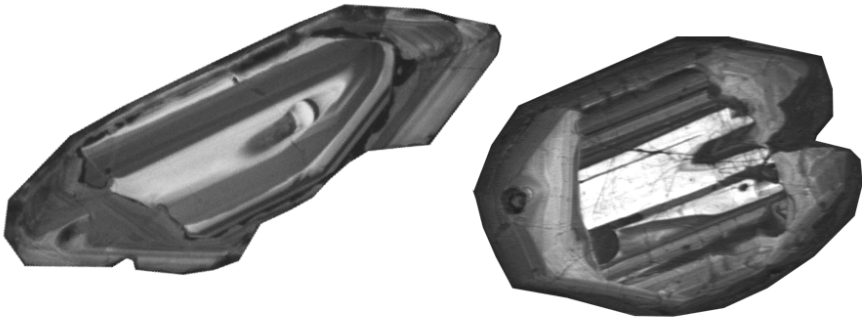

VIII International SHRIMP Workshop
6-10 September, 2016
Granada, Spain

Index

Multiple sulfur isotopes with SHRIMP-SI: analytical protocols for identification of mass-independent and mass-dependent fractionation sulfur signatures

Ávila, JN, Ireland, TR, Holden, P and Lanc, P

Research School of Earth Sciences, The Australian National University

Sulfur isotopes have been used to address a wide variety of questions and processes about the evolution of Earth's atmosphere and hydrosphere. The four-isotope analysis of sulfur allows the distinction of different reaction pathways during geological and biological processing of sulfur. Of particular note in isotope geochemistry is the fractionation of S isotopes in the early Earth where correlated variations in $\Delta^{33}S$ and $\Delta^{36}S$ are apparent with a ratio of approximately -1. The variations of $\Delta^{33}S$ and $\Delta^{36}S$ measured in rocks older than ~2.4 Ga have been attributed to mass-independent fractionation (MIF) of sulfur isotopes in atmospheric source reactions. On the other hand, measurements of multiple sulfur isotopes in some post-Archean sulfides have found non-zero $\Delta^{33}S$ and $\Delta^{36}S$ produced by mass-dependent biogeochemical fractionation (MDF) that show a different $\Delta^{33}S/\Delta^{36}S$ relationship (~ -7) than that found for Archean rocks. Therefore, quantifying the relationships between $\Delta^{33}S$ and $\Delta^{36}S$ offers the possibility to decouple signatures produced from mass-independent processes from those produced from mass-dependent processes.

Over the past few years, there have been major advances on ion microprobe measurements of sulfur isotopes. One of our recent goals has been to optimize the SHRIMP-SI detection system for measurement of multiple sulfur isotopes (^{32}S, ^{33}S, ^{34}S, and ^{36}S). Due to the large abundance difference between the major (^{32}S and ^{34}S) and minor isotopes (^{33}S and ^{36}S) and the presence of sulfur in different proportions in minerals, different analytical protocols need to be adopted. For instance, the addition of each isotope requires a longer analytical time simply because of the lower abundances of ^{33}S and ^{36}S relative to ^{32}S and ^{34}S. Analysis of ^{33}S only requires an additional few minutes to get the required statistics (to around 0.1‰ in $\Delta^{33}S$). Four isotope analysis including ^{36}S requires approximately 20 minutes to achieve 0.2‰ precision in $\Delta^{36}S$ in sulfides. The analysis of sulfate is more difficult because the proportion of S in this mineral is far lower than in sulfide, which results in ion signals a factor of two or more lower. Accuracy of measurements ($\delta^{34}S$, $\delta^{33}S$, $\delta^{36}S$, $\Delta^{33}S$, and $\Delta^{36}S$) is assessed by analysis of sulfur reference materials (e.g., Ruttan and Balmat pyrite, Canyon Diablo troilite, Norilsk chalcopyrite, Anderson pyrrhotite, Balmat galena).

SHRIMP-SI has been used to identify preserved isotopic signatures of the ancient atmospheric and oceanic chemistry as well as biological activity and overprinted secondary processes (e.g., magmatic and hydrothermal) in sulfides. Analytical protocols for SHRIMP-SI multiple sulfur isotope analysis of a suite of sulfide reference materials will be presented as well as examples of high precision multiple sulfur data of MIF ($\Delta^{33}S/\Delta^{36}S \sim -1$) and MDF ($\Delta^{33}S/\Delta^{36}S \sim -7$) sulfur signatures.

Age and origin of charnockitic rocks from Luis Alves Craton, South Brazil

Basei, MAS[1], Bhattacharya, S[2], Campos Neto, MC[1], Sato, K[1], Tassinari, CCG[1], Harara, OMM[3] and Siga Junior, O[1]

1: Geoscience Institute, University of São Paulo, Brazil
2: Indian Statistical Institute, Calcutta, India
3: Geoscience Institute, Paraná Federal University, Brazil

The Luis Alves Craton corresponds to a continental fragment that occurs between Ribeira (N) and Dom Feliciano (S) Neoproterozoic belts, in the southern part of Brazil. Its basement rocks consist of gneisses and migmatites, among which high-grade metamorphic associations characterized by the presence of orthopyroxene can be found. Regional studies involving zircon U-Pb ages and Hf isotope analyzes provide important constraints for the evolution of the high-grade gneisses and to infer the time when the protoliths of the charno-enderbitic rocks were extracted from the mantle.

Two localities were examined in greater detail, one of them consists of a large cut of 150m length in the BR280 road near Guaramirim City, and the other site is a large quarry of the Infrasul Mining Company, near Joinville City. Both places have excellent outcrops of charnockitic rocks with clear

evidences of magmatic differentiation as the main process to explain the compositional variation found. Centimetric to metric bands of amphibolites, enderbites, charnockites (predominant rock), and mafic granulite enclaves occurs in both areas. Pink leucogranite cross cutting the banding are also observed in both locations.

The charnockites have a mineral assemblage: Plag-Qtz-Opx-Opaque±K-fls±Hbl, with some secondary amphibole in Opx. Porphyroblastic amphibole and plagioclase defines the gneissic foliation. Petrographic studies of the mafic granulite enclaves provide textural evidence of hornblende breakdown producing orthopyroxene and plagioclase on the one hand and ilmenite deposition at the edges of hornblende on the other; these being good indicators of the progressive metamorphic pathway to high grade. It is proposed that these mafic granulite enclaves represent restites generated during the deep-crustal anatexis and magmatic differentiation process that formed the charnockites. The protoliths of the mafic granulite enclaves could be considered as hydrated basalts (or gabbros), that undergone hornblende-dehydration melting in the lower continental crust.

SHRIMP and LAICPMS zircon analyzes carried out on the rocks from both localities, including most of the described litho-types yield different ages. In the BR 280 Road the values are concentrated around 2.5Ga (enclaves of mafic granulites, enderbites and charnockites) while the leucogranite cutting the banding indicated 2.3Ga. On the other hand, in the Infrasul Quarry all ages of the five rocks analyzed are around 2.18Ga.The two U-Pb age clusters of 2.50 and 2.18Ga indicate a gap of almost 300Ma between the formation of the charnockitic rocks of BR280 and Infrasul quarry.

The Hf isotopic data of both locations are very similar, and impossible to establish a consistent difference between them. The vast majority of εHf(t) values is slightly negative (-9.0 to 0.0) and the Hf-T_{DM} model ages are all predominantly Archean with values ranging from 3.0 to 3.2Ga proving the crustal origin of these rocks. Considering the differences in U-Pb ages and the similarities in the Hf model ages in both sets, it can be proposed that the studied charnockitic rocks were formed and simultaneously metamorphosed in deep crustal levels, representing the melting at 2.5 and 2.18 Ga of the material extracted from the mantle and accreted at the base of the crust around 3.0Ga.

Heat-induced diffusion in zircons: effects on U-Th-Pb ages and oxygen isotopes.An experimental study at 1400 ºC

Bea, F, Montero, P, Molina, JF and Scarrow, JH

Department of Mineralogy and Petrology, University of Granada, Spain

The study of zircons inherited by magmatic rocks may yield important information about the nature of the magmatic sources and the evolution of magmas but the consequences of their permanence in a hot magmatic environment are not yet well known. These might be important for the U-Th-Pb isotope system, because Pb^{+2} has much lower diffusivity than U^{4+} and Th^{4+}, and for the oxygen isotope system because oxygen is always present in the phases surrounding the inherited zircon, be these a magma or a solid mineral if the zircon is an inclusion fluid phase. Diffusion effects, on the other hand, would be hardly noticeable for the Sm-Nd system or for Hf isotopes because all involved ions have similarly low diffusivity. Previous 3D numerical models of Pb diffusion and zircon solution kinetics revealed that pre-magmatic zircons suspended in magma can only be perceptibly disturbed at 800–830 °C, but this requires more than 1 Myr. At higher T all pre-magmatic zircons in contact with common magmas would be dissolved before diffusion to be effective. Zircons shielded from the melt, on the other hand, can resist much higher temperatures and are surrounded by solid minerals that, in contrast to a melt, do not act as sinks for Pb^{2+}.

To check the results of numerical models, here we present the results of diffusion in natural zircons that were heated at 1400 ºC during up to six months. To avoid thermal decomposition, zircons were embedded in finely powdered silica. We used zircon concentrates from two different rocks, a peraluminous ca. 485 Ma granite in which most zircon grains contain ca. 605 Ma cores, and a metaluminous calc-alkaline 320 Ma tonalite with very uniform zircons. We found that zircons from the peraluminous granite resist heating better than the calk-alkaline tonalite but suffer from marked intra-grain diffusion effects because the grains heterogeneity. After 6 months at 1400 ºC, roughly equivalent to 5 Myrs at 900 ºC, we found that the ca 485 Ma rims yielded considerably older ages, and that the ca 605 Ma age of the cores was totally faked. We also found that the $\delta^{18}O$ of cores and rims, peaking at 6

and 8 respectively, changed and converged to one single value around 9. This may cause wrong provenance estimations based on oxygen isotopes. The highly homogeneous zircons from the tonalite, in contrast, were little affected.

Genetic relationship between gabbro and foidolite counterparts of the Proterozoic polyphase Gremyakha-Vyrmes massif (Kola Peninsula): accessory mineral testing

Belyatsky, BV[1], Lepekhina, EN[1], Antonov, AV[1], Rodionov, NV[1], Balashova, YuS[1], Sorokhtina, NV[2], Shevchenko, SS[1] and Sergeev, SA[1,3]

1: CIR, A.P.Karpinsky Geological Institute (VSEGEI), St-Petersburg, Russia
2: Department of Geochemistry, Vernadsky Institute, RAS, Moscow, Russia
3: Institute of the Earth Sciences, St-Petersburg University, Russia

The largest Proterozoic polyphase Gremyakha-Vyrmes massif is an example of the unique combination of petrology contrasting intrusive rock complexes, among which are: the complex of ultramafic and mafic rocks, foidolite complex and alkaline granites complex. The massif of 19 km long is located in the central part of the Kola Peninsula within the Late Archaean complex of the Kola-Belomorian granite-gneisses and confined to one of the faults of the Belomorides and Karelides joint zone. Intensive magmatism within this zone manifested at 2.45 Ga and lasted for more than 550 m.y., and about 1.9 Ga was accompanied by alkaline magmatism. At this time, it was formed Gremyakha-Vyrmes polyphase massif, the rocks of which are dating on average 1.97 – 1.87 Ga [Savatenkov et al., 1998, 1999; Bea et al., 2001]. Ultramafics and alkaline granitoids compose two separate bodies, and foidolite occur in the central part of the massif. One of the models of the massif formation suggests generation of major complexes from two independent mantle sources, and the ultramafic rocks and granites were formed from a common source with addition of crustal component while foidolites were appeared from an independent source and were not genetically related to ultramafics. It is assumed simultaneous intrusion of all magmatic phases – 1885 ± 20 Ma, and the similarity of Sr-Nd isotope signatures of gabbro-peridotites and granitoid series, and the difference from the respective foidolite signatures (Bea et al., 2001; Arzamastsev et al., 2006). However, field observations have revealed a clear link ultramafics and foidolites, while the relationships of these rocks with granites, apparently, determined by tectonic contacts, and accordingly granites could be melted and intruded later than ultramafics and alkaline rock series (Polkanov et al., 1967; Sorokhtina et al., 2010, 2012). The available geochronological data show significant age variations: for ultramafic-mafic rocks from 1810 to 1973 Ma, alkaline rocks – from 1870 to 2070 Ma, and for alkaline granite and syenite complex – from 1800 to 1940 Ma. As a result, the age of the rocks varies within 150 m.y. interval. At the same time, carbonatites have the youngest Rb-Sr age among the massif rocks – 1765 Ma (Savatenkov et al., 1999), that either reflects their later origin, or the imprint of metamorphism developed within the Kola Peninsula at about 1.75 Ga. It can be assumed on the basis of these observations that the rocks of mafic-ultramafic series and foidolites had a single mantle source and were derived by differentiation of a single alkaline-ultramafic magma which evolution led initially to the formation of mafic-ultramafic rocks, and then foidolites genetically linked with carbonatites and rare-metal mineralization (Sorokhtina et al., 2012).

To verify the age of crystallization of the existing intrusive, late-magmatic and post-magmatic phases, as well as relationships and genetic link between gabbro and foidolite, which together comprise about 80% of the massif volume, we have studied the U-Pb system of indicative accessory minerals (zircon, titanite, pyrochlore and apatite) separated from 10 gabbro and 8 foidolite samples. The obtained due to local analysis of these minerals by U-Pb SHRIMP-II results are shown in Figures 1-5.

Conclusions

Alkaline-gabbro Gremyakha-Vyrmes massif has been active for a minimum of 200-250 m.y. Thus, the sequence of the main intrusive phases (gabbro and foidolite) was as follows: the main gabbroic phase injection was 1981.7±5.9 m.y. ago, and over the next 40-50 m.y. there was a gradual cooling down to 700-800°C with the closing of the U-Pb titanite system at 1944±17 m.y. ago, foidolite crystallization began at 1894±12 Ma, according to U-Pb zircon data. Further massif cooling with the crystallization and recrystallization of accessory titanite, apatite and pyrochlore occurred around 1830–1840 Ma. Ore-deposit process with the-rare metal mineralization is fixed by different isotopic systems at 1760–1740 Ma, apparently it was impact on the U-Pb gabbro apatite system. To sum up, the gabbro

and foidolite intrusions have no direct genetic link and their spatial juxtaposition in a single complex can be explained due to structural and tectonic factors and increased permeability of this lithosphere, as well as a long-lived thermal activity of the upper mantle.

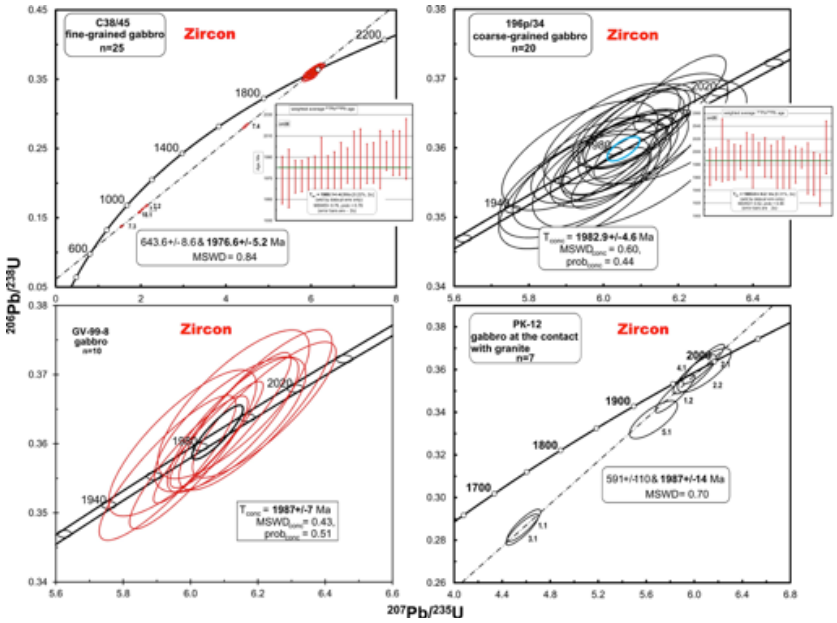

Fig.1. U-Pb concordia diagrams for zircon from the Gremyakha-Vyrmes gabbro. The average zircon age for all gabbro samples is: 1981.7 ± 5.9 Ma

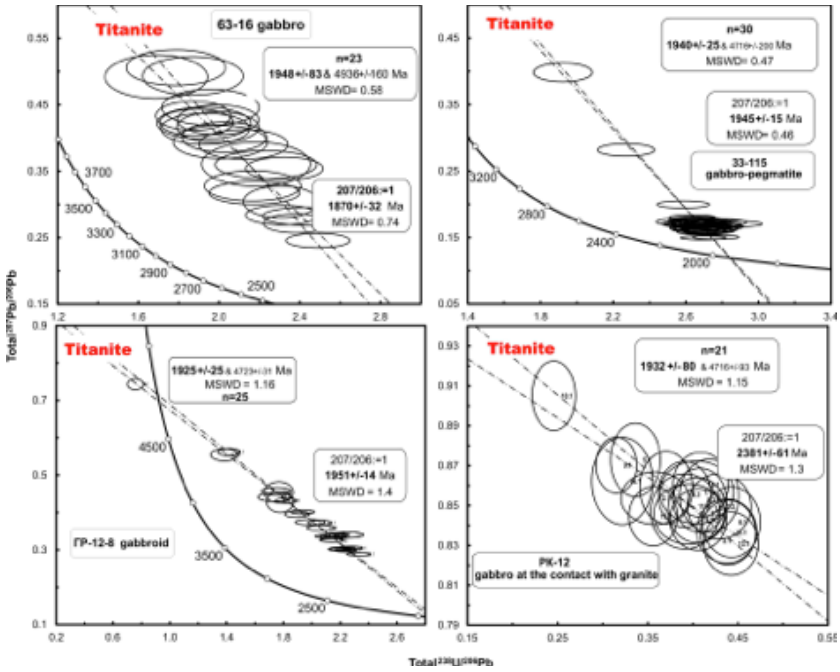

Fig.2. Total $^{238}U/^{206}Pb$ vs $^{207}Pb/^{206}Pb$ diagrams with concordia for titanite from Gremyakha-Vyrmes gabbro. The average titanite age for all studied gabbro samples is: 1944 ± 17 Ma

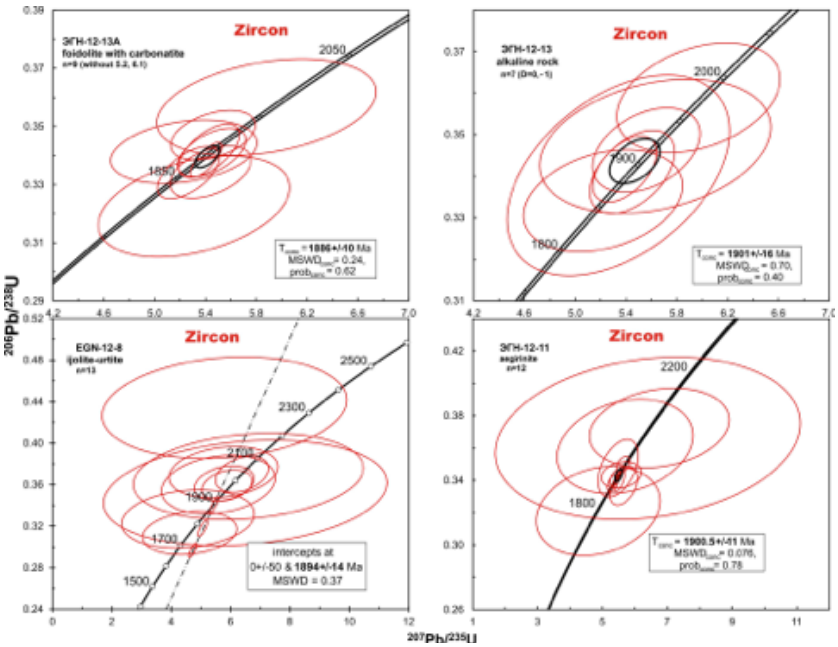

Fig.3. U-Pb concordia diagram for zircon from foidolites of the Gremyakha-Vyrmes massif. The average zircon age for foidolites: 1894 ± 12 Ma.

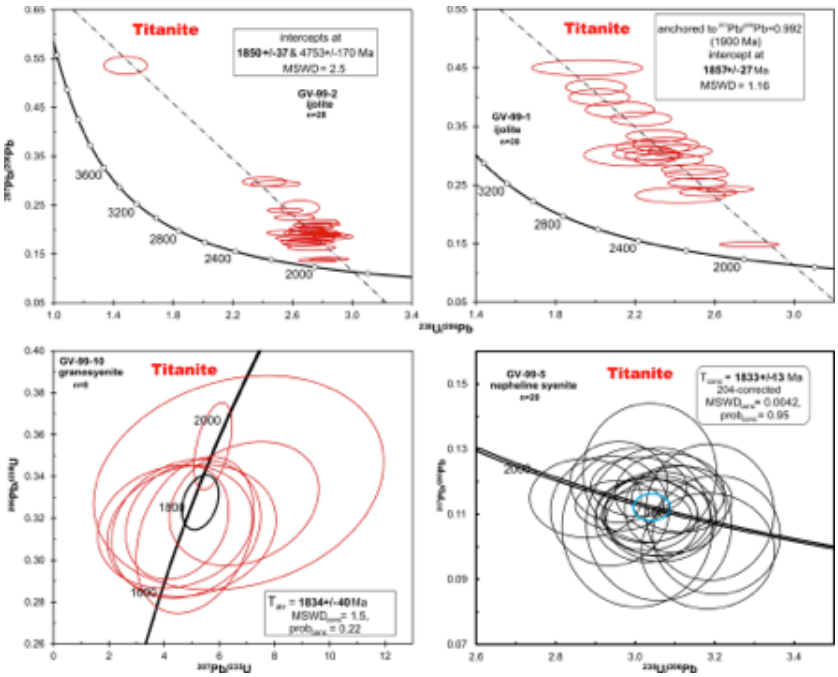

Fig.4. U-Pb concordia diagrams for titanite from foidolites of Gremyakha-Vyrmes polyphase massif. The average titanite age for foidolites: 1838 ± 21 Ma.

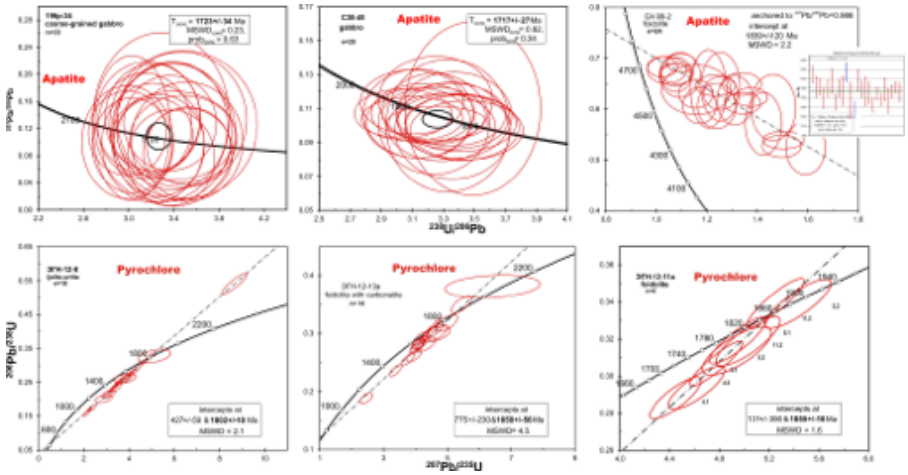

Fig.5. U-Pb concordia diagram for pyrochlore and apatite from gabbros and foidolites of the Gremyakha-Vyrmes massif. The average age of the pyrochlore and apatite from foidolites is almost the same: 1830 ± 25 and 1839 ± 68, respectively, while apatite from gabbro has significantly younger age: 1719 ± 21 Ma (2σ).

Acknowledgements

This research was done within the framework of the state contract with Sevzapnedra (Rosnedra) K41.2014.014.

References

Arzamastsev, AA, Bea, F, Arzamastseva, LV, Montero, P. (2006) Proterozoic Gremyakha-Vyrmes polyphase massif, Kola Peninsula: an example of mixing basic and alkaline mantle melts. Petrology 14(4), 361–389.

Bea, F, Arzamastsev, A, Montero, P, Arzamastseva, L. (2001) Anomalous alkaline rocks of Soustov, Kola: evidence of mantle-derived metasomatic fluids affecting crustal materials. Contributions to Mineralogy and Petrology 140, 554–566.

Polkanov, AA, Eliseev, NA, Eliseev, NE, Kavardin, GI. (1967) Gremyakha-Vyrmes massif on the Kola Peninsula. Moscow, Nauka, 236 p [in Russian].

Savatenkov, VM, Pushkarev, YuD, Sergeev, AV, Sulimov, RB. (1999) Carbonatites of the Gremiakha-Vyrmes massif (Russia) as an indicator of the new ore-deposit specialization. Geology of Ore Deposits 41(5), 449–454.

Savatenkov, VM, Sulimov, RB, Sergeev, AV, Goncharov, GN, Pushkarev, YuD. (1998) Sm-Nd, Rb-Sr and Pb-Pb isotope systematics of basites-ultrabasites in Gremiakha-Vyrmes massif: implication for the role of crust-mantle interaction while the magma generation and Ti-ore-forming process. Proceedings of the Russian Mineralogical Society 5, 15–25.

Sorokhtina, NV, Kogarko, LN, Shpachenko, AK. (2010) New data on mineralogy and geochemistry of rare-metal mineralization of the Gremiakha-Vyrmes massif. Doklady Earth Sciences 434(1), 1240–1244.

Sorokhtina, NV, Kogarko, LN, Shpachenko, AK, Groznova, MV, Kostitsyn, YuA, Roshchina, IA, Gredina, IV. (2012) Geochemistry and age of the complex of alkaline metasomatic rocks and carbonatites of the Gremyakha-Vyrmes massif, Kola Peninsula. Geochemistry International 50(12), 975–987.

Interpretation of U-Pb SHRIMP zircon ages for the oldest metamorphic complex (Ukrainian Shield)

Berezhnaya, NG and Sergeev, SA

Centre of Isotopic Research, Russian Geological Research Institute (CIR VSEGEI), St-Petersburg, Russia

The Bug Granulite-Gneiss complex (BGG) is located in the Dniester-Bug province in the south-western part of Ukrainian Shield. The BGG evolution demonstrates multiple Archaean and Proterozoic events. Its Archaean rocks are exposed in the Bug-Ros' block and outcrops along Southern Bug river. The main rock type are Early Archaean gneissic enderbites (~70%), some mafic and ultramafic lithologies (~10%), Mesoarchaean to Neoarchaean metasediments (Lobach-Zhuchenko et al., 2014). The oldest crustal component is gneissic enderbites has an age of ca 3750 Ma that appears to be of igneous derivation (Claesson et al., 2015; Bibikova et al., 2013).

In our sampling area gneissic enderbite contains a huge of enclaves of mafic granulites, metaperidotites and metaorthopyroxenites. Samples for zircon separation were collected from the Odessky quarry. There are fine-grained non-migmatized hypersthene–plagioclase granulite UR-132 and coarse-grained gneissic enderbite UR-108.

Based on their external morphology, texture in BSE and CL images, geochemical composition and isotopic age (Fig.1), all studied zircons from granulite UR-132, were subdivided *de bene esse* into five (I-V) groups and from enderbite – into two (A-B) groups (Table 1).

At least two versions of interpretation are possible: First version was developed in our recent article (Lobach-Zhuchenko et al., 2016). Zircons of group I indicate the protolith age for mafic granulite 3659±19 Ma, zircons from group II presumably contain some inheritance from older felsic rocks, ca 3.75 Ga, zircons III date 3588±7 Ma granulite metamorphism, whereas zircons VI and V are characterized by either 2.4 Ga or 2.1 Ga old homogeneous rims, reflected Proterozoic HPT metamorphism. According to the second version, zircons I and III from mafic granulite are rather indistinguishable in morphology, age and geochemistry. Hf content in zircons I and III lay within 6500-9000 ppm interval. Thus, they may have magmatic origin, but its size and geochemistry are in conflict with both rock texture and characteristic of genuine magmatic zircon from mafic rocks.

Zircons from the gneissic enderbite UR-108 show two different types of CL patterns. Type A zircon comprise large prismatic or oval pink color grains. CL and BSE images reveal a planar-banded zoning or a sector zoning in the fractured cores surrounded by homogeneous rims. Cores demonstrate (in ppm): Hf 8150-10200, U 40-100, Y 570-920, Yb 210-270, Gd 10-20. Th/U ratios are 0.9-1.3. One best-preserved core shows concordant age of 3670±11 Ma (Table 1, Fig.1). Most of zircons A altered and yields the discordant ages. Rims and maximally altered cores are around 2.7 Ga old. Cores of zircons A are very similar to cores in zircons I and III from mafic granulites UR-132. Type B represents large oval (500–300 μm) muddy brown and strongly fractured grains. CL images show dark cores and light rims. In contrast to zircons A, cores contain (in ppm): Hf 11150-18400, U 1500-2300, Y 800-1870, Yb 450-830, Gd 10-15. Th/U ratios are 0.07-0.1. Age of cores in type B zircons vary between 2627±9 to 3352±75 Ma. Zircons B from enderbite, like zircons II from mafic granulite, have high REE and U content. Rims of both (A and B) zircon types yield different Proterozoic discordant ages between 2.1 and 2.4 Ga, as well as the subcorcondant age around 2080 Ma. Generally, zircons A and B from gneissic enderbite (UR-108) by its geochemistry and age have a similar appearance to zircons I-III from granulite UR-132.

We presume that the magmatic protolith of mafic granulites, during intrusion, was contaminated by host enderbite material and zircon I-III is inherited from protolith of enderbites, which was earlier identified as diorite in composition (Claesson et al., 2015, Shumlyanskyy, 2012). Hf content of 7500-9000 ppm in zircon I and III is typical for zircon of Archaean diorites. Initial $^{177}Hf/^{176}Hf$ values for magmatic zircons I are in a range of 0.280348–0.280598 and display εHf (t=3.66 Ga) values from -3.4 to +5.8. The $(^{176}Hf/^{177}Hf)_I$ of zircons III are in a range of 0.280312–0.280439, and their εHf (t=3.59 Ga) values vary from -5.2 to -0.7. LA–ICPMS Lu–Hf isotope analysis of enderbite zircons (e.g. 06-BG35, at Shumlyanskyy, et al., 2015) also show εHf(t) variations from -5.2 to -0.8, like in oldest zircons of mafic granulite UR-132.

Conclusions

– Protolith of gneissic enderbite was formed 3.66 Gy ago (age of diorite magmatic crystallization).

– Protolith of of mafic granulite (intrusive rock) was contaminated by older enderbite material, including 3.4-3.66 Ga old zircon xenocrysts. Entirely magmatic zircon of this stage is absent.

– 2.6 Ga - granulite-facies metamorphism recorded in rims growth and in altered zircons B type from gneissic enderbite.

– 2.1–2.4 Ga old rims show metamorphic overprint during some stages of Proterozoic HPT metamorphism.

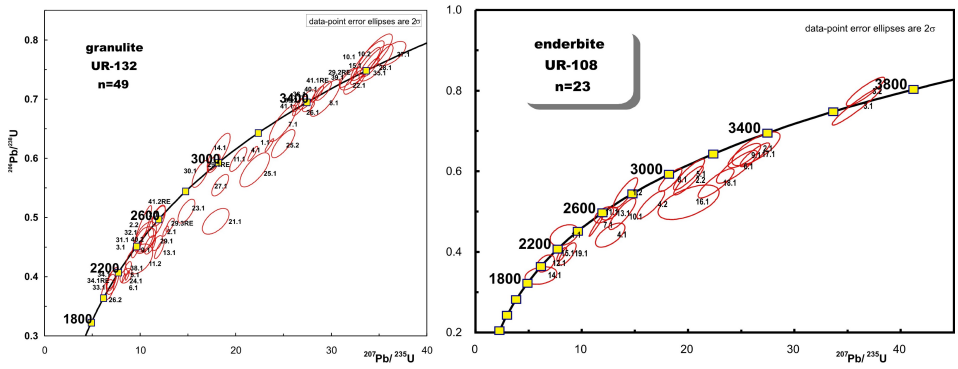

Fig.1 U-Pb concordia diagrams for all zircon varieties from mafic granulite (UR-132) and enderbite (UR-108) of the BGG, Ukrainian Shield.

References

Bibikova, EV, Fedotova, AA, Kirnozova, TI, Fugzan, MM, Claesson, S, Il'insky, LS, Stepanyuk, LM, Shumlyansky, LV. (2013) Isotope-geochronological (U-Th-Pb, Lu-Hf) study of the zircons from the Archean magmatic and metasedimentary rocks of the Podolia domain, Ukrainian Shield. Geochemistry International 51(2), 87–108.

Claesson, S, Bibikova, E, Shumlanskyy, L, Dhuiml, B, Hawkesworth, CJ. (2015) The oldest crust in the Ukrainian Shield – Eoarchaean U-Pb and Hf-Nd constrains from enderbites and metasediments. Journal of Geological Society of London, Special Publication 389, 227–253.

Lobach-Zhuchenko, SB, Balagansky, VV, Baltybaev, ShK, Bibikova, EV, Chekulaev, VP, Yurchenko, AV, Arestova, NA, Artmenko, GV, Egorova, JuS, Bogomolov, ES, Sergeev, SA, Skublov, SG, Presnyakov, SL. (2014) The Orekhov–Pavlograd Zone, Ukrainian Shield: Milestones of its evolutionary history and constraints for tectonic models. Precambrian Research 252, 71–87.

Lobach-Zhuchenko, SB, Kaulina, TV, Baltybaev, ShK, et al. (2016) The long (3.7-2.1 Ga) and multistage evolution of the Bug Granulite–Gneiss Complex, Ukrainian Shield, based on the SIMS U-Pb ages and geochemistry of zircons from a single sample. Journal of Geological Society of London, Special Publication (in press).

Shumlyanskyy, LV. (2012) Isotope geochemistry of the granite boulder from pseudo conglomerate of the Teteriv Series, North-Western region of the Ukrainian shield. Mineralogical Journal 34(1), 54–62 [in Ukrainian].

Shumlyansky, L, Hawkesworth, C, Dhuime, B, Billström, B, Claesson, S, Storey, C. (2015) 207Pb/206Pb ages and Hf isotope composition of zircons from sedimentary rocks of the Ukrainian shield: Crustal growth of the south-western part of East European craton from Archaean to Neoproterozoic. Precambrian Research 260, 39–54.

Table 1. Zircon varieties in the Archaean enderbites and mafic granulites of the BGG, Ukrainian Shield

Zircon type	Morphology, max. size, μm	Cores, Rims. Analytical spot diameter 25μm	CL	Hf, U, ppm, Th/U	Age, Ga
UR-132 – mafic granulite					
I	Prismatic/Oval, Isometric 500x250	Zoned cores 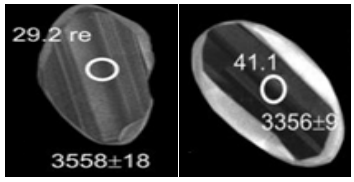 Rims	Weak Light	6500-7400, 60-260, 0.4-1.1 6400-7100, 20-30, 0.4	3.66 - 2.37 2.55
II	Oval 500x300	Cores + inclusions 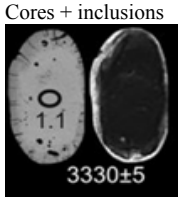 Clear Rims	Dark Light	8500-13000, 770-2030, 0.1-0.9 9600-9800, 30-100, 0.03-0.4	3.42 - 3.56 2.40-2.06
III	Isometric 500x250	Sector-zoned cores 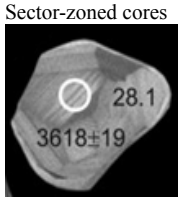 Rims	Light Light	6650-9800, 45-55, 0.7-1.6	3.62-3.33
IV	Isometric/Oval 200x100	Cores (I-III type)  Homogeneous rims	Dark Light	7900, 20, 0.9 7130-9760, 20, 0.4	2.48
V	Isometric/Oval 200x100	Cores (I-III type) 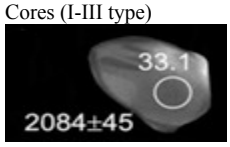 Homogeneous rims	Gray Light	6700-6900, 15-40, 0.01-0.9	2.08-2.10
UR-108 - gneissic enderbite					
A	Prismatic/Oval Isometric 500x250	Sector-zoned cores 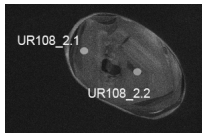 Homogeneous rims	Light Gray	8150-10200, 40-100, 0.9-1.3	3.67-2.70 2.10-2.40
B	Oval 500x300	Cores+ inclusions 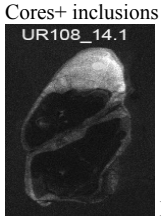 Rims	Dark Light	11150-18400,1500-2300, 0.1 1380, 430, 0.2 9240-9530, 25-30, 0.7-0.9	3.35-2.63 2.70 2.10-2.40

Dissecting SQUID 2.5: The amazing innards of our data reduction package

Bodorkos, S[1], Magee, CW, Jr.[1], Bowring, J[2], Main, P[1] and Cross, A[1]

1: Geoscience Australia Canberra ACT, Australia
2: College of Charleston, Charleston SC USA

The Microsoft Excel-based SQUID 2.50 software for SHRIMP data reduction was developed by Ken Ludwig (formerly of the Berkeley Geochronology Center) in 2009, in response to community demand for increased flexibility in data processing, with specific reference to extended run tables, and customised and/or complex data reduction procedures. The Task feature was a particularly important innovation in SQUID 2.50, allowing researchers to develop and easily share custom data reduction routines.

Unfortunately, SQUID 2.50 is dependent on Excel 2003, which (as of April 2015) is no longer supported by Microsoft. An attempt to upgrade SQUID 2.50 for use in a newer version of Excel failed owing to a variety of factors, including security enhancements and fundamental changes to the Excel object-model post-2003. However, the data-handling methodology and arithmetic underpinning SQUID 2.50 seems fundamentally sound, as indicated by comparisons between high-precision SHRIMP and CA-IDTIMS $^{206}Pb/^{238}U$ results on well characterised zircons (Magee et al., this volume). The widespread acceptance and uptake of SQUID 2.50 has led Geoscience Australia (GA) to collaborate with the College of Charleston's Cyber Infrastructure Research and Development Lab for the Earth Sciences (CIRDLES) in working toward redeploying SQUID 2.50 methodology and arithmetic in an open-source, platform-independent environment.

The initial aim of this project is to reverse engineer SQUID 2.50 in Java. Rigorous replication of Excel results in Java is essential to verifying the technical success of the port, and the SQUID 2.50 algorithms will then be useable as a baseline against which future improvements in data-reduction methodology can be benchmarked. One significant and ongoing challenge is the unravelling of the calculations implemented in SQUID 2.50 via Microsoft's Visual Basic for Applications (VBA) language. The code underpinning SQUID 2.50 has been open-source since 2009, but the VBA modules are poorly documented, and extraction of the logic and algorithms for re-implementation in Java has proven difficult. Nevertheless, we have made some promising initial progress, and all of the calculations replicated thus far are bundled in a Java application "Calamari", which is being demonstrated at this Workshop.

We developed a parser for the XML files produced by the SHRIMP control software, replicated the Tukeys Biweight algorithm frequently used by SQUID 2.50, and used these features to convert the 10 'integrations' (ion counts and SBM counts), collected during each scan of each mass-station, into total ion counts and total SBM counts for that peak (as shown by the 'condensed XML' SQUID-worksheet labelled with the name of the input datafile). This procedure incorporates the collector deadtime correction for ion counts, and the SBM zero correction for SBM counts. At low count-rates (i.e. when the median of the 10 ion-count integrations at a mass-station is less than 100), we have replicated SQUID 2.50's assessment of the most-outlying integration as a potential exclusion on the basis of Poisson statistics, and our implementation faithfully replicates idiosyncratic behaviour exhibited by the VBA code when the median is not an integer.

We reproduced the arithmetic used to estimate the count-rates (i.e. "[mass] cts/sec"), as typically displayed near the left-hand sides of the StandardData and SampleData sheets of a SQUID-workbook. Subsequent work focused on the replication of ratios of measured nuclides, as defined in the Isotope Ratios window of SQUID 2.50's Task Editor. Following custom calculations for specific scenarios (i.e. single-scan data, and ratios where total ion counts of either numerator or denominator are less than 32) and SBM-normalisation of ion-count data if desired, the first step for each ratio is double-interpolation of the numerator and denominator counts for adjacent scans (using the method described by Dodson, 1978), to the time-midpoint of the four mass-stations involved. In this fashion, N–1 ratios are generated (where N is the number of scans), and we faithfully replicated the time-stamps, values and errors of each of the N–1 measured-nuclide ratios calculated for each combination of analysis and "ratio of interest", as shown on the Within-Spot Ratio sheet of a SQUID-workbook.

The next step is to calculate the "mean of ratios" from the double-interpolated data, by choosing one of the two methods proffered by SQUID 2.50: "spot average" or "linear regression to spot midtime". Both of these calculation methods feature correlated errors on adjacent interpolated ratios

(arising from the fact that adjacent ratios initially shared data from the same scan: Ludwig, 2009), and both are rigorously replicated in Java. The implementation includes an assessment of statistical coherence, which if failed leads to an assessment of the statistical effect of sequentially deleting each of the constituent data-points. The deletion offering the largest statistical improvement is assessed against stringent criteria for permission (the deletion generally needs to improve the MSWD of the calculation by a factor of 3–5 **and** remove all excess scatter: unless both conditions are met, the proposed deletion is considered unwarranted). The result of the calculation is a per-spot mean ratio and its percentage error, displayed in uncoloured columns near the left-hand sides of the StandardData and SampleData sheets of a SQUID-workbook) and we successfully replicated both "spot average" and "linear regression" calculations.

During this process, we discovered that "linear regression" calculations in which none of the constituent data-points qualifies for exclusion yield values and errors corresponding to the Y-intercept of the linear regression (i.e. at time = 0), rather than the value and error resulting from linear interpolation to the burn-midtime. There is no obvious explanation for this VBA implementation (especially as the full linear interpolation **is** implemented to calculate ratio value and error in any case where one of the constituent data-points **does** qualify as a permissible outlier), and it is possible that it is an unintended bug.

Other, confirmed bugs are evident in the "downstream" section of the code, the most egregious of which lies within the calculation of the percentage error associated with the 207-corrected $^{206}Pb/^{238}U$ ratios. Simple inspection of the formulae in the relevant cells of a SQUID-workbook shows that the numeric decay constant used is that of ^{232}Th, rather than ^{238}U; it follows that all percentage errors associated with 207-corrected $^{206}Pb/^{238}U$ ratios are underestimated by a factor of ~3 (i.e. lambda238/ lambda232). This is easily verified by inspecting the correspondingly larger (and correctly calculated) percentage errors associated with the 204-corrected and 208-corrected $^{206}Pb/^{238}U$ ratios.

Finally, it is essential to note that the focus of our work thus far (which represents nearly 6 months of effort from 2–3 people) has been almost entirely arithmetical, and it is obvious that very significant additional arithmetic unravelling remains to be done. Furthermore, no work has yet been done on a user interface, and no data-reduction customisation is yet available (at the time of writing, even the input XML is hard-wired). Developing the capability and usability that the SHRIMP community has come to expect from SQUID 2.50 will require substantial additional resourcing if the project is to be completed in a timely fashion. We estimate that a total SHRIMP community contribution of USD300,000 (cash or dedicated expertise) will be needed in order to advance the current work to a functioning production version of re-implemented SQUID 2.50 by the time of the 2018 SHRIMP Workshop. Fewer resources will result in (at best) correspondingly longer timeframes for completion. It remains possible that the work done thus far will be shelved, as neither GA nor the College of Charleston can continue to support the project in its current form without assistance.

References

Dodson, MH. (1978) A linear method for second-degree interpolation in cyclical data collection. Journal of Physics E: Scientific Instruments. 11 296.

Ludwig, K. (2009) Errors of isotope ratios acquired by double interpolation. Chemical Geology. 268 24-26.

Advanced Cyber Infrastructure for Geochronology as a Collaborative Endeavor: A Decade of Progress, A Decade of Plans

Bowring, JF[1] and McLean, NM[2]

1: Department of Computer Science, College of Charleston, Charleston, SC, USA
2: Department of Geology, University of Kansas, Lawrence, KS, USA

The Cyber Infrastructure Research and Development Lab for the Earth Sciences (CIRDLES.org) has worked collaboratively for the last decade with geochronologists from EARTHTIME to build a first-of-its-kind cyberinfrastructure geared to ensuring transparency and reproducibility in geoscience workflows. This allows geochemists to focus on geochemistry research and to be engaged in the

development of algorithms, interactive user interfaces, and data outputs without having to author a large codebase or master computer science and software engineering principles. The computer science community also benefits by acquiring research opportunities to improve development process methodologies used in the design, implementation, and sustainability of domain-specific software. We are actively engaged in refining and extending that work to serve additional geochronology domains during the next decade.

The term Cyber Infrastructure is used in many contexts and does not have a hardened definition. We are developing a working definition of cyberinfrastructure for science: a collaboratively and sustainably evolving socio-technical system of systems including humans, software, computing devices, and electronic storage intended to support and advance open science and ensure reproducibility.

Sam Bowring of Massachusetts Institute of Technology (MIT) pioneered this collaboration between geochronologists and computer scientists to develop what he called "cradle to tomb" cyberinfrastructure to support the flow of data for geochronology from the field to the laboratory to publicly accessible online databases. He drove the establishment of EARTHTIME in 2001 as a community-driven initiative with the goal of calibrating Earth history and developing the geochronological techniques necessary to produce high precision dates. These techniques included the collaborative development of robust open source software tools to support the scientific workflows of geochronologists, including data reduction, analysis, and archiving. The resulting tools *Tripoli* and *ET_Redux*, developed by the authors with others, now play a key role in U-Pb geochronology by isotope dilution thermal ionization mass spectrometry (ID-TIMS).

Our first major collaborative software development effort was the program *Tripoli*, which is designed to interactively and visually process raw TIMS U-Pb data, and it has become a workhorse for the TIMS community. During the creation of *Tripoli*, we unwittingly entered into cyberinfrastructure development and evolution as we realized there was a possibility to use the internet – also known as the cloud - to establish and maintain models and instances of commonly used parameters as well as analytical results. We developed an architecture that provided standard data schemas so that users of *Tripoli* could create, store, and share versioned models of their parameters, like tracer isotopic compositions, and results.

ET_Redux (formerly *U-Pb_Redux*) is a free open-source software system that provides end-to-end support for the reduction of raw mass spectrometer (TIMS - in concert with *Tripoli*, and LA-ICPMS) data to U-Pb dates. The system automates the analytical and scientific workflows of data acquisition, statistical filtering, data analysis and interpretation, publication, community-based archiving in online databases, and the download, compilation and comparison of data from different laboratories to support collaborative science. Innovations for LA-ICPMS include allowing users to implement and compare both 'intercept' and 'downhole' data reduction techniques, recognition of sample-to-sample uncertainty correlations deriving from sample-standard bracketing, and implementation of log-ratio analysis for handling compositional data.

The EarthChem database used in this system – GeoChron.org – depends on keyed references to the System for Earth Sample Registration (SESAR) database that stores metadata about registered samples. These keys are each a unique International Geo Sample Number (IGSN) assigned to a sample and to its derivatives. *ET_Redux* provides for interaction with this archive, allowing analysts to store, maintain, retrieve, and share their data and analytical results electronically with whomever they choose and depends on an open standard for the data elements of a complete reduction and analysis of U-Pb data. *ET_Redux* provides one-click archiving - the analyst can save their partial or completed data and results in the cloud at Geochron.org as often as they wish and retrieve or share them just as easily. The analyst fully controls who accesses these files, and can switch from private to public access, for instance, when a study incorporating that data is published.

This collaborative work is difficult – it took the authors and others years to move from prototypes to a functioning and still-evolving system. In addition to the complex nature of the geochemists' workflows and the mathematics and statistics used to handle the data, there emerged many cultural differences between computer science and geoscience. At the simplest level was the difference between 0-based and 1-based indexing of matrices. At the most complex level was learning to see the world as the other domain did. Some practical cyberinfrastructure solutions emerged in the form of a common language complete with dictionary, visualizations, process maps, and prototypes. Along the way we've continually discovered and refined how to conduct collaborative domain-specific software

engineering. One main attribute of this collaborative process is its iterative nature and the management of continuous change. The authors and our colleagues have communicated weekly if not daily via all manner of media for the better part of 10 years as *Tripoli* and *ET_Redu*x have evolved and gone into production. We place our development efforts into the public domain to help explore new ways in which software systems built for scientific inquiry can remain sustainable in the face of constant advances and change.

During the next decade, we intend to extend our *ET_Redux* cyberinfrastructure to new isotope systems and to new instrumentation. The original *U-Pb_Redux*, built for U-Pb isotope dilution thermal ionization mass spectrometry (ID-TIMS), was developed as an exemplar software system, whose basic components could be re-purposed. For instance, the vector-graphics interactive concordia plots with SVG/PDF output used for ID-TIMS U-Pb geochronology were reused for LA-ICPMS data, which will debut for that community in a workshop at the 2016 national meeting of the Geological Society of America. Other modules, such as specialized data structures that model discrete versioned parcels of information, like decay constants, isotopic tracers, or reference material isotopic compositions (Bowring et al., 2011), are being reused for our current development effort to capture, archive, and re-calculate U-series carbonate and silicate data. For instance, constructing sea level curves using multiple decades of U-Th geochronology of corals requires capturing the state of uranium and thorium decay constants over multiple refinements of their values and uncertainties. Many of the same data reduction, uncertainty propagation, data visualization, and data archiving capabilities now developed for *ET_Redux* could be extended to SHRIMP U-Pb geochronology as well.

With Geosciences Australia, we have begun to explore the addition of SHRIMP data and workflows to *ET_Redux*, building on our TIMS and LA-ICPMS U-Pb functionality. During 2016, Jim Bowring and Simon Bodorkos have worked to successfully demonstrate the replication of the basic arithmetic implemented by Ken Ludwig in Squid 2.5 (Ludwig, 2009) with an open source project written in Java called *Calamari*: https://github.com/CIRDLES/ET_Redux/wiki/SHRIMP:-Intro. Next, we seek to collaborate with the SHRIMP community to complete replication of Ken Ludwig's U-Pb SHRIMP data reduction and uncertainty propagation algorithms from Squid 2.5, providing a viable, Excel-independent software package. Once this pressing need is met, we look to continue our collaboration with the SHRIMP community to explore adding new statistical approaches developed for *ET_Redux* (McLean et al., 2011; 2016), integrate existing concordia and weighted mean plots and calculations and data table and database outputs, and to create new data reduction and interpretation visualizations required by the SHRIMP community.

References

Bowring, J, Horstwood, M, Gehrels, G. (2013) Resolving bias in laser ablation geochronology. Eos Trans. AGU 94(24), 217. doi:10.1002/2013EO240010.

Bowring, JF, McLean, NM, Bowring, SA. (2011) Engineering cyber infrastructure for U-Pb geochronology: Tripoli and U-Pb_Redux. Geochem. Geophys. Geosyst. 12, Q0AA19. doi: 10.1029/2010GC003479.

Horstwood, M, Gehrels, G, Bowring, JF. (2010) Improving consistency in laser ablation geochronology. EOS Trans. AGU 91(28), 247. doi:10.1029/2010EO280003.

Ludwig, KR. (2009) SQUID 2: A User's Manual, rev. 12 Apr, 2009. Berkeley Geochron. Ctr. Spec. Pub. 5, 110 p.

McLean, NM, Bowring, JF, Bowring, SA (2011). An algorithm for U-Pb isotope dilution data reduction and uncertainty propagation, Geochem. Geophys. Geosyst. 12, Q0AA18. doi:10.1029/2010GC003478.

McLean, NM, Bowring, JF, Gehrels, G (2016). Algorithms and software for U-Pb geochronology by LA-ICPMS. Geochem. Geophys. Geosyst. 17. doi:10.1002/2015GC006097.

Youngest exposed granite and its geochemistry: the 0.8 Ma Kurobegawa Granite

Cambeses, A[1], Bea, F[1] and Ito, H[2]

1: Department of Mineralogy and Petrology, University of Granada, Spain
2: Nuclear Risk Research Center, Central Research Institute of Electric Power Industry, Japan

Granite is a major constituent of the Earth's crust and deciphering the genesis and evolution of the youngest known granite may contribute to the understanding of the crustal evolution of our planet. Younger granites may have experienced the least effects from later metamorphism and/or diagenesis. Here we focus on the analytical results of zircon U-Th-Pb age and composition of the *c*. 0.8 Ma Kurobegawa Granite, Hida Mountain Range of central Japan (Fig. 1A). The Kurobegawa Granite is the youngest known exposed granite on Earth (Ito et al., 2013).

The Kurobegawa Granite is vertically zoned in Upper, Middle, and Lower Units composed, from bottom to top, of granodiorites to granites (Fig. 1B; Wada et al., 2004). Variably shaped Microgranular Mafic Enclaves (MMEs) are present throughout the pluton (Fig. 1B). Notably, in some areas extensive mingling/mixing is recognised between granitic units and MMEs, forming the hybrid Unit (Fig. 1B). We consider two representative specimens, sampled near the northern rim of the Kurobegawa Granite: i) a large sample, *c*. 4.5 kg, composed of medium-grained felsic granite intermingled with MMEs (Fig. 1C); and ii) a small sample, *c*. 0.7 kg, composed of an MME cut by an aplite vein (Fig. 1D).

The MMEs are diorites to tonalites characterized by a medium-grained, equigranular hypidiomorphic texture. They contain plagioclase, acicular amphibole, biotite and interstitial alkali feldspar and quartz. Accessory phases include apatite, titanite, epidote, zircon, magnetite and pyrite. The texture of the host granite is coarse- to medium-grained and inequigranular. It is composed of large crystals of plagioclase, alkali feldspar, biotite and quartz in a fine-grained matrix with the same mineralogy and minor amphibole. Accessory phases in the granites are apatite, zircon, monazite, epidote, titanite and magnetite.

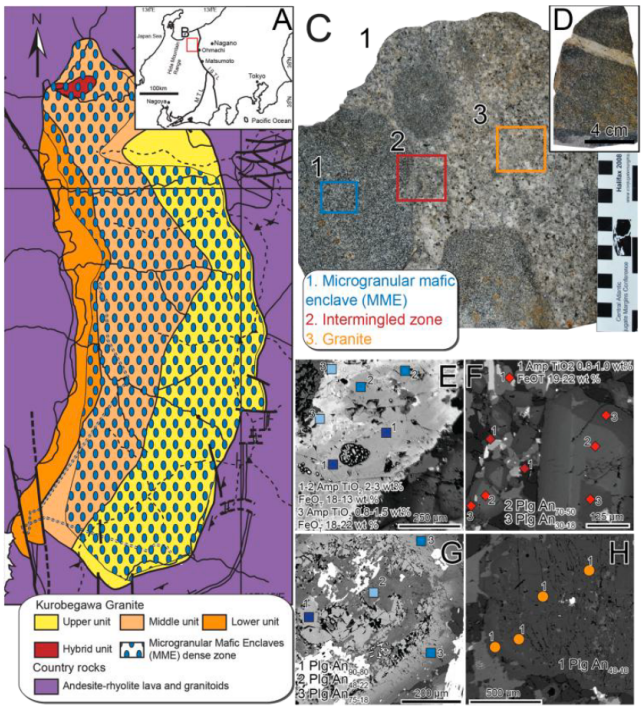

Figure 1. A) Location of the Kurobegawa Granite in Hida Mountain Range and B) simplified geological map (modified from Wada et al., 2004). C and D) Hand-specimen studied samples. E-H) Representative back-scattered electron images showing phase relationships and their main compositional variations. Colours are the same as in Figure C.

Textural evidence of mingling and mixing processes (Figs. 1E-1H) includes: normal and reversed oscillatory-zoned plagioclase, spongy-cellular plagioclase included in large plagioclase, patchy-zoned

amphibole and ovoid quartz megacrysts. Textures and mineral chemistry allowed identification of different types of phases formed during different crystallization stages. Large amphiboles in the MMEs have high-TiO_2 (2-3 wt %) and low-FeO_T (18-13 wt %) magnesiohastingsite cores (Fig. 1E). Rims, edenites to hornblendes, are patchy-zoned with low-TiO_2 (0.8-1.5 wt %) and high-FeO_T (18-22 wt %) (Fig. 1E). Notably, in the intermingled zone fine-grained amphibole has reequilibrated to low-TiO_2 (0.8-1 wt %) and high-FeO_T (19-22 wt %) edenite to hornblende (Fig. 1F). Plagioclase also reflects open mixed system crystallization conditions, e.g., spongy bytownite (An_{90-80}) included in andesine-oligoclase (An_{48-22}) overgrown by zoned bytownite to oligoclase (An_{75-18}) are common in the MMEs (Fig. 1G). By contrast, large plagioclases in the granite have homogeneous andesine-oligoclase composition (An_{40-10}) (Fig. 1H). However, in the intermingled zone fine-grained matrix plagioclases show evidence of reequilibration with labradorite cores (An_{70-50}) and a sharp overgrowth of oligoclase (An_{30-18}) (Fig. 1F). Biotite in the MMEs is zoned with low-Al_2O_3 (12.5-13.5 wt %) and high-TiO_2 (4.2-4.9 wt %) core to rim trend. A reversed core-rim trend is detected in large biotites from the granites with high-Al_2O_3 (14.2-13.5 wt %) and low-TiO_2 (4.2-3.2 wt %). Nevertheless, fine-grained biotites from the intermingled zone have intermediated composition with $Al_2O_3 \approx$ 13 wt % and $TiO_2 \approx$ 4.5-3.2 wt %.

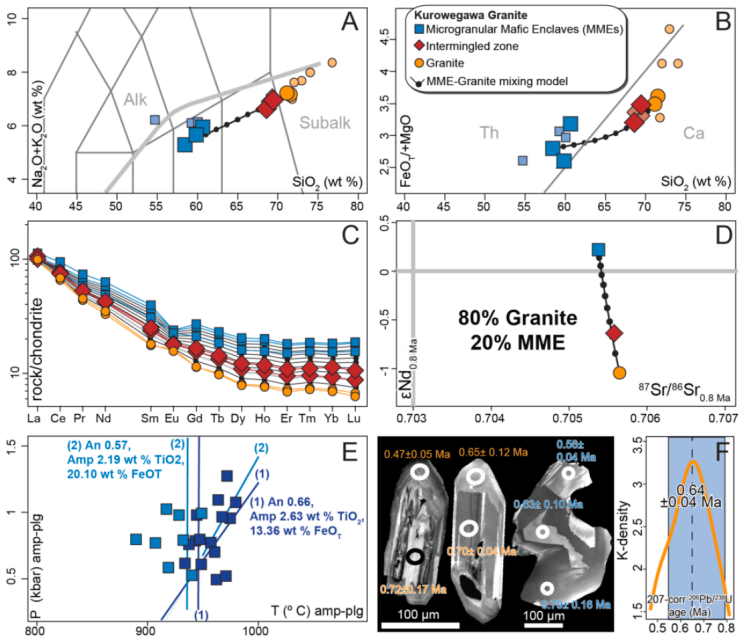

Figure 2. Whole-rock composition of the Kurowegawa Granite: A) Total alkalis vs SiO_2 (TAS); B) FeO_T/MgO vs SiO_2; C) Chondrite-normalised diagram; and D) εNd_t vs. $^{87}Sr/^{86}Sr_t$. We also add a two end-member mixing model. E) Temperature estimates, calculated with the amphibole-plagioclase thermometer and pressure estimates, calculated with the amphibole-plagioclase barometer. F) New U-Th-Pb SHRIMP ages determined in granite and Mafic Microgranular Enclave. Small and light coloured symbols from Wada et al. (2004).

The MMEs have a subalkaline ($SiO_2 \approx$ 58-61 wt %, $Na_2O+K_2O \approx$5.3-5.9 wt %), medium-K ($K_2O \approx$1.8-2.2 wt %), tholeiitic ($FeO_T/MgO \approx$ 2.6-3.2) and metaluminous composition (ASI≈ 0.90-0.95) (Fig. 2A and 2B). The granites have subalkaline ($SiO_2 \approx$ 71 wt % $Na_2O+K_2O \approx$ 7 wt %), high-K ($K_2O \approx$ 3.8 wt %), calc-alkaline ($FeO_T/MgO \approx$ 3.5-3.6) and slightly peraluminous compositions (ASI≈ 1.02) (Figs. 2A and 2B). In silicate Earth-normalised diagrams both type of rocks have negative anomalies in Ba Nb, Ta and Ti and positive anomalies in K and Pb. All the rocks are enriched in LREE relative to HREE: $La_N/Lu_N \approx$5.6-6.3 in MMEs and $La_N/Lu_N \approx$ 14.2-15.6 in granites; and flat or only slight negative Eu anomalies: $Eu/Eu^* \approx$0.8 in MMEs and $Eu/Eu^* \approx$1.1 in granites (Fig. 2C). These compositions are similar to those of high-K calc-alkaline supra-subduction magmas. Moreover, the isotopic composition of these rocks varies from $\varepsilon Nd_t \approx$0.22 and $^{87}Sr/^{86}Sr_t \approx$ 0.70537 in the MMEs to $\varepsilon Nd_t \approx$ -1.04 and $^{87}Sr/^{86}Sr_t \approx$0.70565 in the granites (Fig. 2D) with similar Nd model age *c*. 0.7 Ga in both rock types. Notably, the whole-rock composition of the intermingled zone and hybrid unit rocks from Wada et al. (2004) fit with a simple two end-member mixing model with 20% of MME and 80 % of granite (Figs. 2A-2D). Thus, it is supporting the importance of mingling/mixing processes in Kurobegawa Granite formation.

Thermobarometric estimations have been determined for the MMEs using the amphibole-plagioclase thermometer of Holland and Blundy (1994) and the amphibole-plagioclase barometer of Molina et al. (2015). In the 1-10 kbar pressure range, temperatures for the MMEs are 890-980ºC (95% c.i. 945±10 ºC, n=23) (Fig. 2E). For amphibole-plagioclase pairs estimated pressures vary from 0.4-1.2 kbar (95% c.i. 0.8±0.08 kbar, n=23) over a range of 900 to 1000ºC (Fig. 2E). These data suggest that the Kurobegawa Granite emplacement and subsequent intrusions of MMEs took place at *c*. 3 km depth.

The granite contains abundant zircons. These are colourless, transparent, euhedral, large bipyramid-terminated prisms with an average size of 175 μm x 75 μm (Fig. 2F). Under the cathodoluminescence microscope they are dark grey to pale grey, with a marked oscillatory zoning. Some cores have patchy texture with oscillatory zoned overgrown (Fig. 2F). Twenty-one measurements on 15 grains yielded medium to high concentrations of U (254-932 ppm) and Th (127-812 ppm) with Th/U = 1.1-3.0 and perceptible common lead (f^{206} 3-17%). They are, therefore, discordant. The discordia, however, is correctable yielding the weighted means (errors reported at 2σ) 207-corrected $^{206}Pb/^{238}U$ interval of 0.47-0.81 Ma with average of 0.64±0.04 Ma (95% c.i., n=21) (Fig. 2F). Significantly, older ages were found in patchy cores, whereas younger ages correspond to rims (Fig. 2F). Only one zircon was found in the MME small specimen that was big enough for SHRIMP analysis (Fig. 2F). It is colourless stubby, euhedral and equant to elongated bipyramidal prisms with a size of 400 μm x 300 μm (Fig. 2F). Cathodoluminescence images revealed patchy zonation (Fig. 2F). Three determinations in this grain yielded an age range of 207-corrected $^{206}Pb/^{238}U$ of 0.56-0.79 Ma (Fig. 2F).

The petrographic, mineral chemistry and whole-rock composition of the Kurobegawa Granite and coeval MMEs indicate in-situ complex mafic-felsic mingling/mixing processes. This process apparently took place at c. 0.6 Ma although the age range from core to rim detected in zircons 0.5-0.8 Ma agrees with variable zircon overgrowth episodes. Our results favour the model of multiple small-scale felsic intrusion over a period of 2 millions years rather than large magma chamber, as was proposed by Ito et al. (2013). In addition, the lower pressure emplacement conditions of the Kurobegawa Granite highlight the importance of magmatic intrusion in the Hida Mountain Range rapid uplift process.

References

Holland, T, Blundy, J. (1994). Non-linear interactions in calcic amphiboles and their bearing on amphibole-plagioclase thermometry. Contributions to Mineralogy and Petrology 116, 433-447.

Ito, H, Yamada, R, Tamura, A, Arai, S, Horie, K, Hokada, T. (2013) Earth's youngest exposed granite and its tectonic implications: the 10–0.8 Ma Kurobegawa Granite. Sci. Rep. 3, 1306.

Molina JF, Moreno JA, Castro A, Rodríguez C, Fershtater GB (2015) Calcic amphibole thermobarometry in metamorphic and igneous rocks: New calibrations based on plagioclase/amphibole Al-Si partitioning and amphibole/liquid Mg partitioning. Lithos 232:286–305.

Molina, JF, Scarrow, JH, Montero, P, Bea, F. (2009) High-Ti amphibole as a petrogenetic indicator of magma chemistry: evidence for mildly alkalic-hybrid melts during evolution of Variscan basic-ultrabasic magmatism of Central Iberia. Contributions to Mineralogy and Petrology 158, 69-98.

Wada, H, Harayama, S, Yamaguchi, Y (2004) Mafic enclaves densely concentrated in the upper part of a vertically zoned felsic magma chamber: The Kurobegawa granitic pluton, Hida Mountain Range, central Japan. Geological Society of America Bulletin 116, 788-801.

Diffusion-induced disturbances of the U-Th-Pb isotope system in zircon as consequence of thermal shock: a SHRIMP study in granitic enclaves hosted in SE Spanish lamproites

Cambeses, A, Montero, P, Scarrow, JH, Molina, JF and Bea, F

Department of Mineralogy and Petrology, University of Granada, Spain

What determines whether zircons are preserved in high-temperature systems is not yet well understood. The presence of pre-magmatic zircons in mantle-derived rocks (e.g., Pilot, 1998; Bea et al., 2001) is contradictory to their instability both at high-temperature and in high-solubility environments (Watson and Harrison, 1983). To evaluate this process it is essential knows the kinetics and diffusion

rates of zircon under disequilibrium conditions. Bea and Montero, (2013) modelled the diffusion of Pb^{2+}, U^{4+} and Th^{4+} in pre-magmatic zircons as a consequence of thermal shock. They considered the effect of a variation of isotopic ratios and, then, the causes of 'spurious' ages (Fig. 1A and B). In the present work, we evaluated the thermal shock effect in zircons from a natural laboratory of granitic enclaves found in lamproite dyke rocks from the SE Spain Neogene Volcanic Province (NVP).

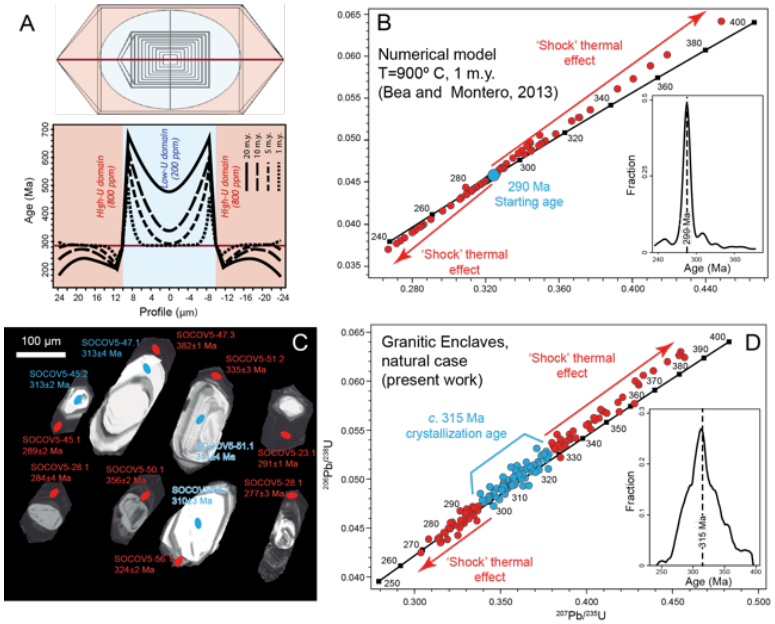

Figure 1. A) Numerical modelling of diffusion of a zircon with compositional domains as a consequence of thermal shock, note the age disturbance as a consequence of diffusion from high-U to low-U domains (modified from Bea and Montero, 2013). B) Wetherill Concordia plot showing the diffusion effect caused by thermal shock of a zircon with an age of 290 Ma (modified from Bea and Montero, 2013). C) Cathodoluminescence images and ages of representative analyzed zircons from the granitic enclaves of Socovos lamproites. D) Wetherill Concordia of SHRIMP data obtained from zircons from granite enclaves from Socovos lamproites. The probable age of these granites is c. 315 Ma.

The NVP is located in south-east Spain in the Betic Cordillera, it comprises a wide compositional range of magmatism: calc-alkaline; high-K calc-alkaline; lamproites; and alkali basalts (e.g., López-Ruiz and Rodríguez-Badiola, 1980). The Socovos fault ultrapotassic rocks are located in the north-west of the NVP and are mostly emplaced as dykes and minor volcanic edifices (Pérez-Valera et al., 2013). The easternmost dykes contain abundant granitic enclaves with variable size from metric to centimetric scales and rounded contacts. All the granitic enclaves have the same petrographic and compositional characteristics. They have remarkable partially melted textures that grade from rim to cores, although the enclaves have not disintegrated (Cambeses et al., accepted). Zircon is a common accessory phase in these granites in which it is typically shielded by large crystals of feldspar and quartz.

Granitic enclaves contain zircons with variable morphologies, although the main zircon population is prismatic, colourless, with sizes from 250 μm x100 μm to 150 μm x100 μm (Fig. 1C). Under the cathodoluminescence microscope, they show magmatic oscillatory zoning and, in general, compositional domains with low cathodoluminescent rims, high-U, and low-U cores (Fig. 1C). The U-Th-Pb data of 219 concordant SHRIMP analysis show a polymodal age distribution. Some *c.* 60 % the ages are Carboniferous, 270-390 Ma. These were obtained in oscillatory zoned grains, both cores and rims, which suggests a magmatic origin (Figs.1C and 1D). The rest of data are cores of *c.* 20 % Neoproterozoic, *c.* 615 Ma, and minor Mesoproterozoic, Paleoproterozoic and Archean zircons.

Carboniferous ages have a distribution spread along the Whetherill concordia plot. Two dispersive age trends are observed: i) the first shows a reverse discordia that reaches *c.* 385 Ma with the youngest interception at around *c.* 315 Ma (Fig. 1D); and ii) the second includes younger ages from *c.* 270 Ma to *c.* 310-320 Ma (Fig. 1D). In addition, these Carboniferous ages have a main cluster at *c.* 315 Ma (Fig. 1D). The *c.* 315 Ma age is typical of Variscan granites from the Central Iberian Zone (cf., Bea et al., 2003), which we suggest corresponds to the basement through which the lamproite magmas rose (Cambeses et al., accepted). The crystallisation age of the granitic enclaves, therefore, is *c.* 315 Ma (Fig. 1D). However, the wide age range detected in lamproite granitic enclaves does not correspond with basement granitoids from the Central Iberian Massif Zone (cf., Bea et al., 2003). This wide age

interval is apparently a consequence of diffusion-induced disturbances in the zircon U-Th-Pb isotopic system as a consequence of thermal-sock. This was induced by high temperature lamproite magmas, that, in the case of Socovos lamproites, reached *c.* 1200 ºC (Cambeses et al., submitted). Under these conditions the faster diffusion coefficient of Pb^{2+} relative to U4+ and Th^{4+} (cf., Cherniak , 2010) favours mobilization of Pb from higher to lower concentration domains. This effect modifies the zircon crystallization age resulting in a wide range of 'spurious' ages (Figs. 1C and 1D). Our observation of a natural example fits with the numerical modelling example of Bea and Montero (2013), of a shielded zircon with compositional domains (Figs. 1A, 1B and 1D). In agreement with these authors and considering that U concentrations in the analyzed zircons varies from high cathodoluminescent cores *c.* 250 ppm to less cathodoluminescent rims *c.* 15000 ppm (ratio *c.* 1/60) in a lamproite magma at a temperature of *c.* 1200 ºC less than one month was enough to generate the diffusion in the zircons.

The granite enclaves hosted in the Socovos lamproites provide a good natural case study to observe the diffusion processes caused by thermal shock in zircons. Our results highlight the importance of diffusion processes in zircons associated with high-temperature environments and how these result in 'spurious' ages in the main analyzed grains. As a result, in-situ U-Th-Pb determinations on zircons from high-temperature systems should be considered carefully when interpreting ages obtained.

References

Bea, F., Fershtater, G.B., Montero, P., Whitehouse, M., Levin, V.Y., Scarrow, J.H., Austrheim, H., Pushkariev, E.V., 2001. Recycling of continental crust into the mantle as revealed by Kytlym Dunite zircons, Urals Mounts, Russia. Terra Nova 13, 407-412.

Bea, F., Montero, P., 2013. Diffusion-induced disturbances of the U–Pb isotope system in pre-magmatic zircon and their influence on SIMS dating. A numerical study. Chemical Geology 349-350, 1-17.

Bea, F., Montero, P., Zinger, T., 2003. The nature and origin of the granite source layer of Central Iberia: evidence from trace element, Sr and Nd isotopes, and zircon age patterns. Journal of Geology 111, 579–595.

Cambeses, A., García-Casco, A., Scarrow, J.H., Montero, P., Pérez-Valera, L.A., Bea, F., submitted. Mineralogical evidence for lamproite magma mixing and storage at mantle depths: Socovos fault lamproites, SE Spain. Lithos.

Cambeses, A., Montero, P., Scarrow, J.H., Molina, J.F., Bea, F., accepted. Caracterización del basamento Bético: Un estudio U-Th-Pb SHRIMP en circones de enclaves graníticos Variscos incluidos en lamproítas de la Región Volcánica Neógena del sureste de España. Geotema.

Cherniak, D.J., 2010. Diffusion in accessory minerals: zircon, titanite, apatite, monazite and xenotime. Reviews in Mineralogy and Geochemistry 72, 827–869.

López-Ruiz, J., Rodriguez-Badiola, E., 1980. La región volcanica neogena del sureste de España. Estudios Geologicos 36, 5-36.

Pérez-Valera, L.A., Rosenbaum, G., Sánchez-Gómez, M., Azor, A., Fernández-Soler, J.M., Pérez-Valera, F., Vasconcelos, P.M., 2013. Age distribution of lamproites along the Socovos Fault (southern Spain) and lithospheric scale tearing. Lithos 180-181, 252-263.

Pilot, J., Werner, C.D., Haubrich, F., Baumann, N., 1998. Palaeozoic and Proterozoic zircons from the Mid-Atlantic ridge. Nature 393, 676-679.

Watson, E.B., Harrison, T.M., 1983. Zircon saturation revisited: temperature and composition effects in a variety of crustal magma types. Earth and Planetary Science Letters 64, 295-304.

SHRIMP zircon oxygen isotope composition as an indicator of mantle-crust interaction in the Ossa-Morena Zone, SW Iberia, Variscan magmatism: the Burguillos del Cerro plutonic complex

Cambeses, A, Scarrow, JH, Montero, P, Molina, JF and Bea, F

Department of Mineralogy and Petrology, University of Granada, Spain

Syn-orogenic igneous rocks record tectonomagmatic processes, providing information about mantle and crustal sources tapped during terrane accretion. Unpicking the components of hybrid magmas is the key to assessing the importance of mantle and crustal contributions. Throughout the European Variscan orogenic province mafic-intermediate 'calc-alkaline' stocks are common within granitoid

plutons (cf., Pitcher, 1993). However, the extent to which such magmas may be used as markers of tectonomagmatic context is a matter of some discussion. The most extensive expression of the Variscan province magmatism is the Iberian Massif. In the south of the massif, the Ossa-Morena Zone (OMZ) continental block, formed of Neoproterozoic to Carboniferous rocks, juxtaposed with the Central Iberian Zone (CIZ) and the South Portuguese Zone (SPZ) during the early Carboniferous.

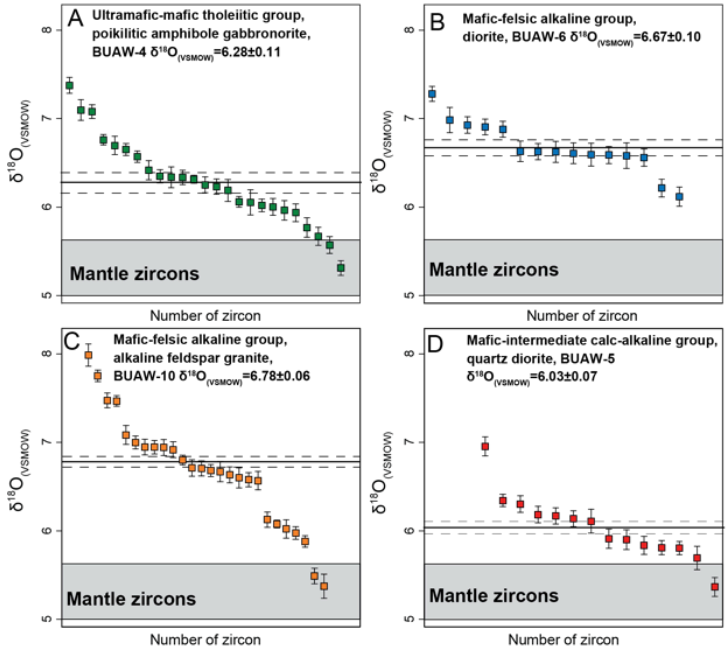

Figure 1. SHRIMP zircon oxygen isotope compositions of the Burguillos del Cerro plutonic complex: A) ultramafic-mafic tholeiitic group poikilitic amphibole gabbronorite, (BUAW-4). B) Mafic-felsic alkaline group diorite, (BUAW-6). C) Mafic- felsic alkaline group alkali feldspar granite, (BUAW-10). D) Mafic-intermediate calc-alkaline group quartz diorite, (BUAW-5).

The Variscan plutons in the OMZ have a broad compositional spectrum comprising gabbros and diorites through quartz diorites to granodiorites and granites. This suggests a complex interplay of magmas derived from mantle and crustal sources (cf., Casquet and Galindo, 2004, Cambeses et al., 2015). The Burguillos del Cerro plutonic complex crops out over an area of about 100 km^2 in the central part of the OMZ. It has a rounded morphology and comprises ultramafic-mafic, intermediate and subordinate felsic rocks (Pons, 1982; García-Casquero, 1995). The petrography, mineral chemistry and whole-rock composition permit classification of the Burguillos del Cerro plutonic complex rocks in four broad groups: i) ultramafic-mafic tholeiitic group; ii) mafic-felsic alkaline group; iii) mafic-intermediate calc-alkaline group and; iv) subordinate felsic peraluminous group (Cambeses, 2015). Notably, all of these compositionally varied plutonic rocks were coeval with a SHRIMP zircon U-Th-Pb age range of 336-338 Ma (Cambeses, 2015).

The SHRIMP zircon oxygen isotopes from the Burguillos del Cerro plutonic complex groups show heterogeneity and, thus, variable components of mantle and crust. The average magmatic zircon $\delta^{18}O_{(VSMOW)}$ values of the three main Burguillos groups are similar (Fig. 1): the ultramafic-mafic tholeiitic group 6.28 ± 0.11; the mafic-felsic alkaline group diorite 6.67 ± 0.10 and alkali feldspar granite 6.78 ± 0.06; and the mafic-intermediate calc-alkaline group 6.03 ± 0.07. However, a wide dispersion is observed in with grains having both low $\delta^{18}O_{(VSMOW)}$ of 5.31 ± 0.08 typical of mantle-derived zircons (cf., Valley, 2003) and higher $\delta^{18}O_{(VSMOW)}$ 7.99 ± 0.12 (Fig. 1).

The strong temporal and spatial relationships of the Burguillos del Cerro plutonic complex rock groups and their wide range of magmatic zircon O isotopic compositions reflects a change in the magma composition during zircon crystallisation. Three different magma sources have been identified in the Burguillos del Cerro Plutonic complex (Cambeses, 2015): two basic mantle-derived, the first alkaline from the lithosphere and the second tholeiitic from the asthenosphere, and a third crustal-derived acid peraluminous partial melt of OMZ basement metasediments. The oxygen isotope composition of the Burguillos del Cerro plutonic complex zircons resulted, we suggest, from variable contributions of mantle- and crustal-derived components during magma crystallisation.

Compositionally heterogeneous magmas mixed and crystallised leading to the formation of hybrid rocks.

The Carboniferous, Visean age, 336-338 Ma, determined for the Burguillos del Cerro plutonic complex decouples its formation from a subduction-related tectonomagmatic context. It was emplaced instead between two Variscan collisional events related to an intra-orogenic episode of extension/ transtension coeval with sedimentary basin development; high-temperature low-pressure metamorphism; and mid-crustal intraplating of ultramafic-mafic sills (e.g., Cambeses et al., 2015).

References

Cambeses, A., 2015. Ossa-Morena Zone Variscan 'calc-alkaline' hybrid rocks: interaction of mantle- and crustal-derived magmas as a result of intra-orogenic extension related intraplating. Ph.D. thesis, University of Granada, 478 p.

Cambeses, A., Scarrow, J.H., Montero, P., Molina, J.F., Moreno, J.A., 2015. SHRIMP U-Pb zircon dating of the Valencia del Ventoso plutonic complex, Ossa-Morena Zone, SW Iberia: middle Carboniferous extension-related 'calc-alkaline' magmatism. Gondwana Research 28, 735-756.

Casquet, C., Galindo, C., 2004. Magmatismo varisco y postvarisco en la Zona de Ossa-Morena. In: Vera, J.A., (ed.), Geología de España. Sociedad Geológica de España-Instituto Geológico Minero España, Madrid, 194-199.

García-Casquero, J.L., 1995. Intrusión múltiple y cuerpos ígneos politípicos: El Complejo Igneo de Burguillos del Cerro, un ‘macizo diorítico zonado’ en el Basamento Varisco de la Península Ibérica. Boletín Geolçógico y Minero 106, 379-398.

Pitcher, W.S., 1993. The Nature and Origin of Granite. Chapman and Hall, London, 321 p.

Pons, J., 1982. Un Modele d’evolution de Complexes plutoniques: Gabbros et Granitöides de la Sierra Morena Occidentale. Ph.D. thesis, University of Paul Salvatier Touluse, 451 p.

Valley, J.W., 2003. Oxygen isotopes in zircon. In: Hanchar, J.M., Hoskin, P.W.O. (eds), Zircon, Reviews in Mineralogy and Geochemistry, 53. Mineralogical Society of America/Geochemical Society, Washington, DC, 343-385.

Sedimentary provenance of the southern Paraná Basin based on U-Pb geochronology, and O and Hf isotopes on detrital zircons

Canile, FM[1], Babinski, M[1], Rocha-Campos, AC[1] and Fanning, CM[2]

1: Instituto de Geociências, Universidade de São Paulo, São Paulo, Brazil.
2: Research School of Earth Sciences, Australian National University, Canberra, Australia.

The Paraná Basin is the largest Gondwanan sedimentary basin in South America, it comprises about 1.4 million km^2 and its rocks can be found in Brazil, Argentina, Uruguay and Paraguay. The studied area in Santa Catarina, Brazil, is an outcrop called the “White Column”, since these rocks were first studied by Israel C. White in 1908, and the place is known as the Classic Geologic Section of the Gondwana Continent in Brazil. The section includes sedimentary rocks from late Paleozoic-early Mesozoic units from Paraná Basin, named from base to top: Rio do Sul Formation, Rio Bonito Formation (Triunfo, Paraguaçu and Siderópolis members), Palermo Formation, Irati Formation, Serra Alta Formation, Teresina Formation, Rio do Rasto Formation (Serrinha and Morro Pelado members) and Botucatu Formation. U-Pb, O and Hf isotope data were obtained from detrital zircons from these eleven units in order to constrain the provenance of the sediments, as well as to contribute to the understanding of the evolution of the basin.

U-Pb ages determined on 2350 detrital zircon grains range from 242 Ma to 3.4 Ga, and among them 1941 grains below discordance filters (±10%) were used to construct relative probability diagrams for the studied units (Figure 1). O isotopic compositions were obtained on the same U-Pb spots of 242 zircons grains that were representative of the main age populations. Following the O isotopic analyses (Figure 2), Hf isotopic measurements were carried out on the same zircon grains and other ones, totalizing 417 grains analysed for Hf (Figure 3). These analyses allowed us to identify sources with the same U-Pb ages but different isotopic signatures suggesting they come from different terranes.

The lowermost basal unit (Rio do Sul Formation) show only the four main detrital age groups (Figure 1), Neoarchean (2.7-2.5 Ga), mid-Paleoproterozoic (2.0-1.8 Ga), Grenvillian (1.1-0.9 Ga) and Brasiliano (850-490 Ma), that are present in all the studied units and that reflect the importance of the Precambrian basement bordering the east side of the basin, such as Dom Feliciano, Kaoko and Namaqual-Natal belts as source areas. The data confirm previous studies (e.g. Bigarella at al., 1967) that point out to an ice cap located to the west in the African side bringing detritus to the basin from SSE to NNW. However, some Grenvillian grains present O and Hf isotopic signatures that point to a crustal filiation, which suggest that part of them could be from rocks located in Argentina and not only from Africa that presents juvenile Grenvillian rocks. These detritus were able to travel long distances probably due the paleogeographic links between the Phanerozoic Basins of the West Gondwana (Limarino and Spalletti, 2006). A few grains of ~2.0 Ga present isotopic signatures that indicate a juvenile filiation and that have no compatibility with any source described in the literature. As the proportion of these grains decreases along the section, they were interpreted as part of the local basin basement, a cratonic block that was uplifted during the early deposition stages of the section (Rio do Sul and Rio Bonito Formations) and subsequently eroded or covered by sediments from the overlying units. This hypothesis is supported by data from Holz et al. (2006) which show that a huge source area was uplifted in the Santa Catarina area and from Milani et al. (1998) proposition of more than one cratonic block forming the basement of the Paraná Basin.

The uppermost unit of the Rio Bonito Formation, Siderópolis Member, shows an important change in the source of detritus since it contains a Permian age-peak (290-266 Ma) that persists towards the top of the section (Figure 1). Despite the Choiyoi Group being pointed as the main source of Permian zircons observed in the Paraná Basin (e.g. Rocha-Campos et al., 2011, Sato et al., 2015), our isotopic data together with the study of the shape of these zircons show that other West Gondwana Permian rocks from Argentina, particularly from the North Patagonian Massif, could also be possible sources. These zircons probably reached the studied area by the process of erosion of these Permian terranes and the subaquatic transport of the debris over long distances (rounded grains) and not only from the air through volcanic ash falls (prismatic grains).

It is also from the Siderópolis Member to upsection that Ordovician to Carboniferous zircon grains with crustal isotopic signatures that connect them to sources from Argentina, such as the Sierras Pampeanas and Famatiano Belt, become abundant, showing that the proximal source areas (Precambrian) are no longer the main source of sediments to the basin. This is confirmed by the data from Milani and Ramos (1998) that show a regional onlap from the south to north for the Rio Bonito and Palermo Formations. This characteristic persists at least until the deposition of the Rio do Rasto Formation, when the material begins to be reworked.

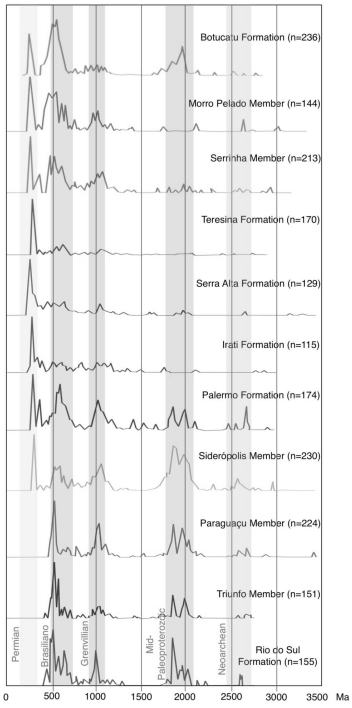

Figure 1 – Probability curves of detrital zircon ages from the Paraná Basin.

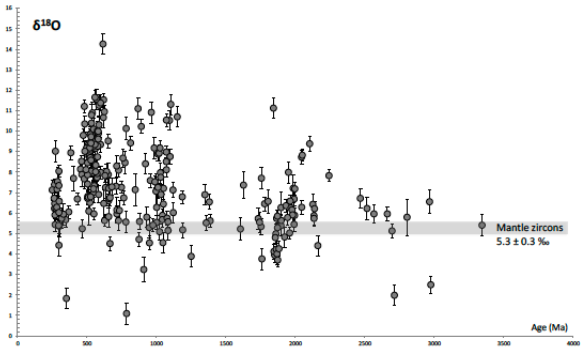

Figure 2 – Age versus $\delta^{18}O$ diagram for the detrital zircons from the Paraná Basin.

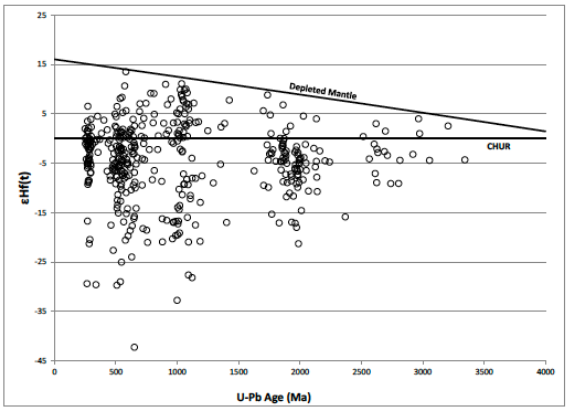

Figure 3 – Age versus Ɛ Hf(t) diagram for the detrital zircons from the Paraná Basin.

References

Bigarella, JJ, Salamuni, R, Fuck, RA. (1967) Striated surfaces and related features developed by Gondwana ice sheets (State of Paraná, Brazil). Palaeogeography, Palaeoclimatology, Palaeoecology 3, 265-276.

Holz, M, Küchle, J, Philipp, RP, Bischoff, AP, Arima, N. (2006.) Hierachy of tectonic control on stratigraphic signatures: Base-level changes during the Early Permian in the Paraná Basin, southernmost Brazil. Journal of South American Earth Sciences 22, 185-204.

Limarino, CO, Spalletti, LA. (2006) Paleogeography of the upper Paleozoic basins of southern South America: An overview. Journal of South American Earth Sciences 22, 134-155.

Milani, EJ, Faccini, UF, Scherer, CM, Araújo, LM, Cupertino, JA. (1998) Sequences and stratigraphic hierarchy of the Paraná Basin (Ordovician to Cretaceous), Southern Brazil. Geologia USP-Série Científica 29,125-173.

Milani, EJ, Ramos, VA. (1998) Orogenias paleozoicas no domínio sul-ocidental do Gondwana e os ciclos de subsidência da Bacia do Paraná. Revista Brasileira de Geociências, 28(4), 473-484.

Rocha-Campos, AC, Basei, MAS, Nutman, AP, Kleiman, LE, Varela, R, Llambias, E, Canile, FM, da Rosa, OCR. (2011) 30 million years of Permian volcanism recorded in the Choiyoi igneous province (W Argentina) and their source for younger ash fall deposits in the Paraná Basin: SHRIMP U-Pb zircon geochronology evidence. Gondwana Research 19, 509-523.

Sato, AM, Llambías, EJ, Basei, MAS, Castro, CE. (2015) Three stages in the Late Paleozoic to Triassic magmatism of southwestern Gondwana, and the relationships with the volcanogenic events in coeval basins. Journal of South American Earth Sciences 63, 48-69.

White, IC. (1908) Final report of Dr. I. C. White, chief of the Brazilian Coal Commision: July 1st, 1094 to May 31st, 1906. Imprensa Nacional, Rio de Janeiro, CPRM, 617p.

History of SHRIMP Development-A Personal Perspective

Clement, SWJ

Ion Optical ConsultingPrince Edward Island, Canada

Based on the personal recollections of the author, the origins of the first SHRIMP instrument at the Australian National University will be described and the factors which determined the initial design will be outlined. The course of the actual design and construction will be followed in a somewhat anecdotal fashion. The author will then go on to describe the subsequent construction of SHRIMP II and the decision to begin building and marketing the instruments commercially, along with the development of various options such as the Multiple Collector and the Cesium ion source. The design and construction of the two specialised instruments built at the Research School of Earth Sciences, the SHRIMP RG and the SHRIMP SI, will also be discussed briefly.

Data reduction beyond Excel 2003: Challenges and opportunities for the SHRIMP community

Cross, A[1], Bodorkos, S[1], Bowring, J[2], Main, P[1], Sircombe, K[1] and Magee, C[1]

1: Resources Division, Geoscience Australia, GPO Box 378, Canberra, ACT 2601, Australia
2: Department of Computer Science, College of Charleston, Charleston, South Carolina, USA

The advent (in 1999) of the Microsoft Excel-based SQUID software for SHRIMP data reduction, written by Ken Ludwig (formerly of the Berkeley Geochronology Center), revolutionised work practices and (in conjunction with its companion add-in ISOPLOT) data-reporting for the majority of SHRIMP laboratories. “SQUID 1” was followed in 2009 by SQUID 2.50, developed in response to community demand for a more flexible data processing tool, capable of processing extended run tables, and implementing customised and/or complex data reduction procedures. The Task feature was a particularly important innovation, allowing researchers to develop and easily share their data reduction routines.

Unfortunately, SQUID 2.50 is dependent on Excel 2003, which (as of April 2015) is no longer supported by Microsoft. An attempt to upgrade SQUID 2.50 to a newer version of Excel failed due to a wide variety of factors well beyond the “debugging” of code, including security enhancements and fundamental changes to the Excel object-model post-2003. Nevertheless, the methodology and arithmetic underpinning SQUID 2.50 is fundamentally sound (as indicated, for example, by comparisons between SHRIMP and CA-IDTIMS U–Pb results on well characterised zircons), and the widespread acceptance and uptake of SQUID 2.50 has led Geoscience Australia (GA) to collaborate with the College of Charleston’s Cyber Infrastructure Research and Development Lab for the Earth Sciences (CIRDLES) in working toward redeploying SQUID 2.50 methodology and arithmetic in an open-source, platform-independent environment. It is hoped that this work will provide the foundation for future advances in SHRIMP data processing.

The ID-TIMS community pioneered open-source, platform-independent, U–Pb data reduction via UPb_Redux (now named ET_Redux). This software was developed in collaboration with CIRDLES, and has been cited in 194 journal articles to date. Recently, the LA-ICP-MS U–Pb community has also developed open-source data reduction software using ET_Redux. Working with CIRDLES to redeploy SQUID 2.50 into ET_Redux will significantly strengthen ties with the ID-TIMS and LA-ICP-MS U–Pb communities, and provide a much stronger foundation for inter-comparison of data-reduction protocols between techniques.

Nonetheless, significant challenges remain. Although it has been open-source since 2009, the SQUID 2.50 code is largely undocumented, and has proven difficult to unravel to the point of re-implementation. GA and CIRDLES have made some promising initial progress in this regard, which will be described and demonstrated at this Workshop. However, delivery of a production replacement for SQUID 2.50 is several years away at the current rate of progress and resourcing. More timely completion of this project will require strong support and investment from the wider SHRIMP community.

Looking for a new calcite reference for SHRIMP isotope analyses: preliminary data

Czupyt, Z and Wierzbowski, H

Polish Geological Institute – National Research Institute, Warszawa, Poland

Oxygen and carbon isotope compositions of calcite microfossils or high-resolution isotope traverse sections through calcite macrofossils may be measured using an ion microprobe. High analytical accuracy and precision of the ion microprobe isotope measurements can be established by repeated analyses of isotopically homogenized calcite references. Unfortunately, commercially available calcite references are not tested for the isotope homogeneity in the microscale and specific references used for the microprobe analyses (as UWC-3 or Mex; cf. Rollion-Bard et al., 2007; Kozdon et al., 2009) are prepared in small amounts only.

In order to find a new calcite reference material for ion microprobe analyses we have tested, using a SHRIMP IIE/MC device, housed in the Polish Geological Institute – National Research Institute in Warsaw, oxygen isotope homogeneity of three commercially available calcite isotope standards (NBS 18, NBS 19, and IAEA-CO-1) provided by IAEA, and have compared they to the UWC-3 ion microprobe reference (see Table 1). We have also compared $\delta^{18}O$ values of two skeletal, fossil calcites (OK1 – Kimmeridgain oyster shell from central Poland, and BRT8 – Kimmeridgian belemnite rostrum from the Russian Platform) measured by SHRIMP microprobe during multiple calibrations to different standards.

All the references are made of natural marbles. Several small grains of each reference, along with small fragments of two skeletal calcite samples were placed in the centre of the standard SHRIMP II mount (diameter of 35 mm) and carefully polished. A 15kV, 9 nA Cs^+ primary beam was focused to 20 µm spot on the target producing a ~200 nA secondary beam. O^{16-} and O^{18-} were measured simultaneously on Faraday cups. An additional ~330 eV electron beam was used to neutralize surface charging.

Table 1. Isotope data of calcite references tested

Calcite reference	Mean $\delta^{18}O$ – reference values	Mean $\delta^{18}O$ – microprobe analyses	Number of microprobe analyses of $\delta^{18}O$	Standard deviation of microprobe analyses of $\delta^{18}O$
NBS 18	-23.20‰ VPDB	-23.19‰ VPDB	28	0.27
NBS 19	-2.20‰ VPDB	-2.19‰ VPDB	22	0.26
IAEA-CO-1	-2.40‰ VPDB	-2,40‰ VPDB	26	0.19
UWC-3	-17.82‰ VPDB	-17.83‰ VPDB	26	0.29

Our preliminary results have indicated medium oxygen isotope homogeneities of NBS 18 and NBS 19 references. The same applies to an available portion of UWC-3 standard, provided by J. Valley (Table 1). IAEA-CO-1 reference is characterized by much better oxygen isotope homogeneity. The IAEA-CO-1 reference may, therefore, be used for oxygen isotope analyses of calcites in the Micro-area Analysis Laboratory of the Polish Geological Institute – National Research Institute until a new reference characterized by high internal homogeneities of both oxygen and carbon isotope signals is selected and tested.

Multiple oxygen isotope analyses of two natural calcites and calcite references have revealed the presence of small to moderate differences in measured $\delta^{18}O$ values during calibration to different references applied (Table 2). This points to the importance of the selection of an appropriate reference material for the ion microprobe analyses of oxygen isotope composition of calcareous fossils.

Table 2. Oxygen isotope data of skeletal calcites tested

Calcite	Reference, $\delta^{18}O$ (standard phosphoric acid method)	Mean $\delta^{18}O$ (calibration to NBS 18)	Mean $\delta^{18}O$ (calibration to NBS 19)	Mean $\delta^{18}O$ (calibration to IAEA- CO-1)	Mean $\delta^{18}O$ (calibration to UWC-3)	Number of micro-probe analyses
OK1	*-2.29‰** VPDB	-2.33	-2.50	-2.56	-2,36	8
BRT8	*-1.74‰** VPDB	-3.24	-3.50	-3.52	-3.30	10
NBS 18	-23.2‰ VPDB	-	-23.02	-23.04	-23.14	28
NBS 19	-2.20‰ VPDB	-1.90	-	-2.21	-1.97	22
IAEA-CO-1	-2.4‰ VPDB	-2.11	-2.50	-	-2.17	26
UWC3	-17.82‰ VPDB	-17.85	-17.81	-17.82	-	26

** $\delta^{18}O$ values of two fragments of skeletal calcities measured by means of phosphoric acid and microprobe methods may have differed originally due to internal inhomogeneity of the samples.*

Acknowledgement

We are grateful to John Valley for kind providing a small amount of UWC-3 ion microprobe reference material of the University of Wisconsin-Madison (USA) and to Stanisław Hałas from the University of Maria Curie-Skłodowska in Lublin (Poland) for providing IAEA CO 1 and NBS-19 standard materials.

References

Kozdon, R, Ushikubo, T, Kita, NT, Spicuzza, Valley, JW. (2009) Intratest oxygen isotope variability in the planktonic foraminifer *N. pachyderma*: Real vs. apparent vital effects by ion microprobe. Chemical Geology 258, 327–337.

Rollion-Bard, C, Mangin, D, Champenois, M. (2007) Development and application of oxygen and carbon isotopic measurements of biogenic carbonates by ion microprobe. Geostandards and Geoanalytical Research 31, 39–50.

Metasomatic zircon growth under granulite-grade conditions: some examples

Dunkley, DJ[1,2,3], Hiroi, Y[4], Harlov, DE[5], Shiraishi, K[3] and Motoyoshi Y[3]

1: Institute of Geological Sciences, Polish Academy of Sciences, Warsaw, Poland; daniel.dunkley@twarda.pan.pl
2: Department of Applied Geology, Curtin University, Perth, Western Australia
3: National Institute of Polar Research, Tachikawa, Japan
4: Chiba University, Chiba, Japan
5: GeoForshungsZentrum, Potsdam, Germany

Zircon modification and production in granulite-grade terranes, is most commonly attributed to reactions occurring at peak or post-peak temperature conditions, typically in association with partial melting and/or the crystallisation of anatectic melt. Although this is the case in many instances, the effects on zircon of metasomatic processes, either on the micro-scale with the diffusion of elements between rocks of differing composition, or on the micro- to macro-scale with the infiltration of fluids from external sources, can be observed in atypical petrological associations. Here we present three case studies where zircon growth in metasomatic assemblages provides new perspectives on processes during high-grade metamorphic events.

1) Units of dolomite-calcite marble gneiss in the Ediacaran-Cambrian Lützow-Holm Complex of eastern Dronning Maud Land, east Antarctica contain extensive development of coarse scapolite-diopside skarn where adjacent to felsic charnokitic gneiss, and in desilicated ‘xenoliths’ (Satish-Kumar et al., 2006). Zircon dissolution and growth during fluid-driven skarnification is demonstrated by internal replacement of pre-existing zircon crystals and

neoblastic zircon growth interstitial to phlogopite in metasomatic rinds on 'xenoliths'. Multiple discrete times of growth indicate repetition of fluid-driven processes during an extended period of high-temperature metamorphism (Dunkley, 2010).

2) In the highest-grade section of the Lützow-Holm Complex, post-high strain tectonic activity includes the emplacement of weakly-deformed dismembered veins of clinopyroxenite across gneissic lithologies (Motoyoshi and Ishikawa, 1997). Although the veins have been interpreted as mafic dykes, mineralogy reflects compositions controlled by host lithologies rather than basaltic magma. Where veins intersect felsic lithologies, they are thin and discrete, whereas veins across graphite-sulphide-rich metapelitic gneiss 'blow-out' to clinopyroxenite-pyrite pegmatite produced by metasomatism in association with oxidising fluids. Zircon from this pegmatite mostly consists of a generation of equant neoblastic grains and rims, with an age that slightly postdates the dominant growth of metamorphic zircon in host gneisses.

3) The amphibolite-grade to granulite-grade transition in the southern margin of the East Dharwar Craton of peninsula India involves widespread charnockitisation of granitoid gneisses at the end of the Archean. Zircon modification and growth proceeds in multiple stages, with earlier stages having compositions and textures commonly found in amphibolite-grade to granulite-grade felsic gneisses, but later stages in the highest-grade gneisses being associated with terrane-wide depletions in U, Th, REEs and other elements. These depletions have been variably attributed to melt extraction or infiltration of oxidising brines from lower crustal sources (Harlov et al., 2015).

References

Dunkley, DJ. (2010) Textural Diagnosis of Zircon Re-equilibration by Fluids and Melts during high-T Metamorphism. Goldschmidt 2010, Geochimica et Cosmochimica Acta, 74(11) Supp. 252.

Harlov, DE, Dunkley, DJ, Hansen, E, Ishwar-Kumar, C. (2015) Zircon Trace Element Chemistry as a Function of Metamorphic Grade along a Traverse of Lower Archean Crust, Shevaroy Block, Southern India. Goldschmidt Abstracts, 2015, 1183.

Motoyoshi, Y, Ishikawa, M. (1997) Metamorphic and structural evolution of granulites from Rundvågshetta, Lützow-Holm Bay, East Antarctica. In: Ricci CA (ed.) The Antarctic Region: Geological evolution and processes, Terra Antarctic Publications, 65-7.

Satish-Kumar, M, Motoyoshi, Y, Suda, Y, Hiroi, Y, Kagashima, S. (2006) Calc-silicate rocks and marbles from Lützow-Holm Complex, East Antarctica, with special reference to the mineralogy and geochemical characteristics of calc-silicate mega-boudins from Rundvågshetta. Polar Geosci., 19, 37-61.

Suffering zircon from a Variscan lower crustal environment: U-Pb ages and oxygen isotopic compositions in mafic and felsic granulites from the Serre Massif (Calabria, Italy)

Fiannacca, P[1], Williams, IS[2], Cirrincione, R[1] and Hegner, E[3]

1: Department of Biological, Geological and Environmental Sciences, University of Catania, Italy
2: Research School of Earth Sciences, The Australian National University, Australia
3:Department of Earth and Environmental Sciences, Ludwig-Maximilians-Universität München, Germany

Metagabbros from the base of a near-complete cross section of Variscan continental crust, in the Serre Massif (Calabria-Peloritani Orogen, southern Italy; Cirrincione et al., 2015), have long been considered to be layered intrusions of latest Neoproterozoic age, metamorphosed under granulite-facies conditions at the end of the Variscan Orogeny. Previous dating of the granulitic metagabbros provided reliable ages of ~300-290 Ma for late Variscan metamorphism, but less convincing ages of ~593-564 Ma for the original mafic magmatism (Schenk & Todt, 1989; Micheletti et al., 2008; Fornelli et al., 2011). Peak P-T conditions for the metagabbros are ~1.1 GPa at ~ 900°C (Acquafredda et al., 2008), corresponding to a typical MP/HT granulite-facies lower crustal environment. Constraining the crystallization age of the original magma body is important to confirm or disprove earlier suggestions that late Precambrian magmatism played an important role in the formation of peri-Gondwana crust in

the southern Calabria-Peloritani Orogen (e.g., Fiannacca et al., 2013). This inference is contrasted by evidence for Permian and Triassic ages for similar gabbroic intrusions in northern Calabria (Liberi et al., 2011). Furthermore, the Serre Massif is well known to share many similarities with the Ivrea crustal section (southern Alps), where a Permian event led to magmatic underplating of a Mafic Complex in the lower crust and intrusion of granites in the upper crust (e.g., Sinigoi et al., 2010). Different ages for the gabbro protolith have different implications for the role of mafic components in the formation of the granitoids of the Serre Batholith which form the middle to upper portions, c. 13 km thick, of the crustal section exposed in the Serre Massif (Fiannacca et al., 2015; in press). This role might be either old mafic crust undergoing partial melting and forming I-type, geodynamically unrelated granitoids, or late Palaeozoic mantle-derived mafic magma, mixing with coeval crustal melts, or triggering partial melting as underplated magmas at the base of the crust.

Most of the zircon grains from a basal metagabbro appear to be either metamorphic or older grains with metamorphic rims. SHRIMP U-Pb dates have a wide range from ~3.2 Ga to ~270 Ma. The majority of the older cores yield ~720–450 Ma, the youngest of which possibly placing an upper limit on the age of magmatism. The maximum age for the metamorphism is ~313 Ma. All of the metamorphic zircons have high $\delta^{18}O$ values (9.3–10.6‰), indicating crystallization in the presence of sediment-derived fluids. Older zircon cores have lower $\delta^{18}O$ values (6.1–9.2‰), of which only three are <7.5‰. There is no evidence for primary zircon crystallized from a mantle-derived magma. Instead, the oxygen isotopes have a strong sediment signature, consistent with the large amount of detrital zircon in the sample. The εNd value of the metagabbro, calculated at 290 Ma, is -2.1, falling in the reported range of -0.9 to -3.4 for similar rock samples (Caggianelli et al., 1991); the values calculated for 550 Ma range from -0.8 to -2.4, suggesting a high degree of older crust in the mantle-derived magma. The O and Nd isotopic signature of the metagabbro might therefore indicate that prolonged residence of a sediment-'contaminated' mafic magma in the deep crust has largely modified the zircon $\delta^{18}O$ and some U-Pb dates, making it hard to determine the gabbro emplacement age. If the ~450 Ma zircon age is that of a detrital zircon, however, the gabbro magmatism must be younger.

This hypothesis has been tested by studying two samples of felsic granulites hosting the metagabbro with the aim of defining the depositional ages of the arenitic protoliths and, therefore, to place constraints on the maximum emplacement age of the original gabbros. The U-Pb analyses of zircon grains from the felsic granulite samples show that prolonged residence under lower crustal conditions has resulted in significant migration and clumping of the radiogenic Pb, more so than in the metagabbro, despite the metamorphic conditions being in the range of common granulite-facies metamorphism. The metamorphic zircon, in contrast, shows no evidence for such migration, suggesting that it is newly grown, not older zircon recrystallised. Both samples give a metamorphic age of ~300 Ma. Because of the Pb mobilisation, the ages of the detrital zircon cores cannot be determined reliably. In one of the felsic granulite samples, however, the youngest cores are ~400 Ma, providing a best estimate for the maximum depositional age of the arenite protoliths, and supporting the conclusion that the gabbro is not of Precambrian age, but rather ~400 Ma or younger.

Previous cases of zircon "suffering" like that from the Serre lower crust have been reported from older rocks from more extreme crustal environments, such those affected by UHT metamorphism. Why the relatively young zircon from the Calabrian lower crust has been so strongly affected by intracrystalline redistribution of radiogenic Pb has yet to be determined.

References

Acquafredda, P, Fornelli A, Piccarreta, G, Pascazio, A. (2008) Multi-stage dehydration-decompression in the metagabbros from the lower crustal rocks of the Serre (southern Calabria, Italy). Geological Magazine 145, 397-411.

Caggianelli, A, Del Moro, A, Paglionico, A, Piccarreta, G, Pinarelli, L, Rottura, A. (1991). Lower crustal granite genesis connected with chemical fractionation in the continental crust of Calabria (southern Italy). European Journal of Mineralogy 3, 159-180.

Cirrincione, R, Fazio, E, Fiannacca, P, Ortolano, G, Pezzino, A, Punturo, R. (2015) The Calabria–Peloritani Orogen, a composite terrane in Central Mediterranean; its overall architecture and geodynamic significance for a pre-Alpine scenario around the Tethyan basin. Periodico di Mineralogia 84 (3B), 701–749.

Fiannacca, P, Williams, IS, Cirrincione, R, Pezzino, A. (2013) The augen gneisses of the Peloritani Mountains (NE Sicily): granitoid magma production during rapid evolution of the northern Gondwana margin at the end of the Precambrian. Gondwana Research 23, 782–796.

Fiannacca, P, Cirrincione, R, Bonanno, F, Carciotto, MM. (2015) Source-inherited compositional diversity in granite batholiths: the geochemical message of Late Paleozoic intrusive magmatism in central Calabria (southern Italy). Lithos 236-237, 123–140.

Fiannacca P, Williams IS, Cirrincione R. (in press) Timescales and mechanisms of batholith construction: constraints from zircon oxygen isotopes and geochronology of the late Variscan Serre Batholith (Calabria, southern Italy). Lithos.

Fornelli, A, Langone, A, Micheletti, F, Piccarreta, G. (2011) Time and duration of Variscan high temperature metamorphic processes in the south European Variscides: constraints fromU–Pb chronology and trace element chemistry of zircon. Mineralogy and Petrology 103, 101–122.

Micheletti, F, Fornelli, A, Piccarreta, G, Barbey, P., Tiepolo, M. (2008) The basement of Calabria (southern Italy) within the context of the Southern European Variscides: LA-ICPMS and SIMS U–Pb zircon study. Lithos 104, 1–11.

Schenk, V, Todt, W. (1989) The age of the Adriatic crust in Calabria (southern Italy): constraints from U–Pb zircon data. Terra Abstracts 1, 350.

Sinigoi, S, Quick, JE, Demarchi, G, Peressini, G. (2010). The Sesia magmatic system. Journal of the Virtual Explorer 36, 1-33.

Why SHRIMP IV?

Foster, JJ [1], Clement, S[2]

1: Australian Scientific Instruments, Australia
2: Ion Optical Consulting, Crapaud, PEI Canada

Following the success of SHRIMP SI, a commercial variant of the instrument, SHRIMP IV has been designed. SHRIMP SI has been improved in its performance by the persistence of Peter Holden in locating sources of secondary ion instability and this information was taken into account when designing SHRIMP IV. Stephen Clement did the ion optical redesign of the primary and secondary columns on advice regarding problems encountered in SHRIMP SI.

The new instrument has features that are not currently available in SHRIMP SI.

The source chamber has been redesigned completely so that both the primary and secondary columns are supported on optical benches as in SHRIMP II rather than being located by the chamber walls.

The chamber is not a single block of stainless steel as in SHRIMP SI but has a removable lid to allow easy access for maintenance and troubleshooting.

The instrument incorporates a new sample stage that uses Smarac motors instead of in vacuum steppers. The new stage is self-indexing and has been shown to be highly reproducible in position and can be moved very rapidly. There is virtually no gas load from the piezo linear motors.

The primary column can be used with both positive and negative ion sources.

Provision for scanning the primary beam across a target and for depth profiling has been incorporated into the new design.

SolidWorks has been used to model the entire source so that working drawings for the instrument can be produced.

No changes have been made to the ESA or magnet, but the single collector can be replaced by the ASI built AMC (advanced multicollector).

Geochronological Constraints on the Exhumation and Emplacement of Subcontinental Lithospheric Mantle Peridotites in the Westernmost Mediterranean

Garrido, CJ

Instituto Andaluz de Ciencias de la Tierra (IACT), CSIC-UGR, Granada, Spain

Exhumation of subcontinental mantle peridotite in the Western Mediterranean has been attributed to different tectonic processes including pure extension, transpression, or alternating contractive and extensional processes related with continental subduction followed by extension, before final their contractive intracrustal emplacement. Any model trying to explain the exhumation and emplacement of subcontinental lithospheric mantle peridotites in the westernmost Mediterranean should take into account the available geochronological constraints, as well as the petrological and geochemical processes that lead to internal tectono-magmatic zoning so characteristic of the Betic and Rif orogenic peridotites.

Different studies have suggested a Hercynian, Cenozoic-Mesozoic or an Alpine age for the late tectono-magmatic evolution and intra-crustal emplacement of Betic-Rif peridotites. The pervasive presence of Mesozoic U-Pb zircon ages in Ronda UHP and HP garnet pyroxenites does not support a Hercynian age for the intracrustal emplacement of the peridotite. A hyper-extended margin setting for is in good agreement with the Jurassic extensional event that pervasively affected ALKAPECA terrains (i.e. the Alboran, Kabylides, Peloritani, and Calabria domains) in the western Mediterranean due to the opening of the Piemonte-Ligurian Ocean. However, a Jurassic age and a passive margin tectonic setting do not account, among other observations, for the late Miocene thermochronological ages recorded in zircons rims (U-Pb) and garnets (Lu-Hf) in garnet pyroxenites from the Betic-Rif peridotites, the pervasive Miocene resetting of U-Pb zircon and monazite ages in the overlying Jubrique crustal section, the supra-subduction radiogenic signature of late pyroxenite intrusive dikes in the Ronda peridotite, and the arc tholeiitic affinity of late mantle-derived, gabbroic dykes intruding in the Ronda and Ojen plagioclase lherzolites. These data are more consistent with a supra-subduction backarc setting for the Paleocene Alpine evolution of the Alboran peridotite massifs due to slab rollback in the westernmost Mediterranean.

Several geodynamic models have proposed initial south directed migration of the orogenic arc in a more easterly position (south of the Balearic Islands) during the Paleogene before the closure of the Paleo-Tethys Ocean and collision with the Algerian margin. This early emplacement for the Ronda Peridotite (approx. 25-23 Ma) in such an easterly position would provide a common origin for the peridotite bodies found in the Kabylies in Algeria, and in the Betics-Rif. We propose that after thinning and extension in a back-arc setting recorded in the Ronda spinel tectonite domain and the recrystallization front, the final Miocene exhumation of Ronda Peridotite is associated with early folding and later but probably synkinematic shearing of the SCLM in a contractive geodynamic setting. This process is recorded in the low-pressure plagioclase tectonite domain of the Ronda peridotite and the supra-subduction bonititic affinity of late intrusive pyroxenites.

Mineralogy of the high-latitude bryozoans from the Admiralty Bay (King George Island, South Shetland Islands), Antarctica

Hara, U and Jasionowski, M

Polish Geological Institute-National Research Institute, Warsaw, Poland

Glacjal fjordic bryozoan community from the Admiralty Bay (King George Island, South Shetland Islands, Antarctica) dominated by the ascophoran neocheilostomes of umbunulomorphs of *Arachnopusia aviculifera*, *Inversiula nutrix*, *Cellarinella watersi*, *Cellarinella nutti*, and lepraliomorphs of *Smittina obicullata*, *Osthimosia* sp., schizoporellid of *Isoschizoporella similis*, phidoloporoid of the *Reteporella frigida*, hippothoomorph of *Celleporella Antarctica*, anasciform flustrines of aspidostomatid of the *Larvopora mawsoni* and cellarioid of the *Cellaria aurorae* have been chosen for the detailed mineralogical studies (Hara et al. 2010, see also Pabis et al. 2014). The analyzed samples derived from the different parts of the Admiralty Bay (King George Island, South Shetland Islands) within the range of the depths of 15 to 280 meters.

All the cheilostome bryozoan skeletons belonging to Flustrina, Umbonulomorpha and Lepraliomorpha from the Admiralty Bay are composed of intermediate magnesium calcite (IMC) of the Mg content ranges from ca 4.3 to 6.5 wt% $MgCO_3$. It should be noted that the previously published data on mineralogy and elemental geochemistry of Antarctic bryozoan skeletons showed that Antarctic bryozoans are composed of low magnesium calcite (LMC) with the average mol% $MgCO_3$ content as low as 1.9 % (ca. 1.6 wt% $MgCO_3$) see Borisenko & Gontar (1991, *fide* Kuklinski & Taylor, 2008. For comparison the late Ypresian Antarctic fossil flustrines represented by free-living bryozoans belonging to Lunulitidae and Otionellidae (*Lunulites* and *Otionellina*) have been used for the analyses and they showed the low-magnesium calcitic skeletons with magnesium content in the calcite ranged from 0.9 % to 1.4 % (wt% $MgCO_3$). Strontium concentration in the Admiralty Bay skeletons varies in narrow range between 2020 and 2220 ppm, however, in the fossil analyzed lunulite samples the strontium content was higher ranged from 2300 to 3000 ppm.

The recent Admiralty Bay bryozoan skeletons exhibit $\delta^{18}O$ and $\delta^{13}C$ values typical of cool marine water. Their $\delta^{18}O$ ranges from ca. 2.25 to 4.3 PDB with most data clustering between 3 and 4 % PDB. The $\delta^{13}C$ varies from ca. -1 to +1.5 PDB with most data plotted between +0.5 and + 1.5 PDB. No isotopic trends related to bathymetry were observed. The obtained isotopic data are in excellent agreement with environmental conditions prevailing in the Admiralty Bay, indicating precipitation in equilibrium with the ambient water both for oxygen as well usually for dissolved inorganic carbon (DIC). The mean annual water temperatures in the Admiralty Bay are between ca -0.5 and -0.3 ºC fluctuating seasonally from -1.8 to +1.8ºC (Lipski, 1987). It is worth mentioning that the $\delta^{18}O$ values from the whole skeletons or their large fragments are considerably less isotopically variable (2.9-3.3 PDB) than those measured in small samples comprising only tiny colony fragments. It means probably that the whole skeletons record mean environmental conditions (temperature and water isotopic composition), whereas small samples witness the seasonal fluctuations.

Four distinct bryozoan assemblages were discerned based on the range of features such as bryozoan community structure, species richness and biomass and they are strongly associated with the number of environmental factors such as substrate type, water depth - 15-60 m, 60-120 m, 120-200 m and 240-280 m, location within the basin, hydrodynamic regime, influence of the suspended matter inflow or glacial disturbance.

The most favourable conditions with the greatest taxonomic diversity occurred at the depth of 120-200 m, where the fauna settled on the muddy substrate with some stones, in the central part of the fjord.

References

Borisenko, YA, Gontar, VI. (1991) Skeletal composition of cold-water bryozoans (in Russian). Biologia Morya, 1:80-90.

Hara, U, Jasinowski, M, Presler, P. (2010) Geochemistry and mineralogy of bryozoan skeletons from Admiralty Bay (South Sheltland Islands, Antarctica: a preliminary account, p. 56. Terra Nostra, 15th International Conference IBA.

Kukliński, P, Taylor, PD. (2009) Mineralogy of Arctic bryozoan skeletons in a global context. Facies, 55: 489-500.

Lipski, M. (1987) Variations of physical conditions, nutrients and chlorophyll a contents in Admiralty Bay (King George Island, South Shetland Islands, 1979). Polish Polar Research, 8: 307–332.

Pabis, K, Hara, U, Presler, P, Siciński, J. (2014) Structure of the bryozoans communities in an Antarctic glacjal fjord (Admiralty Bay), Polar Biology 37: 737-751.

Ba Isotopic Analysis of Chondrules from the Sayama Meteorite: Application for Development of ^{135}Cs-^{135}Ba Chronometry in the Early Solar System

Hidaka, H[1, 2], Higuchi, T[2] and Yoneda, S[3]

1: Department of Earth and Planetary Sciences, Nagoya University, Nagoya 464-8601, Japan
2: Department of Earth and Planetary Systems Science, Hiroshima University, Higashi-Hiroshima 739-8526, Japan
3: Department of Science and Engineering, National Museum of Nature and Science, Tsukuba 305-0005, Japan

Early alteration processes that probably occurred on the primitive asteroids are important activities for understanding the evolution of the solar system and the differentiation of solar planetary materials. Aqueous alteration in the early solar system is one of the primitive activities in the asteroidal bodies (DuFresne and Anders, 1962). The presence of hydrous minerals observed in the CI and CM2 chondrites provides evidence that aqueous alteration occurred on the meteorite parent body (Barber, 1981; Tomeoka and Buseck, 1985; Zolensky et al., 1989). Isotopic studies using the decay of short-lived radionuclides put temporal constraints on the occurrence of early activities in the CI and CM chondrites. The ^{135}Cs-^{135}Ba isotopic system in chondritic materials is expected to work as a sensitive chronometer for aqueous processes on the parent bodies, because Cs is one of the elements that react strongly with water. To develop the ^{135}Cs-^{135}Ba chronometry, precise determination of the Ba isotopic compositions in the early solar system materials is required. However the following features are considered disadvantageous and make the search for radiogenic ^{135}Ba from the early solar system materials difficult: (1) the existence of additional s-process nucleosynthetic components originating from pre-solar grains; (2) the relatively low Cs/Ba elemental ratio in chondritic materials, and (3) the possibility of redistribution of Cs after the aqueous alteration. Isotopic excesses of ^{135}Ba correlated with the Cs/Ba elemental ratios were found in the chondrules from the Sayama meteorite (Hidaka and Yoneda, 2013). This suggests that radiogenic ^{135}Ba was selectively adsorbed as ^{135}Cs in serpentine produced from olivine by an early aqueous alteration process on the parent body.

The Sayama meteorite fell in 1986, and was recognized as a meteorite of CM2 in 2000. The mineralogy of the Sayama meteorite is similar to those of highly altered CM meteorites such as EET83334 and ALH88045, which are characterized as the most phyllosilicate-rich members (Yoneda et al., 2001), showing an extensive signature for aqueous alteration on the meteorite parent body. As a result of mineralogical observation of the thin section of the Sayama meteorite, it is reported that around half of the olivine in several chondrules is replaced by serpentine (Yoneda et al., 2001). Our previous study of Ba isotopic analyses of chemical leachates from the chondrules of the Sayama meteorite shows evidence of the presently extinct short-lived radionuclide ^{135}Cs (half-life 2.3 Ma) in the early solar system and selective adsorption of ^{135}Cs into phyllosilicates in association with aqueous activity on the primitive meteorite parent body. The data suggest the remobilization of Cs in the meteorite parent body. The purpose of this study is to find geochemical evidence for redistribution of alkaline elements as a result of the aqueous activity on the early solar materials.

In our previous study, 35 chondrules with diameters from 100 to 600 μm were handpicked from the matrix portion of the Sayama meteorite. Although most of them were consumed in the previous isotopic study with complete decomposition and chemical treatments (Hidaka and Yoneda, 2013), two remained, and were used for SHRIMP analysis in this study. The polished section was prepared from these two chondrules. Prior to the SHRIMP analysis, the observation of two-demensional (2D) Raman spectra were performed on the thin section to collect spatially resolved chemical images of serpentinized phases transformed from olivine in chondrules on the thin section. Determination of the elemental concentrations of Rb, Sr, Cs and Ba was performed with a SHRIMP at Hiroshima University. The samples were sputtered with a 5 nA O_2^- primary ion beam. The mass resolution (M/ΔM at 1% of peak height) was set at 9000 to resolve the oxide ion species (MO^+) from the mass region in this study. The masses of ^{86}Rb, ^{87}Rb+^{87}Sr, ^{88}Sr, ^{120}(^{28}Si$_2$^{16}O$_4$), ^{133}Cs, ^{135}Ba, ^{137}Ba, ^{138}Ba, ^{139}La, and ^{140}Ce and backgrounds (at masses of 85.5 and 140.5) were monitored. Standard glass SRM 612 obtained commercially from NIST was used for the calibration of secondary ion ratios to the elemental concentrations.

It is known that the Sayama meteorite (CM2) shows an extensive signature for aqueous alteration on the meteorite parent body, and that most of the primary minerals in the chondrules are replaced to phyllosilicates as the result of the aqueous alteration. In this paper, it is confirmed from the observation of two-demensional (2D) Raman spectra that a part of olivine in a chondrule collected from the Sayama chondrite is serperntinized. As the result of SHRIMP analyses, elemental redistribution of Rb, Sr, Cs, and Ba probably caused by intensive aqueous alteration was observed on the microscale in chondrule grains from the Sayama meteorite. The data showed that alkaline elements such as Rb and Cs are heterogeneously redistributed in the chondrule. The elemental abundances of these four elements vary widely in individual micro-scale regions (Rb: 0.19 ~ 7.9 ppm, Sr: 2.4 ~ 33 ppm, Cs: 0.03 ~ 3.0 ppm, and Ba: 0.25 ~ 4.7 ppm). We expected that these alkaline elements have been selectively adsorbed in a specific phases. Although it is still unclear, serpentine is one of the candidates as a specific material for selective uptake of alkaline elements. The serpentinized phases identified by the micro-Raman observation showed high Rb/Sr and Cs/Ba ratios up to 0.69 and 1.1, respectively, which are 2.3 to 14 times higher than in the CI chondritic level. Furthermore Ba isotopic analysis provided variations of ^{135}Ba/^{138}Ba and ^{137}Ba/^{138}Ba in the chondrule. Although we carefully selected the

analytical points for micro-region isotopic measurements of Ba to find isotopic evidence of radiogenic ^{135}Ba, the existence of initial ^{135}Cs in the solar system is still unclear from this study. Interference from additional nucleosynthetic components in the solar primitive materials is one of the major problems in this study. Based on the stellar model, a correction was made in this study to detect radiogenic ^{135}Ba by subtraction of the s-process component. The isotopic excess from radiogenic ^{135}Ba is considered to be too small to be detected by in-situ analysis in the current situation, finding specific phases having a much higher Cs/Ba elemental abundance ratio (>10) is required.

References

Barber, DJ. (1981) Matrix phyllosilicates and associated minerals in C2M carbonaceous chondrites. GCA 45, 945-970.

DuFresne, ER, Anders, E. (1962) One the chemical evolution of the carbonaceous chondrites. GCA 26, 1085-1114.

Hidaka, H, Yoneda, S. (2013) Radioactive Cs capture in the early solar system. Sci. Rep. 3, 1330 (6 pp).

Hidaka, H, Higuchi, T, Yoneda, S. (2015) Redistribution of alkaline elements in association with aqueous activity in the early solar system. ApJ 815, 76 (6pp).

Tomeoka, K, Busek, PR. (1985) Indicators of aqueous alteration in CM carbonaceous chondrites: Microtextures of a layered mineral containing Fe, S, O and Ni. GCA 49, 2149-2163.

Yoneda, S, Ebihara, M, Oura, Y, Okada, A, Kusakabe, M, Nakamura, T, Nagao, K, Naraoka, H. (2001) Sayama meteorite: A new CM chondrite fall in Japan with highly aqueous altered textures. LPSC 32, 2034 (abstract).

Zolensky, ME, Bourcier, WL, Gooding, JL. (1989) Aqueous alteration on the hydrous asteroids: Results of EQ3/6 computer simulations. Icarus 78, 411-425.

Preliminary report of stable isotope analysis with 5-head advanced multi-collector

Horie, K[1, 2], Takehara, M[1] and Magee CW.[3, 4]

1: National Institute of Polar Research, Tachikawa, Japan
2: Department of Polar Science, The Graduate University for Advanced Studies (SOKENDAI), Tachikawa, Japan
3: Australian Scientific Instruments, Fyshwick, Australia
4: Community Safety and Earth Monitoring Division, Geoscience Australia, Canberra, Australia

National Institute of Polar Research's Second SHRIMP, installed in 2014, is first SHRIMP-IIe with the 5-head advanced multi-collector (AMC). The previous SHRIMP multi-collector uses the central triplet heads or a Faraday cup at the axial position, with the option to ion optically transfer the beam to a fixed DDEM at the rear of the multicollector. The 5-head AMC consists of fixed axial head and four moveable heads and can install 5 independently positionable Faraday cups. This feature of the 5-head AMC allows a wider variety of high precision, in-situ isotope geochemistry using SHRIMP, such as 4 sulfur isotope analysis (^{32}S, ^{33}S, ^{34}S, and ^{36}S). Over the last two years, we tried to analyze oxygen isotopes (^{18}O/^{16}O) with OH^- or ^{17}O in zircon and apatite, boron isotopes (^{11}B/^{10}B) in tourmaline, magnesium isotopes (^{24}Mg, ^{25}Mg, and ^{26}Mg), plus Al concentration in olivine, chlorine isotopes (^{37}Cl/^{35}Cl) and so on. In this presentation, we report preliminary data of composition dependent matrix effect on magnesium isotopes in olivine and isotopic ratios of chlorine (^{37}Cl/^{35}Cl) and sulfur (^{34}S/^{32}S) in apatite.

Magnesium isotopes potentially offer new insights into a diverse range of geological processes, including the formation of carbonate sediments, weathering, evaporation and condensation in the solar nebula, and evidence for extinct radionuclides in the early solar system. An O_2^- primary ion beam of 2.1 nA was used to sputter an analytical spot of ~25 μm diameter on polished synthetic olivines (Norman et al. 2006). ^{24}Mg, ^{25}Mg, and ^{26}Mg were detected by the Faraday cups at low mass (LM), intermediate low mass (ILM), and intermediate high mass (IHM), respectively. The width of collector slit at LM was a 200 μm, and all others were 300 μm. In addition to Mg isotopes, ^{27}Al was measured at high mass (HM) head with a 300 μm slit. As shown in Figure 1, the analysis of the olivines demonstrates a composition dependent matrix effect in which systematically heavier isotopic

compositions were measured in the olivines with lower Mg# Unlike the laser ICPMS fractionation, this trend does not seem to be linear, particularly at high Mg*.

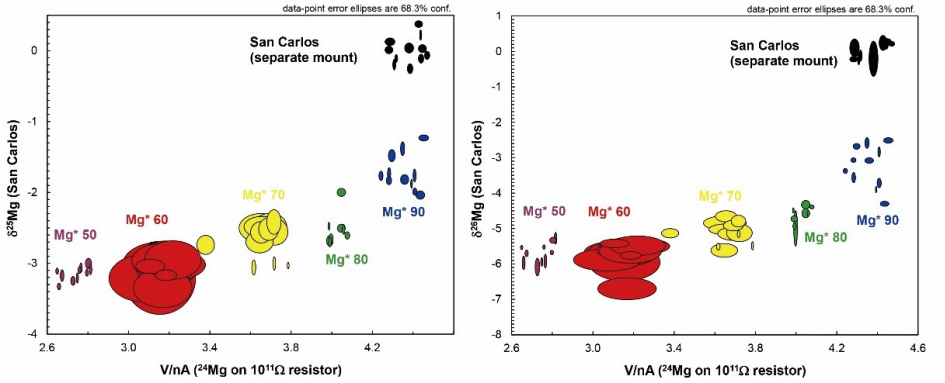

Figure 1 $^{25}Mg/^{24}Mg$ and $^{26}Mg/^{24}Mg$ isotopic compositions measured by SHRIMP-IIe/AMC on olivines with Mg = 50-90, as a function of signal intensity of ^{24}Mg (volts).*

Halogens play an important role in a range of magmatic to hydrothermal processes since they can influence, the density and viscosity of melts, the evolution of magmatic systems, the transport of metals in fluids and the environmental impact of gas emissions on the atmosphere during degassing processes. Chlorine isotopes (^{35}Cl and ^{37}Cl) in various apatites were analyzed with 2 sulfur isotopes (^{32}S and ^{34}S). ^{32}S, ^{34}S, ^{35}Cl, and ^{37}Cl were detected at LM, ILM, IHM, and HM, respectively. ^{32}S, ^{35}Cl ,and ^{37}Cl were measured on 10^{11} Ω resistors in current mode, while ^{34}S was measured using the capacitor (iFlex) in charge mode.

Durango apatite had a raw $^{37}Cl/^{35}Cl$ ratio of 0.316765, with a mean spot internal standard error of 0.1‰, and a spot-to-spot standard deviation of 0.17‰. Setting the Durango value to 0.4‰ (Boyce, personal communication) yielded a pooled value of 0.4 ± 0.11‰. This was within error of the eight successfully run BGC Fish Canyon apatites (0.49 ± 0.11‰) and eight of the 10 MIT Fish Canyon apatites (0.42 ± 0.05‰).

With only ~100,000 cps of ^{34}S, there was no expectation of high precision on the $\delta^{34}S$ analyses for 3 minute acquisitions. The analytical precision was predictably poor, and it is our understanding that ~20 minute analyses are required for high precision (Economos pers. com). However, the main purpose of this run was to test the overnight MC-autoanalysis and to get some reasonable Cl data, while finding and staying on the S peaks. Long duration experiments suggest that $\delta^{34}S$ and $\delta^{37}Cl$ have different down-hole fractionation trends in the apatite matrix, complicating the use of the precise $\delta^{37}Cl$ to correct for downhole $\delta^{34}S$ drift

The Fish Canyon apatites have mean $\delta^{34}S$ values within 0.7‰ of each other, and were about 4 permil heavier than Durango (set to 5‰). The marine fossils were about 20 permil heavier, a value consistent with Phanerozoic marine sulphate. The $\delta^{34}S$ values of the fossils are broadly compatible with a marine origin, and there is S and Cl isotopic variability, the meaning of which would require liaising with a paleontologist to interpret.

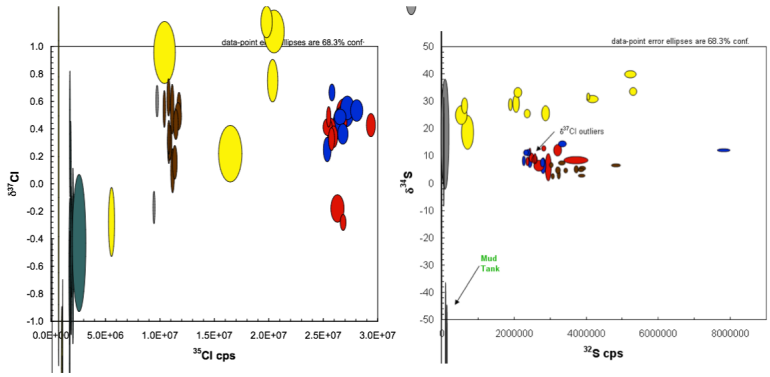

Figure 2 $\delta^{37}Cl$ and $\delta^{34}S$ values for various apatites. Yellow= various marine fossils; Blue Fish Canyon from BGC; Red= Fish Canyon from MIT; Teal= Mud Tank; Brown= Durango; Grey= Experimental.

References

Norman, ND, McCulloch, MT, O'Neill, HSC, Yaxley, GM. (2006) Magnesium isotopic analysis of olivine by laser-ablation multi-collector ICP-MS: Composition dependent matrix effects and a comparison of the Earth and the Moon. JAAS 21, 50-54.

Community-derived uncertainty propagation and data reporting standards in LA-ICP-MS U-Pb geochronology to improve data interpretation and inter-laboratory comparison

Horstwood, MSA[1] and the LA-ICP-MS U-Th-Pb Network[2]

1: NERC Isotope Geosciences Laboratory Geochronology & Tracers Facility, British Geological Survey, UK
2: www.plasmage.org

Over the last several years the laser ablation (LA-)ICP-MS U-Th-Pb community has attempted to co-ordinate its knowledge and pool community resources to better understand issues affecting the accuracy (*sensu stricto*) of LA-ICP-MS U-Th-Pb data (www.plasmage.org). Through a series of international workshops and collaboration with the EARTHTIME community, new data reporting protocols have been defined along with new reference values for commonly used zircon, monazite and titanite reference materials which more accurately define the material sampled during LA analysis. A new uncertainty propagation workflow has been determined identifying key random and systematic uncertainty components, producing new guidelines on when each of these components should be propagated and how this should be considered in data interpretation and comparison. These new protocols (see Horstwood et al. 2016) should help improve the peer-review process and more accurately define the calibration factors required in LA analysis. Better understanding of the components of uncertainty within LA-ICP-MS data now enable more appropriate comparison and interpretation of data at different uncertainty levels to better resolve age differences and aid international comparison.

Newer initiatives include the investigation of data processing packages and the quantification of any variable outputs, and the production of a zircon reference material set to allow demonstration of lab performance through validation and the interrogation of systematic bias between materials. Experiences in defining these new pathways will be shared to contribute to any parallels that might exist with current efforts to implement new data handling software within the SHRIMP community.

References

Horstwood, MSA, Košler, J, Gehrels, G, Jackson, SE, McLean, NM, Paton, C, Pearson, NJ, Sircombe, K, Sylvester, P, Vermeesch, P, Bowring, JF, Condon, DJ, Schoene, B. (2016) Community-Derived Standards for LA-ICP-MS U-(Th-)Pb Geochronology – Uncertainty Propagation, Age interpretation and Data Reporting. Geostandards and Geoanalytical Research doi: 10.1111/j.1751-908X.2016.00379.x

The united plates of East Antarctica: nature and extent of a Tonian Oceanic Arc Super Terrane (TOAST) in eastern Dronning Maud Land, East Antarctica

Jacobs, J[1,2], Elburg, MA[3], Opås, B[1], Läufer, A[4], Ruppel, A[5], Estrada, S[5], Henjes-Kunst, F, Montero, P[6] and Bea, F[6]

1: Department of Earth Science, University of Bergen, Norway
2: Norwegian Polar Institute, Tromsø, Norway
3: Department of Geology, University of Johannesburg, South Africa
4: Bundesanstalt für Geowissenschaften und Rohstoffe (BGR), Hannover, Germany
5: Federal Institute of Geosciences and Natural Resources (BGR), Hannover, Germany
6: Department of Mineralogy and Petrology, University of Granada, Spain

An extensive Tonian Oceanic Arc Super Terrane (TOAST) has been recognized in a so far poorly studied area in eastern Dronning Maud Land based on integrated geological-geophysical studies. The TOAST is sandwiched in between Kalahari and Rukerland and consists of a characteristic gabbro-trondhjemite-tonalite-granite suite SHRIMP-dated at ca. 1000-900 Ma. TOAST samples have normalised trace element patterns typical for subduction-related magmas, have mostly a positive initial epsilon Nd and lack significant inheritance, typical for juvenile crust. The TOAST underwent protracted Late Neoproterozoic/Early Palaeozoic crustal reworking, migmatisation and polyphase melt production as a result of accretion-collision tectonics from ca. 650-500 Ma. Airborne geophysics allows us to speculate that the TOAST has a significant southern extent until ca. 77°S, where it abuts against a cryptic craton. The western margin of the TOAST probably represents the Forster Magnetic Anomaly in central Dronning Maud Land, whilst the eastern margin is poorly surveyed at present. We have tested the validity of the southern extension of the TOAST with the help of a U-Pb zircon detrital moraine study from the southern side of the Sør Rondane Mts. One-thousand zircons from nine moraine samples from southernmost Sør Rondane, the Nansen ice field and Steingarden, were dated by LA-ICP-MS. The analyses fall into three major age groups at ca. 1080, 950 and 550 Ma; only very few older Palaeoproterozoic zircons were found. Apart from late-tectonic granites, another common lithology in the moraines is a grey gneiss with a U-Pb zircon age of ca. 1080 Ma, similar to the oldest major age peak found. Rocks of this age are not commonly exposed in Sør Rondane. Similar to TOAST samples, the grey gneisses have a subduction signature with negative Nb/Ta anomalies; however, they are more evolved than the proximate juvenile TOAST. Although rocks with ages of ca. 1080 Ma are common in the Maud and Rayner belts to the E and W, the grey gneisses in the moraines differ from the latter two in that they are much more juvenile. The grey gneisses probably rather represent an early, late Mesoproterozoic phase of the TOAST. A Late Mesoproterozoic/Tonian metamorphic overprint is neither recorded in rocks of the TOAST nor the grey gneisses, indicating that these oceanic arcs probably evolved outboard of Rodinia.

SHRIMP U-Pb analysis of Hematite

Kennedy, AK[1], Courtney-Davies, L[2], Ciobanu, CL[2], Wade, BS[3], Cook, NJ[2], Ehrig, K[4], Talavera, C[1], Condon, D[5] and Tapster, S[5]

1: John de Laeter Centre, Curtin University of Technology, Bentley, WA, Australia
2: School of Chemical Engineering, The University of Adelaide, Adelaide, SA 5005, Australia
3: Adelaide Microscopy, The University of Adelaide, Adelaide, SA 5005, Australia
4: BHP Billiton Olympic Dam, Adelaide, SA 5000, Australia
5: NERC, British Geological Survey, Keyworth, UK

Introduction

The common Fe oxides, hematite and magnetite, are abundant in Iron-Oxide-Copper Gold (IOCG) deposits, and also occur as accessory phases in a wide range of igneous and metamorphic rocks, and, they are the major components in Precambrian Banded Iron Formations. Hematite and magnetite can accommodate a broad range of trace elements within their structures via isostructural exchange mechanisms, and/or coupled substitution mechanisms that conserve overall charge balance (Ciobanu et al., 2013). U, W, Si, Al, can be at % levels, while Sn and Mo can reach 100s of ppm. These trace elements may allow tracking of the provenance of alluvial Fe oxides, and fingerprinting of different types of Fe oxide-bearing ore deposits. In addition, Pb-Pb and U-Pb geochronology of iron oxides (Ciobanu et al., 2013; Courtney-Davies et al., 2016a) will allow us to directly date ore formation, and any subsequent reworking and enrichment process.

Samples

Olympic Dam ore samples containing hematite were studied by optical imaging, and BSE imaging using a FEI Quanta 450 SEM at Adelaide Microscopy, the University of Adelaide. Hematite grains targeted for analysis were identified in a block mount of sample 7295bGM, a deep drillhole sample from the SE part of the Olympic Dam deposit (Ehrig et al., 2012). Figure 1 shows individual hematite grains that are enriched in U and W.

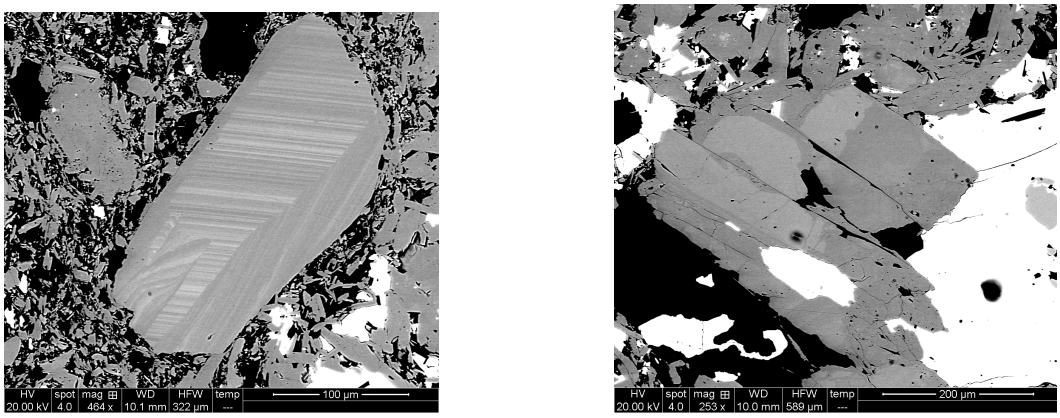

Figure 1. BSE images of hematite grains showing oscillatory zoning and homogeneous core patches from sample 7295bGM (drillhole 1988; 1808,8m; see Ehrig et al., 2012).

Analytical Details

Ion microprobe analytical methods follow those described by Compston et al., 1984; Claoue-Long et al., 1995 and Williams 1998. During initial testing we analysed two points in 7 grains, within a single block mount (7295bGM) of Olympic Dam ore. Data was collected during 6 cycles through nine magnetic field values, corresponding to $^{56}Fe_3{}^{16}O_2{}^+$, $^{204}Pb^+$, BKGD, $^{206}Pb^+$, $^{207}Pb^+$, $^{208}Pb^+$, $^{238}U^{16}O^+$, $^{232}Th^{16}O^+$, $^{238}U^{16}O_2{}^+$, with respective count intervals of 4, 10, 10, 30, 30, 20, 5, 5 and 5 seconds.

Results

Ion yields are acceptable with count rates in the 1000s of c/s for UO^+ and $UO_2{}^+$. The $^{238}U^+$ peak had unacceptably low counts and should not be measured. There was only minor variation of c/s of the molecular $Fe_3O_2{}^+$ reference peak, between and within analyses, suggesting that it is unlikely there is a crystallographic orientation effect on ion yields. Common Pb is present in variable amounts and small corrections are needed, but these are relatively minor corrections for many points, as the ^{204}Pb c/s are close to the background c/s. The distribution of uranium is highly variable between and within grains. For example, in the 4th grain analysed the UO^+ count rate varied from 116 to 4793 c/s. The consistently low Th content of the hematite means that the best correction for common lead is the ^{208}Pb method.

As a result of the observed wide range of U concentrations we decided to test the possibility of producing a $^{207}Pb/^{206}Pb$ vs $^{206}Pb/^{208}Pb$ isochron by treating all ^{208}Pb as common Pb. Figure 2 shows the $^{207}Pb/^{206}Pb$ vs $^{206}Pb/^{208}Pb$ isochron derived from the 11 highest U analytical points. The calculated age of 1574 +5.1/-4.2 Ma is typical of ages obtained in other geochronological studies of Olympic Dam ore (See Ciobanu et al., 2013, for references). This shows that the assumptions, of a single age and a single common Pb composition, are reasonable for the analysed hematite grains.

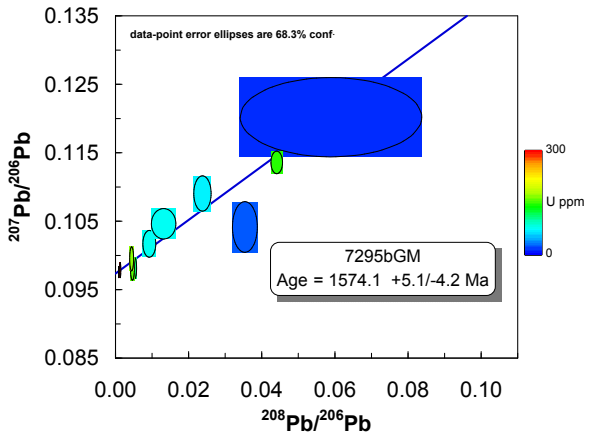

Figure 2. A $^{207}Pb/^{206}Pb$ vs $^{206}Pb/^{208}Pb$ isochron diagram for hematite from sample 7295bGM.

The U-Pb data from a second analytical session on Olympic Dam ore (10.2 OD) was reduced using a SQUID2 task. The $^{206}Pb/^{238}U$ ages for the grains in the 10.2 OD sample are calculated using the normal calibration approach, which assumes the same power law relationship exists between $^{206}Pb^{*}/^{238}U^{16}O$ and $^{238}U^{16}O_2/^{238}U^{16}O$ for both the Reference Material (RM) and unknown. Currently we have no RM, so we used the hematite grains from another block mount, as our RM, with an assumed age of 1584 Ma. Twenty seven analyses of hematite from our RM block were interspersed between the 10.2 OD hematite analyses in this analytical session. Our results are shown in Figure 3.

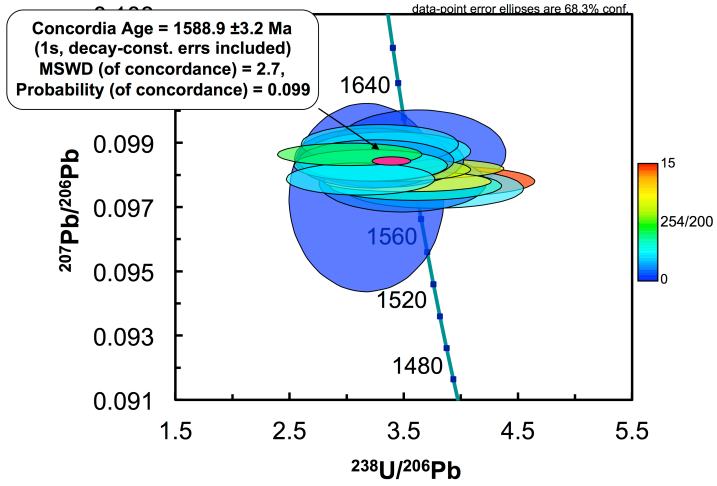

Figure 3. Tera-Wasserburg Concordia diagram for hematite from 10.2 OD, a high-grade bornite rich ore sample previously used for LA-ICP-MS Pb-Pb dating in Ciobanu, et al., (2013). Colour-coding of the points uses the $^{238}U^{16}O/^{56}Fe_3{}^{16}O_2$ peak ratio (254/200) as a proxy for U concentration in hematite. The U decay constants used in calculations are those of Steiger and Jager (1977).

Conclusion

From the above analytical sessions it was conclude that SHRIMP U-Pb and Pb-Pb dating of hematite produces excellent results, if BSE imaging is used to identify grains with hydrothermal oscillatory or sector zoning, or homogeneous undisturbed cores and patches. Currently, we are searching for homogeneous, high U hematite that can be characterised and used as a SIMS RM, and exploring alternate approaches for using iron oxides in geochronology (Courtney-Davies et al., 2016b, in review).

Acknowledgements

This is a contribution to the FOX project (Trace elements in Fe-oxide) sponsored by BHP Billiton and the South Australian Government Department of State Development.

References

Ciobanu, CL, Wade, BP, Cook, NJ, Schmidt Mumm, AS, Giles, D. (2013) Uranium-bearing hematite from the Olympic Dam Cu–U–Au deposit, South Australia: A geochemical tracer and reconnaissance Pb–Pb geochronometer. Precambrian Research 238 129–147.

Claoue-Long, JC, Compston, W, Roberts, J, Fanning, CM. (1995) Two Carboniferous ages: A comparison of SHRIMP zircon dating with conventional zircon ages and $^{40}Ar/^{39}Ar$ analysis. Geochronology, Timescales and Global Stratigraphic Correlation. W. A. Berggren, Kint, D.V., Aubry, M.P., Hardenbol, J., Society for Sedimentary Geology Special Publications. 54: 3-21.

Compston, W, Williams, IS, Meyer, CE. (1984). U-Pb geochronology of zircons from lunar breccia 73217 using a sensitive high-mass resolution ion microprobe. Proceedings of the fourteenth Lunar and Planetary Science Conference, Par 2. Journal of Geophysical Research.

Courtney-Davies, L, Ciobanu, CL, Wade BP, Cook, NJ, Ehrig, K, Cabral, AR, Kennedy, AK, Condon, D, Tapster, S. (2016a) U-Pb geochronology of Fe-oxides: LA-ICP-MS and SHRIMP analysis. 2016 Goldschmidt Conference Abstracts 551.

Courtney-Davies, L, Zhu, Z-Y, Kennedy AK, Ciobanu, CL, Cook, NJ, Ehrig, K, Wade BP. (2016b) Matrix-matched iron-oxide laser ablation ICP-MS U-Pb geochronology using mixed solution standards. (Minerals, Special Ed.:Advances in Mineral Analytical Techniques, in review)

Ehrig, K, McPhie, J, Kamenetsky, V. (2012) Geology and mineralogical zonation of the Olympic Dam Iron Oxide Cu-U-Au-Ag deposit, South Australia. Special Publication Number 16 - Geology and Genesis of Major Copper Deposits, Society of Economic Geologists, p. 237-267.

Steiger, RH, Jager, E. (1977) Subcommission on geochronology: Convention on the use of decay constants in geo- and cosmochronology. Earth and Planetary Science Letters 36: 359-362.

Williams, IS. (1998) U-Th-Pb Geochronology by Ion Microprobe. Applications of Microanalytical Techniques to Understanding Mineralizing Processes. Reviews in Economic Geology. M. A. McKibben, Shanks, W.C., Ridely, W.I. 7: 1-35.

SHRIMP IIe/MC contribution to the genetic investigations of the sulfide mineralization – a case study of pyrite

Krzemińska, E[1], Mikulski, SZ[1], Czupyt, Z[1], Pieńkowski G[1], Wołkowicz S[1] and Wołkowicz K[1]

1. Polish Geological Institute- National Research Institute, Poland

The sulfur isotope composition as a genetic indicator of sulfide mineralization is commonly measured in studies of various terrestrial systems. Among four stable isotopes of sulfur the most abundant are represented by $^{34}S/^{32}S$ ratio ($\delta^{34}S$) that tend to vary systematically within wide range geological settings (Seal, 2006). Sulfur plays a crucial role in the generation of numerous magmatic and hydrothermal ore deposits, thus isotope studies are a powerful tool in interpreting the origin of massive ore deposits and various sings of mineralization including evidences of early microbial activities. The sulfides associated with igneous rocks derived from the mantle are isotopically similar to that of meteorites and have $\delta^{34}S$ values close to 0‰ but sulfide produced by bacteria reduction of sulfate have negative $\delta^{34}S$ values. The isotopic composition is provided increasingly through secondary ion mass spectrometry SIMS technique, which allows to penetrate natural isotopic heterogeneities on a very small scale avoiding other phase inclusions or internal defects.

In this contribution, we report a $\delta^{34}S$ analyses of pyrite collection derived from several localities, that represent different host rocks, geological settings, resulting in a very different processes with the two general objectives: to identify and compare possible sulphur sources by SHRIMP IIe/MC and to acquire information *in situ* about potential isotopic inhomogeneous within single sulphide crystals. Samples that were researched for this study come from wide range terrestrial paleoenvironments. They were represented by: (LI) – pyrite associated with vertebrate skeletal remains, coprolites and petrified wood from clay-pit of an Upper Triassic age, exposed at Lisowice Upper Silesia; (HA) –presumably diagenetic pyrite from lower Halifax Formation (part of Cambro-Ordovician Meguma Group) collected in Nova Scotia, Canada; (KP) – pyrite concretion from Lower Ordovician (Tremadiocian) uranium-bearing Dictyonema Shale horizon belonging to the so-called black shale formation of the Podlasie Depression in E Poland; (TA) – pyrite from quartz deposit, which previously was used for fabrication of porcelain and ferro-silicon, in Taczalin quarry located in central part of the Variscan Fore-Sudetic Block; (RA) pyrite from quartz–sulfide veins and host rocks of the Radzimowice Au–As–Cu abandoned deposit in the Kaczawa Mountains, and (LE) from the Fe prospect in Leszczyniec, both related to Paleozoic (Upper Carboniferous and Cambrian-Ordovician magmatic activity) in the Sudetes that constitute the NE part of the Bohemian Massif.

Previous investigations showed no measureable an orientation effect for pyrite (Kozdon, unpublished data), hence grains were placed almost randomly. Three isotopes of sulfur ^{32}S, ^{33}S, ^{34}S, were measured using focused primary Cs^+ ion beam rastered over an analysis area for a final slightly elliptical spot size of ~18 × 20 µm. A normal incidence electron gun was used for charge compensation. Samples were gold-coated before being loaded into the machine. Stable isotopic compositions are reported as ratios of $^{34}S/^{32}S$ ($\delta^{34}S$) in ‰ relative to the international standard VCDT [Vienna Canyon Diablo Troilite]. High spatial resolution multiple sulfur isotope studies undertaken by multi-collector secondary ion mass spectrometry (SIMS) commonly use well-characterized sulfide reference materials. In all these cases a measurements were standardized with the Ruttan- pyrite reference material, with conventionally determined ref. value of $\delta^{34}S = 1.2 \pm 0.1$‰ (VCDT) (Crowe and Vaughan, 1996).

Several grains of Ruttan were embedded within each megamout close to the desired analytical region of single grains of pyrite samples, and polished to obtain an exposed flat surface. This provides similar beam conditions for measurements of both standards and sample unknowns.

Analyses of sample unknowns were bracketed by measurements of standards every 4-5 measurements. Analyses were performed in automated sequences, with each analysis comprising presputter to remove the gold coating over a rastered. The duration of individual spot analyses was ~6 min. The mean average value of reference Ruttan pyrite was 1.208 ±‰0.074 ‰ (s.d.= 0.24, n=51) and the internal precision for Ruttan during the session was between 0.05 and 0.18 ‰. Typical precision on a single measurement $\delta^{34}S$ of unknown was ±0.06–0.2 ‰ with a few values ±0.28-0.30‰ only noted for a few large negative values of $\delta^{34}S$ (-40‰).

Results

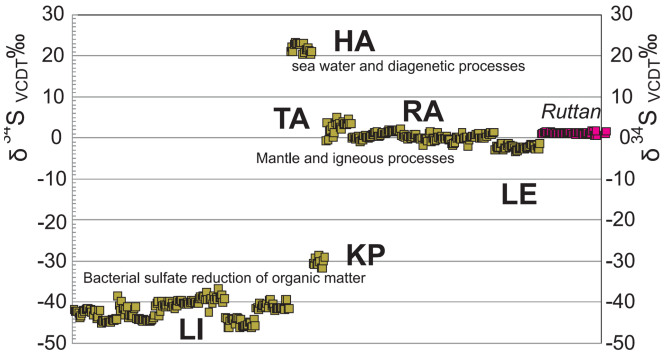

Figure 1.Variations of $\delta^{34}S$ isotope signatures of pyrite (single grains) derived from various environments and Ruttan reference pyrite: All isotopic values in ‰ [VCDT], Abbrev.: (LI) Lisowice, (HA) Halifax formation, (KP) Podlasie Depression, (TA) Taczalin quarry, (RA) Radzimowice, (LE) Leszczyniec.

The complete isotopic dataset is shown in Fig1. One of discussed setting is Upper Triassic clay pit of exposed at LI, famous for its well-preserved vertebrate fossils. Analyses of $\delta^{34}S$ were performed in pyrite developed on remains both of animal (bones) and plant (wood) origin to check a hypothesis of hydrothermal source of mineralization. The $\delta^{34}S$ results however proved that the metabolism of sulfate-reducing bacteria was the only process leading to the development of pyrite mineralization. Very similar bacteria sulfate reduction processes have contributed to the formation of sulfide KP concretion hosted in uranium-bearing Ordovician black shales. These sedimentary formation extending from Scandinavia to Russia, comprise fine -grained, no -metamorphosed, organic-rich, marine deposits considered currently as a potential source rocks for Poland's conventional oil and gas fields.

Pyrite HA, which is abundant in the lower Halifax Formation in Nova Scotia reveals moderately positive values of $\delta^{34}S$. It records an isotopic effect of interactions between seawater and associated hydrothermal activity e.g. shallow thermochemical reduction by H_2S-bearing anoxic bottom waters. On the other hand sulfide-rich Halifax slates are also known as an "acid generated rocks" with their potential hazards of natural oxidation processes within exposure to oxygen and water pyrite rich rocks. It causes the chemical breakdown of the sulfide minerals which releases sulfuric acid, iron and other metals, into the receiving environment, typically a stream, and river, or lake, contaminating aquatic ecosystems.

The last and relatively consistent group of $\delta^{34}S$ results (samples TA, RA, LE) is related to the processes occurring in melts, magma-related, hydrothermal systems of the Sudetes area before and during Variscan orogeny. Sulfur isotopic composition measured on pyrites from RA and LE have range close 0‰, suggesting magmatic and mantle sources for the sulfur (despite different age of magmatic activities). They are distinctly different from those of pyrite in the sedimentary LI, KP ($\delta^{34}S‰ = -40$ to −30‰) systems, and also different from those of evaporates and diagenetic sulfides ($\delta^{34}S‰ = +10$ to +20). The $\delta^{34}S$ values of RA pyrite vary systematically between +2 and –1 ‰. This range however is very narrow. It indicates that the homogenous sulfur isotope compositions may have a similar source for the different samples and reflect an influence of other factors. The granitic of ilmenite series, which were resulted from partial melting of sedimentary protolith, the $\delta^{34}S$ of sulfides was below 0 ‰, while the granitoids of magnetite series that can be considered as resulting from the dominant magmatic protolith the values $\delta^{34}S$ were a greater than 0 ‰. Usually one or several processes including

contamination /assimilation, alteration by seawater may lead to variation of isotopic composition. The LE pyrite reveals a δ^{34}S‰ values between –3.1 and –1.1‰. It suggest that sulfur in MORB-like Leszczyniec Fe prospect was derived largely from magmatic (volcanic) source although with some contribution from seawater sulphate, that is similar mineralisation to volcanic-hosted massive sulfide deposit. Diagram (Fig.1) is shown that the δ^{34}S values of TA sulfides from the quartz vein also fall into a range, which are similar to those of the magmatic rocks (δ^{34}S‰ = −1 to +5). The isotopic composition of a hydrothermal fluid from which the sulfide got deposited and temperatures of deposition were close related to main magmatic range.

Conclusions

The isotope ratio (δ^{34}S) of sulfides measured in situ remains an effective diagnostic tool for the recognition of general origin of sulfur during main event sulfide precipitation and wide range geological settings as well as other very individual factors and influenced processes detectable only by very detailed microanalytical isotopic investigations.

Acknowledgements

The contribution was financed from projects PGI –NRI 61.3207.1502.00.0 and NCN-. DEC-2012/06/M/ST10/00478 of G.P.

References

Crowe D. E. and Vaughan R. G. (1996) Characterization and use of isotopically homogenous standards for in situ laser microprobe analysis of $^{34}S/^{32}S$ ratios. Am. Mineral.81, 187–193.

Mikulski S. Z., Krzemińska E., Czupyt Z. and Williams I. S. (2015) Sulpur isotope measurements of sulphide minerals from the polymetallic ore deposits in the Sudetes on the SHRIMP IIE / MC - ion microprobe. Biuletyn Państwowego Instytutu Geologicznego. 464, 61-78 (in Polish with English abstract & summary).

Seal, RR (2006). Sulfur Isotope Geochemistry of Sulfide Minerals. Reviews in Mineralogy & Geochemistry. 61, 633-677.

The oxygen isotope record of detrital zircon grains from Late Svecofennian metasediments on Fennoscandia-Sarmatia stream as a supplement to the provenance studies

Krzeminska, E, Wiszniewska, J and Czupyt, Z

Polish Geolgical Institute-National Research Institute, Warszawa, Poland

Detailed studies of sediments provenance demonstrate that the age populations of detrital zircons accompanied with other isotope data mirror that of the rock types from which they were derived. The isotopic methods are applied also to the metamorphosed sediments from various Precambrian terranes. Old ages in zircon cores indicate that the zircons can survive up to anatexis. Zircon crystals also hold their original O isotopic composition. If detrital grains despite metamorphic episode, retained primary oxygen isotopes from the time of crystallization (Claesson et al., 2016), such values can be used to discriminate detrital cores populations to better characterize a potential source rocks of clastic material. The fact that the mantle derived δ^{18}O values fall in a narrow range (5.3 ± 0.8‰) allows to use the oxygen signature in zircon as a tracer of the mantle vs crustal origin or hydrothermal fluids interactions.

We present oxygen isotope data of detrital zircon sampled from Late Paleoproterozoic metasediments, which characterize a hidden crystalline basement, close to stream of Fennoscandia and Sarmatia blocks. Core samples represent two isolated deep drillings e.g. Monki and Jastrzebna. The clastic sequences were metamorphosed to greenshist and amphibolite facies respectively, at ca. 1.83 Ga (Krzeminska et al. 2009). Detrital zircon age investigations were done on SHRIMP II at RSES ANU. They identified a wide range of ages from 3.52 Ga to 1.83 Ga (Williams et al. 2009). In details, it has shown a dominant Paleoproterozoic population at 2.1–1.9 Ga, a subordinate Neoarchean group at 2.9 – 2.7 Ga, and rare Paleoarchean grains up to 3.4 Ga. The maximum deposition age of the sequences was

at 1.86 –1.83 Ga, that is at similar period as in the Svecofennian basins known from exposed Fennoscandia.

As a supplement of the provenance studies the investigations of oxygen isotope ratios ($^{18}O/^{16}O$) within detrital cores and metamorphic rims of zircon were realized on SHRIMP IIe MC at PGI-NRI in January 2016. Sample mounts were analyzed with prior removal of existing geochronology spots by repolishing, however oxygen analyses have been precise combined with $^{207}Pb/^{206}$ Pb age record on the same non- metamict zircon cores. The $^{18}O/^{16}O$ ratio expressed as $\delta^{18}O$ relative to Vienna Standard Mean Ocean Water (VSMOW) and results are reported relative to the internal standard of zircon FC1 ($\delta^{18}O$ =5.4 ‰). Thirty four analyses of FC1 made during the time of session, gave an average value of 5.36%±0.05‰. with standard deviation of 0.31.

The proportion of zircon with $\delta^{18}O$ > 6.0‰ increases with younger crystallisation ages and metamorphic overgrowths have heavier O isotope compositions than cores, indicating that the zircon grains record their original, igneous isotope signature. Overgrowths have almost uniform $\delta^{18}O$ values with an average from 9.34 ±0.38‰ (Monki) to 9.05 ± 0.25‰ (Jastrzebna). This range reflects a temperature-dependent fluid interaction influenced to elevated $\delta^{18}O$ values.

The δ18O of detrital cores from Archean zircon population vary between 2.92±0.07‰ and 6.06±0.07‰. From this group about 91% of grains have a mantle-like isotope values close to 5.3 ‰. Only few zircons gave δ18O lower than 5.0‰. They may represent some influence of convective hydrothermal system. A dominant Paleoproterozoic population reveals considerable variability (Fig.1) with slightly elevated δ18O but not extending value of 11 ‰. The average of δ18O for Monki sample is 6.85±0.29‰ and for Jastrzebna sample is 6.01±0.26‰. Slight differences correspond to various characteristics and maturity of sediments e.g. mature paragneises versus immature metagreywackes, respectively.

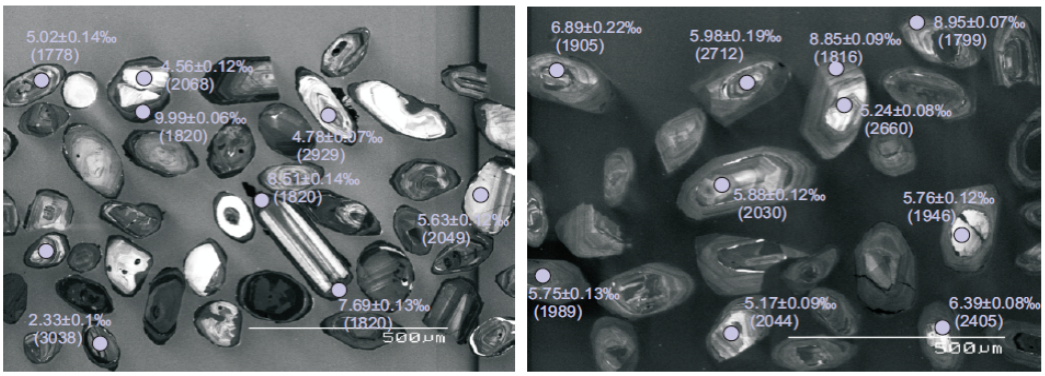

Fig.1. A compilation of $\delta^{18}O$ and Pb –Pb age results of detrital zircons from metasediments (age in brackets, Ma). Samples: Monki (left) and Jastrzebna (right), representing greenshist and amphibolite facies respectively.

In Paleoproterozoic group only 34 % of cores display a mantle – related values, that confirms a post Archean maturation of the crust. Mantle – derived zircons mostly represent cluster age of 2.0 – 1.9 Ga. Considering a potential source, we suppose that isotopic signature corresponds with juvenile rocks ranges from ultrabasics to granitoids from the Osnitsk-Mikashevichy (OM) volcanoplutonic belt known from the westernmost Sarmatia. According to recent geochronological investigations OM was an active continental margin, existing approximately 1980–2000 Ma ago (Shumlyanskyy, 2014). "An active continental margin" setting does not imply the derivation from the mantle, however their source was a subducted oceanic slab, and the overlying mantle wedge vs continental crust (op. ci). For oldest ~3.4 –3.0 Ga Paleoarchean and Neoarchean populations of mantle derived zircon (91%of cores), cannot be correlated to any proximal basement, thus it indicates a distal source of detrital material.

Conclusions

Oxygen isotope investigations reveal that the greenshist and amphibolite metamorphism accompanied with metamorphic fluids do not erase a primary oxygen isotope composition. Differences in zircon core – rim $\delta^{18}O$ values of as much as 5.4 – 6 ‰ have been documented. Oxygen isotope data from detrital cores suggest that older Archean zircon grains represent mostly (91%) mantle derived magmas. Dominated Paleoproterozoic detrital material is composed of mantle – derived juvenile material and supracrustal component. Oxygen isotope signatures of the detrital zircon presented here

might furthermore be indicative of a maturing arc system in this particular region on Fennoscandia-Sarmatia stream.

Acknowledgements

Funding from PGI-NRI projects, especially 61.32071502.00.0 to the senior author has supported presented contribution.

References

Claesson, S, Bibikova, EV, Shumlyanskyy, L, Martin, J, Whitehouse, MJ, Billström K. (2016) Can oxygen isotopes in magmatic zircon be modified by metamorphism? - a case study from the Eoarchean Dniester -Bug Series, Ukrainian Shield. Precambrian Research, 273, 1-11.

Krzeminska, E, Wiszniewska, J, Skridlaite, G, Williams, IS, (2009) Late Svecofenniansedimentary basins in the crystalline basement of NE Poland and adjacent area of Lithuania: ages, major sources of detritus, and correlations. Geological Quarterly, **53**, 255–272.

Shumlyanskyy, L. (2014) Geochemistry of the Osnitsk–Mikashevichy Volcanoplutonic Complex of the Ukrainian Shield Geochemistry International, 52, 912–924.

Williams, IS., Krzeminska, E, Wiszniewska, J. (2009) An extension of the Svecofen-nian orogenic province into NE Poland: evidence from geochemistry and detrital zircon from Palaeoproterozoic paragneisses. Precambrian Research. 172, 234–254.

Metamorphic monazite and zircon SHRIMP ages from the Saglek block, Labrador

Kusiak MA[1], Dunkley DJ[1,2], Wilde SA[2], Sałacińska A[1], Whitehouse MJ[3] and Kielman R[3]

1: Institute of Geological Sciences, Polish Academy of Sciences, Warsaw, Poland
2: Department of Applied Geology, Curtin University, Perth, Western Australia
3: Swedish Museum of Natural History, Stockholm, Sweden

The Nain Complex of coastal Labrador comprises Archean amphibolite to granulite-facies gneisses that include some of the oldest tonalite-trondjemite-granodiorite (TTG) crust preserved on Earth. Samples of felsic orthogneiss and metapelite collected along a 70km north-south coastal traverse from Ramah Bay to Hebron were dated by Sensitive High-Resolution Ion MicroProbe. Tonalitic and granodioritic orthogneisses have petrographic evidence of partial melting at granulite-grade conditions, with subsequent low-grade metamorphism at Little Ramah Bay possibly related to the juxtaposition of the Nain Complex against Paleoproterozoic sediments of the Ramah Group. Magmatic zircon ages of ca. 3.7Ga, are consistent with previous estimates for the protoliths of Uivak I gneiss (Schiøtte et al., 1989). No evidence was found for the recent suggestion of >3.95Ga protoliths to the Uivak I gneiss (Komiya et al., 2015). The new data from Ramah Bay area extends the known outcrop of Uivak I gneiss and suggests continuation in the Nain Complex further north.

Metamorphic ages of ca. 2.7Ga were derived from zircon rims and neoblastic grains in felsic orthogneisses, as well as from monazite in orthogneiss and paragneiss. Felsic orthogneiss from Little Ramah Bay contains zircon rims and neoblastic sector-zoned grains typical of growth from anatectic melt, with a ca. 2.74 Ga age significantly older than a ca. 2.70Ga monazite age from the same sample (Fig. 1a-c). Monazite ages of 2.71Ga were derived from samples of garnet-sillimanite metapelite from Reichel Head, near Ramah Bay, and Shuldham Island in Saglek Fjord, 35km to the south (Fig. 1d-f). The slightly younger age from the orthogneiss may be a result of monazite affected by alteration and during low-grade metamorphism (Fig. 1c). Metamorphic ages are consistent with previous estimates for high-grade metamorphism in the Nain Complex (Schiøtte et al. 1989; Krough and Kamo, 2006). The 30-40 m.y. gap between zircon and monazite ages indicates prolonged metamorphic activity.

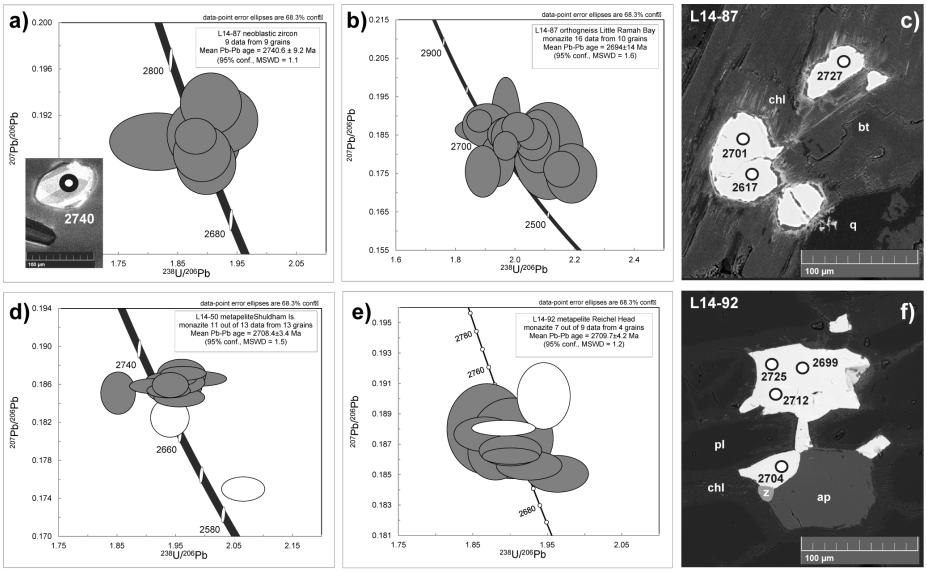

Fig. 1. SHRIMP zircon (a) and monazite (b-f) ages for felsic orthogneiss (a-c) and metapelites (d-f)

Acknowledgements

Field work was carried out with the permission and support of Parks Canada and the Nunatsiavut Government. Research funded by grant NCN No. 2014/15/B/ST10/04245.

References

Krogh, TE, Kamo, SL. (2006) Precise U-Pb zircon ID-TIMS ages provide an alternative interpretation to early ion microprobe ages and new insights into Archean crustal processes, northern Labrador. Processes on the Early Earth, 91-103.

Komiya, T, Yamamoto, S, Aokia, S, Sawaki, Y, Ishikawa, A, Tashiro, T, Koshida, K, Shimojo, M, Aoki, K, Collerson, KD. (2015) Geology of the Eoarchean, > 3.95 Ga, Nulliak supracrustal rocks in the Saglek Block, northern Labrador, Canada: The oldest geological evidence for plate tectonics.

Schiotte, L, Compston, W, Bridgwater, D. (1989) Ion-probe U-Th-Pb zircon dating of polymetamorphic orthogneisses from northern Labrador, Canada. Canadian Journal of Earth Sciences, 26:1533-1556.

POXI, POXI, and SHRIMP Software Update

Lanc, P, Holden, P, Ireland, T and Avila, J

Research School of Earth Sciences, The Australian National University, Australia

Data reduction software for both SHRIMP multi-collector and SHRIMP single collector data have been upgraded with several issues fixed, new features added, and new documentation added. SHRIMP control software has new features for stage drive, automation, peak identification, and new hardware support.

The off-line SHRIMP data reduction software POXI comes in two varieties: single collector, and multiple collector. The single collector version has been updated with various user interface improvements, more accurate deadtime correction, new Squid-like data table output, and more robust run-table peak identification. A draft manual is now available. Multiple collector POXI has a new Sulphur reduction output, new Oxygen data reduction tab, and Excel documentation.

SHRIMP control software has been migrated to NI LabVIEW 2015. Support for new hardware includes new in-vacuum SmarACT ASI stage, Windows tablet interface, cVars, FC4, DMC, and NI

USB thermocouple module support. Some of the new software capabilities include multiple multiple-collector run-tables support, click-to-drive stage live image mode, flexible single collector autotune, single collector charge mode support, and new Element Builder with Mass Scan peak annotations. New application for remote (LAN) ten frames a second live color video has been developed and used for duplicate remote control PC for SHRIMP SI. Off-line spot map location list maker software GPIX has been updated.

Zircon U-Pb age and Hf isotope evidence for provenance change and basin inversion of the Gyeongsang Basin, SE Korea

Lee, T-H[1,2], Park, K-H[2] and Yi, K[1]

1: Korea Basic Science Institute
2: Pukyoung National University

Since the early studies that analyzed detritus materials in sedimentary rocks, the main purposes have been to verify the maximum depositional age, sedimentary provenance and paleocurrent system. U-Pb age determination of detrital minerals, especially zircon and monazite, is a powerful tool for constraining maximum depositional age and potential sediment source studies. However, if the number of probable sedimentary provenances with similar U-Pb ages are either too many or none, it becomes quite difficult to decipher the provenance of detrital materials. However, recently developed Hf isotopic analysis from the same detrital zircon grains used for U-Pb age determinations provides powerful mean for sedimentary provenance studies (e.g., Mueller et al., 2007; Howard et al., 2015).

The Gyeongsang Basin is the largest Cretaceous terrestrial basin formed in the southeastern part of the Korean peninsula. It has important records on paleocurrent system and tectonic history of the Korean peninsula during the early Cretaceous time. So, extensive studies were conducted to investigate the development of the Gyeongsang Basin, but the depositional age of each strata is still insufficiently established in detail.

Detrital zircon U-Pb ages of the Gyeongsang Basin reported by earlier studies are dominated by four age groups; 1800 - 2500 Ma, 210 – 300 Ma, 160 – 200 Ma, and 110 – 140 Ma (Choi et al., 2012; Lee et al., 2015). The first three groups (Precambrian to Jurassic ages) represent detrital materials derived from the Precambrian basement sources and Mesozoic granitoids of the Yeongnam massif surrounding the Gyeongsang Basin. However, the widespread distribution of Precambrian to Jurassic rocks around the Gyeongsang Basin makes it difficult to further resolve the exact sources spatially. By contrast, the sources of 110 – 140 Ma zircons have not been reported from any exposed rock types of the Yeongnam massif yet, probably because the Korean peninsula experienced a significant lull in magmatism associated with changes in drifting direction of the Izanagi plate from Late Jurassic to early Cretaceous. So it is not sure whether such detrital zircons originated from the transient volcanic activity during the early Cretaceous or from the erosion of the exhumed plutonic rocks. Such an absence of any early Cretaceous granitoids in the Korean peninsula makes it difficult to track down potential provenance for early Cretaceous detrital zircons from the Gyeongsang Basin. The main goal of the present study is to determine the maximum depositional ages of the lower to middle strata in Gyeongsang Basin and to investigate its provenance by using U-Pb and Hf isotopic analysis,

U-Pb ages of detrital zircons from the lowermost Nakdong Formation to uppermost Jindong Formation of the Gyeongsang Basin show a wide range from Archean to Cretaceous. Age distribution of detrital zircons from the Gyeoingsang Basin is generally similar to the adjacent rock types. The maximum depositional ages from the Nakdong Formation to Jindong Formation are 127.0 to 99.9 Ma belonging to the period from Aptian to Cenomanian.

The measured $\varepsilon_{Hf}(t)$ values from the detrital zircons of the Gyoengsang Basin vary from -44.0 to 18.2. Among these, most of early Cretaceous zircon grains from the Nakdong Formation to the Haman Formation underlying the Jindong Formation, distributed over the western area of the Gyeongsang Basin, have only negative $\varepsilon_{Hf}(t)$ values reflecting involvement of old continental components. In contrast to the early Cretaceous zircons from the Jindong Formation, distributed over the eastern area of the Gyeongsang Basin, display both negative and positive εHf(t) values. Such a presence of zircons with positive εHf(t) values suggests that more juvenile materials were involved in the volcanics affected the eastern sedimentary successions, indicating growing importance of mantle derived magma.

Therefore, we suggest that tectonic environment of the Gyeongsang Basin was changed from pull-apart basin at the beginning to back-arc basin.

References

Choi, T, Lee, YI, Orihashi, Y. (2012) Mesozoic detrital zircon U-Pb ages of modern river sediments in Korea: Implications for migration of arc magmatism in the Mesozoic East Asian continental margin: Terra Nova 24, p. 156–165.

Howard, AL, Farmer, GL, Amato, JM, Fedo, CM. (2015) Zircon U-Pb ages and Hf isotopic compositions indicate multiple sources for Grenvillian detrital zircon deposited in western Laurentia: Earth and Planetary Science Letters 423, p.300–310.

Mueller, PA, Foster, DA, Mogk, DW, Wooden, JL, Kamenow, G.D, Vogl, JJ. (2007) Detrital mineral chronology of the Uinta Mountain group: implications for the Grenville flood in southwestern Laurentia: Geology 35, 431–434.

Lee, T.-H, Park, K.-H, Yi, KY, Geng, J-z, Li, H-k. (2015) SRHIMP U-Pb ages and Hf isotopic composition of the detrital zircons from the Myogok Formation, SE Korea: development of terrestrial basin and igneous activity during the early Cretaceous: Geoscience Journal, 19, 189-203.

Kovdor pyrochlore U-Pb SHRIMP dating – some challenges and consequences

Lepekhina, EN, Antonov, AV, Belyatsky, BV, Rodionov, NV and Sergeev, SA

Centre of Isotopic Research, AP Karpinsky Geological Institute (VSEGEI), St-Peterburg, Russia

The dating of mineralization and ore-deposited processes is often hindered by the lack of suitable minerals associated with this process. Pyrochlore, complex tantalum-niobate: $A_2B_2X_6Y \times n\ H2O$, where A = [Na, Ca, Mn, Fe^{2+}, Sr, Sb, Cs, Ba, REE, Pb, Bi, Th, U], B = [Nb, Ta, Ti, Al, Fe^{3+}, Zr, Sn, W], X = [O, OH], and Y = [O, OH, F], is the main ore component defining Ta-Nb-rare metal mineralization in carbonatites, granite pegmatites and alkaline metasomatites, and as a mineral that contains high U and Th, can be as a geochronological alternative to zircon in silica undersaturated rocks and deposits.

Pyrochlore is the main host of rare-metal elements of the rocks of carbonatite series, including phoscorites, emerging at different stages of crystallization of carbonated alkaline magma at the mafic-ultramafic polyphase Kovdor massif (North Karelia, Russia). It is a common accessory mineral associated with baddeleyite, zircon, zirkelite, zirkonolite and others (Kukharenko et al., 1965; Subbotin, Subbotina, 2000; Krasnova et al., 2004). In some cases its share reaches significant amounts of rock volume – up to 5 vol.%. Pyrochlore forms octahedral and cube-octahedral crystals from mm up to 2-5 cm (Fig. 1a-c), from light yellow to black colors (Fig. 1c). Mineralogy and the chemical composition features of the Kovdor pyrochlore are described in detail previously (Williams, 1996; Subbotin, Subbotina, 2000; Mikhailova et al., 2016).

Materials and analytical methods

Primary beam of negative charged oxygen ions with 10kV energy focused through 200-m Koehler-aperture on the sample surface so that the size of the elliptical sampling crater was 40×30×2 m during pyrochlore local U-Pb SIMS SHRIMP-II analysis. The intensity of oxygen beam depending on pyrochlore U content was installed at 1-4 nA so that secondary UO^+ emission does not exceed the 1.5 MHz. Secondary ion currents were measured by SEM under single-collector mode and mass scanning. The ion source output 80-m slit in combination with 100-m width of the collector entrance slit provided the device mass resolution at least 5000 excluding isobaric overprint on analysed masses. The $^{202}(Nb_2O)^+$ has been selected as a reference characteristic peak within the Pb, U and Th (oxide) measured masses. The ionic currents of corresponding isotopes (in the mass range from 202 to 254 amu) were successively measured: $^{202}Nb_2O$ – 2s, ^{204}Pb – 20s, background $^{204.5}Pb$ – 10s, ^{206}Pb – from 2 to 10 s, ^{207}Pb – from 4 to 20, ^{208}Pb – from 1 to 10, ^{238}U from 2 to 10, ^{248}ThO – from 0.1 to 2, ^{254}UO – from 0.5 to 4 seconds. The integration time is dependent on the sample age and Pb, U and Th contents. Peak center procedure was performed on the mass-stations – $^{202}Nb_2O$, ^{206}Pb, ^{238}U, ^{248}ThO, ^{254}UO. Each single analysis consisted of 4-5 scans through these masses, and the total analysis time is reached up to 10-15 minutes.

Pyrochlore-331 from sövite II of the Vishnevogorsky massif (Urals) which is Sr-enriched type pyrochlore with 1.5-4.5 wt.% SrO and 1-2.5 wt.% LREE and is represented by octahedral crystals and grains of light brown, yellow and red–brown color, and is characterized by relative areal geochemical homogeneity with the age of 230 ± 1.3 Ma (TIMS) and U content of – 1500 ± 365 ppm, was used as our laboratory standard. The regular over 10 months SHRIMP-II analysis of pyrochlore-331 demonstrates a slight variation of obtained $^{206}Pb/^{238}U$ ratios by using of ln(Pb/U) *vs* ln(UO/U) linear calibration method. The measured $^{206}Pb/^{238}U$ ratios of unknown pyrochlore and standard were normalized to the value of 0.0363 which corresponds to the age of 230 Ma. The average error of measured isotopic ratios for standard pyrochlore varies in the range of 1-2% (2σ) with the number of analyses 10-15 per session (8-10 hours). ^{238}U concentration of the analysed pyrochlore grains was evaluated with respect to the average uranium content of the pyrochlore-331. The measured Pb isotope composition was corrected for common lead contribution according to the model Pb isotope composition at 380 Ma: $^{207}Pb/^{206}Pb$ = 0.851, $^{208}Pb/^{206}Pb$=2.082 and $^{206}Pb/^{204}Pb$=18.35. Raw-data processing and concordia plotting were performed using SQUID 1.0 и ISOPLOT/EX 3.5.

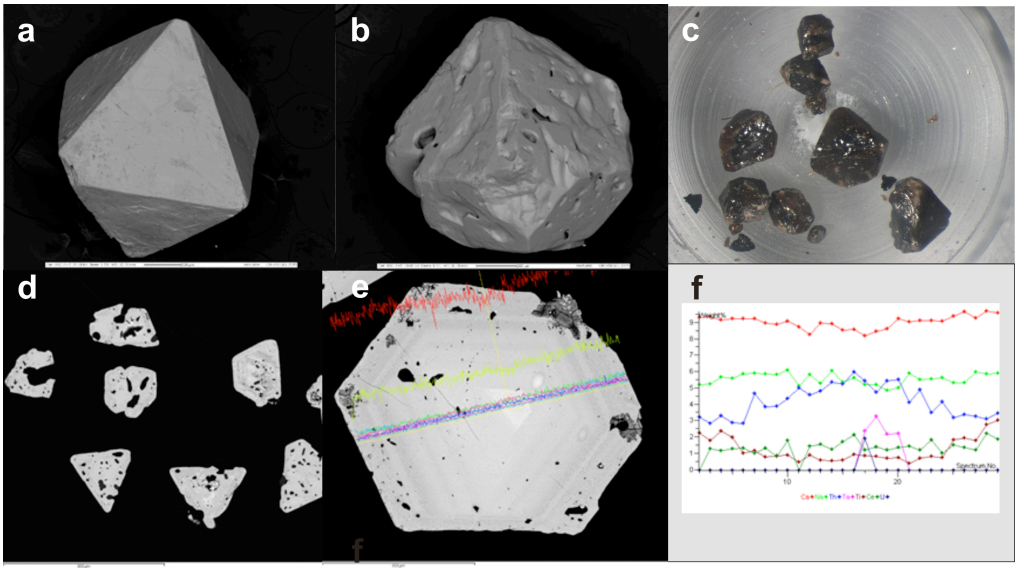

Fig.1. Back-scattered electron (BSE) images of pyrochlore crystals – sample 1069/2 (a) and 1066/3 (b); optic view of dark brown grains of 1079/2 pyrochlore (c); poikilitic pyrochlore grains (d); element profiles (EDS) across single grain (e) and element variations within the grain of Lens I pyrochlore (f).

We studied 5 pyrochlore samples from the early calcite carbonatites, late calcite-dolomite, and phoscorites at vicinity of the Votsuvaara Mountain (Kucharenko et al., 1965). Internal structure of pyrochlore grains examined by scanning electron microscope with energy dispersive spectrometry is characterized by zoning and monotonous with the boundary changes. The most grains are poikilitic due to numerous inclusions of carbonates and apatite (Fig. 1d-f). The Nb–Ta–Ti (a.p.f.u.) diagram shows that the compositions of all samples belong to pyrochlore subgroup (Fig 2a.). Some of pyrochlore compositions in (Ca+Na) – (U+Th+Pb) – (Ba+Sr+REE) diagram fall into the U-pyrochlore, Ba-Sr- and REE- pyrochlore fields (Fig. 2b). Our SIMS study was limited by the presence of UO_2 at 10 wt.% and ThO_2 at 5-7 wt.% or higher.

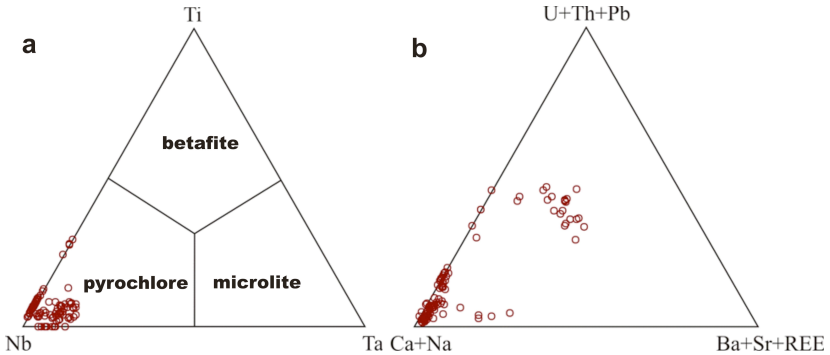

Fig.2. Chemical composition of the studied Kovdor pyrochlores in coordinates of Nb–Ta–Ti (a); and in cations of B site: (Ca+Na) – (U+Th+Pb) – (Ba+Sr+REE) (a.p.f.u.)

Results and conclusions

105 U-Pb SHRIMP-II analyses for 5 pyrochlore samples – about 20 analyses of individual grains in each sample were performed. It should be noted that the studied Kovdor massif pyrochlore differs by significant variations in Th and U, as well as U/Pb ratios, but in generally it is characterized by increased up to 6.5% U and an extremely high Th – up to 40% or more, and high values of Th/U ratio at n×100. It is noted a correlation of calculated U-Pb pyrochlore ages of different samples with variations in uranium, whereas the Th and Pb_{com} have a little effect on this value (Fig.3). Thus, for the most young pyrochlore from 1066-4 sample with the age 291 ± 6 Ma U varies from 3000 ppm to 3%, for sample 1079-2 and the age at 295 ± 9 Ma U changes from 100 ppm up to 6.6%, for "South" sample and 310.0 ± 4.6 Ma U variations are within the 1650 ppm and 6.65%, the 1066-3 sample has the age at 333.0 ± 4.7 Ma, and U content varies from 90 to 2000 ppm, and for the Lens I pyrochlore U from 30 to 400 ppm at the age of 363.4 ±7.8 Ma (Fig.4). The age of the Kovdor alkaline-ultramafic massif according to different isotope dating is within the range of 360-380 Ma (Kramm et al., 1993; Amelin, Zaitsev, 2002; Rukhlov, Bell, 2010; Rodionov et al., 2012) and obtained pyrochlore ages are significantly underestimated and may reflect the influence of the matrix effect or later low-temperature closing of the U-Pb pyrochlore system, as well as the actual chemical and structural transformations of pyrochlore crystals due to the interaction with the late carbonate fluids.

The obtained results of the local analysis of individual pyrochlore samples from Kovdor massif are shown in Figures 3-4 and evidence the principal possibility of the U-pyrochlore and pyrochlore with high U and Th U-Pb dating by SHRIMP-II ion microprobe. An obvious limitation of the method is the similarity of the chemical composition and crystalline matrix of the standard mineral. We used as a standard pyrochlore-331 which is pretty close in age (230 and 380 Ma), Pb_{com} and Th contents to Kovdor pyrochlore from carbonatites and phoscorites but for U it was not the case.

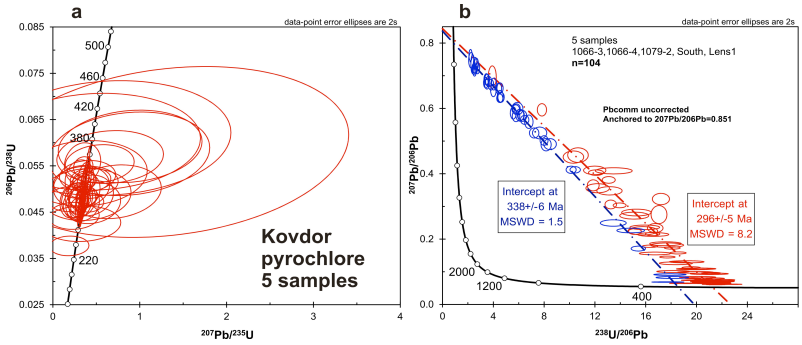

Fig.3. U-Pb concordia diagram for 5 pyrochlore samples from Kovdor carbonatites and phoscorites. Excess age dispersion for studied pyrochlore along concordia from 240 to 400 Ma is evident (a); all 104 pyrochlore analysis in the $^{207}Pb/^{206}Pb$-$^{238}U/^{206}Pb$ coordinates form the two trends with fixed upper intersection with the ordinate at 0.851 which correspond to the ages of 296 ± 5 and 338 ± 6 Ma (b).

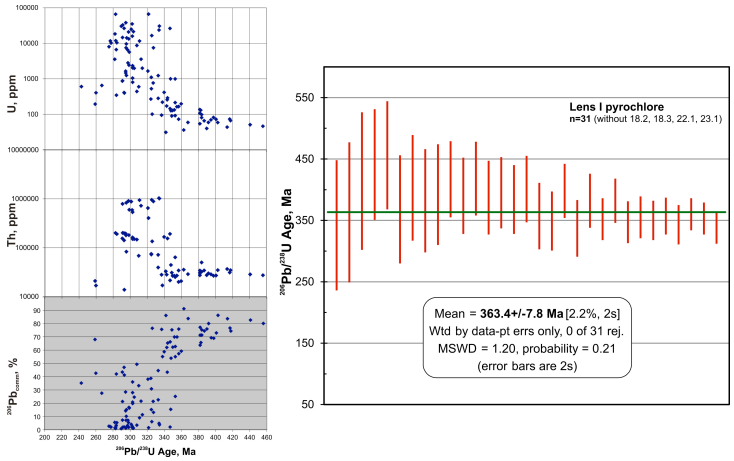

Fig.4. Correlation of calculated $^{206}Pb/^{238}U$ ages of the individual pyrochlore grains with Th, U and common lead ($^{206}Pb_{com}$) contents and the weighted average age calculated for individual grains of Lens I pyrochlore.

Formation and transformation of pyrochlore group minerals from Kovdor carbonatites and phoscorites occur successively in several stages with the corresponding changes of U-Pb pyrochlore systematics. Thus the early pyrochlores and U-pyrochlores crystallized at 364 Ma within phoscorites and early calcite carbonatites (Fig.4), and the Sr- and Ba-pyrochlores of late calcite-dolomite carbonatite formed at 340 Ma, while their re-crystallization with the formation of the Th-pyrochlore rims occured at the later stages of the interaction with metasomatizing fluids 290 m.y. ago (Fig.3). Such evolution of the chemical composition and pyrochlore transformation are known for other alkaline ultramafic massifs of the Karelia-Kola region (Lee et al., 2006; Zaitsev et al., 2012).

Acknowledgements

Our study was carried out in the framework of the state contract with Sevzapnedra (Rosnedra) K41.2014.014 on the pyrochlore collection sampled during 1964-1966 by the researches of the Mineralogy Department of the St. Petersburg State University: Rimsky-Korsakova O.M., Afanasyev B.V., Kirillov A.S., Krasnova N.I.

References

Amelin, Yu, Zaitsev, AN. (2002) Precise geochronology of phoscorites and carbonatites: the critical role of U-series disequilibrium in age interpretations. Geochimica et Cosmochimica Acta 66, 2399–2419.

Krasnova, NI, Balaganskaya, EG, Garcia, D. (2004) Kovdor - classic phoscorites and carbonatites. In: Phoscorites and Carbonatites from Mantle to Mine: the Key Example of the Kola Alkaline Province (Wall, F, Zaitsev, AN, eds), Mineralogical Society Series, Mineralogical Society, London, 10, 99–132.

Kramm, U, Kogarko, LN, Kononova, VA, Vartiainen, H. (1993) The Kola alkaline province of the CIS and Finland: Precise Rb-Sr ages define 380-360 Ma ages for all magmatism. Lithos 30, 33–44.

Kukharenko, AA, Orlova, MP, Bulakh, AG, Bagdasarov, EA, Rimskaya-Korsakova, OM, Nefedov, EI, Ilinsky, GA, Sergeev, AS, Abakumova, NB. (1965) The Caledonian Complexes of Ultrabasic-Alkaline and Carbonatite Rocks on Kola Peninsula and in Northern Karelia (Geology, Petrology, Mineralogy and Geochemistry). Nedra, Moscow, 772 p [in Russian].

Lee, MJ, Lee, JI, Garcia, D, Moutte, J, Williams, CT, Wall, F, Kim, Y. (2006) Pyrochlore chemistry from the Sokli phoscorite-carbonatite complex, Finland: implications for the genesis of phoskorite and carbonatite association. Geochemical Journal 40, 1–13.

Mikhailova, JA, Kalashnikov, AO, Sokharev, VA, Pakhomovsky, YA, Konopleva, NG, Yakovenchuk, VN, Bazai, AV, Goryyainov, PM, Ivanyuk, GYu. (2015) 3D mineralogical mapping of the Kovdor phoskorite-carbonatite complex (Russia). Mineralium Deposita 51, 131–149.

Rodionov, NV, Belyatsky, BV, Antonov, AV, Kapitonov, IN, Sergeev, SA. (2012) Comparative in-situ U–Th–Pb geochronology and trace element composition of baddeleyite and low-U zircon from carbonatites of the Palaeozoic Kovdor alkaline–ultramafic complex, Kola Peninsula, Russia. Gondwana Research 21, 728–744.

Rukhlov, AS, Bell, K. (2010) Geochronology of carbonatites from the Canadian and Baltic Shields, and the Canadian Cordillera: clues to mantle evolution. Mineralogy and Petrology 98, 11–54.

Subbotin, VV, Subbotina, GF. (2000) Pyrochlore group minerals from phoscorites and carbonatites of Kola Peninsula. Vestnik MGTU 3(2), 273–284 [in Russian].

Williams, CT. (1996) The occurrence of niobian zirconolite, pyrochlore and baddeleyite in the Kovdor carbonatite complex, Kola Peninsula, Russia. Mineralogical Magazine 60, 639–646.

Zaitsev, AN, Williams, CT, Wall, F, Zolotarev, AA. (2012) Evolution of chemical composition of pyrochlore group minerals from phoscorites and carbonatites of the Khibina alkaline massif. Geology of Ore Deposits 54(7), 503–515.

TOF-SIMS Development at the Beijing SHRIMP Centre

Liu, D[1], Clement, S[2], Long, T[1], Bao, Z[1], Wang, P[1] and Yang, Z[1]

1: The Beijing SHRIMP Centre
2. Ion Optical Consulting, Prince Edward Island, Canada

This presentation describes a Time-of-Flight Mass Spectrometer currently being developed at the Beijing SHRIMP Centre, in cooperation with the Dalian Institute of Chemical Physics and Jilin University. When fully operational, this new mass spectrometer will complement the existing SHRIMP II instruments currently in use at the Centre. In general, TOF-SIMS instruments cannot achieve the type of precision typical of the SHRIMP or other large ion microprobes based on magnet sector double-focusing secondary analysers. However, the TOF instrument has the advantage of being able to record every secondary ion species emitted from the target, whereas the magnetic sector instruments can only measure a limited number of secondary ion species at one time, depending on the number of detector heads in available in the multiple collector.

The new TOF-SIMS instrument is intended to provide a secondary mass resolution of approximately 8000, defined at the 10% peak height level, with a 10 ns primary pulse. The total path length for secondary ions is approximately 8.2 m and includes two second order, two stage, reflectrons. The target region incorporates a Schwartzchild optical viewing microscope to provide continuous visual monitoring of the target during analysis, independent of the secondary particles being measured. Precise sample positioning is accomplished using individual external drives connected through small edge-welded bellows. Two separate primary columns can be mounted, in addition to an electron gun if required. Primary spot sizes, in critical focusing mode, can be as small as a few microns or less, depending on primary ion species and intensity. Provision has been made for primary scanning to allow imaging in terms of secondary ion distributions, although the main objective has been to achieve the highest precision possible in isotopic or elemental abundance measurements from a single spot in a given analysis time.

The new TOF-SIMS instrument is presently in the initial stage of testing and adjustment.

Acknowledgements

This work is supported by the National Major Scientific Instruments and Equipment Project of China (No. 2011YQ050069).

SHRIMP-TIMS comparison of zircons analysed on the Geoscience Australia SHRIMP

Magee, CW, Jr., Bodorkos, S and Lewis, C

Geoscience Australia Canberra ACT, Australia

An important part of any analytical procedure is to ensure that results are accurate. Geoscience Australia (GA) has been fortunate in that, during the last several years, the use of high-precision CA-ID-TIMS for chronostratigraphy in Australian sedimentary basins has given us access to a substantial selection of precisely dated zircons, which we can use to cross-correlate the SHRIMP and TIMS ages throughout the Phanerozoic. Combined with other double dated samples which have come through our lab, this gives us the ability to plot dozens of doubly dated samples for comparison. Potential sources of disagreement, both geological and analytical, can be investigated using these data. With the exception of two Guadalupian SHRIMP ages, all SHRIMP data presented here was generated in-house on the Geoscience Australia instrument.

Figure 1 shows 22 Permian zircons which have been dated using both CA-ID-TIMS and SHRIMP. Agreement outside of the Guadalupian is quite good. However, both SHRIMP ages from Rowan Event tuffs in the Hunter Basin have SHRIMP ages that are about 1% younger relative to the chemically abraded grains. The Rowan Event samples were analysed with different SHRIMP instruments, different reference zircons, and on different stratigraphic samples, but show surprising agreement with each other despite these differences. One additional Guadalupian sample from the Canning Basin gives a SHRIMP age 2.24% too old. However, the remaining two Guadalupian samples have SHRIMP and TIMS ages that agree within SHRIMP uncertainty.

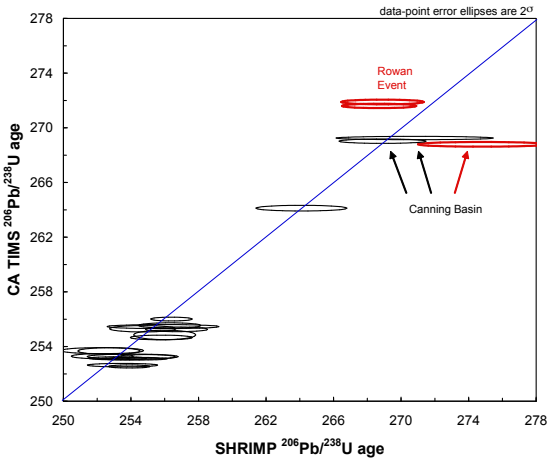

Figure 1. SHRIMP vs. TIMS ages for the Permian.

Aside from these three problematic Guadalupian samples, only one of the SHRIMP-TIMS double dated samples with Temora 2-referenced ages analysed on the GA SHRIMP differ from the CA-ID-TIMS ages by more than 1%, and that analysis (Bishop Tuff, Ickert et al. 2015) is within the (large) uncertainty envelope (Figure 2). Note, however, that with all 29 of these samples, the slope of the SHRIMP vs TIMS line is not quite 1. This is a result of the slope being heavily influenced by the ~ 0.8 Ma Pleistocene Bishop Tuff analysis, in which the SHRIMP and CA-ID-TIMS ages are known to be different due to zircon growth kinetics (Ickert et al. 2015). Excluding this point from the analysis yields a (less precise) line fit within 0.2‰, and well within uncertainty of 1 (Figure 3).

In conclusion, the slope of 1 on the line suggests that, at least at this scale, there is no age-dependency or radiation dose dependency in the accuracy of the SHRIMP. The calibration constant is, within uncertainty, constant. The near zero intercept suggests that either there are no systematic biases, or that we have picked out a reference value for Temora-2 that coincidentally balances out effects of Pb loss, antecrystal ingrowth, and other systematic effects.

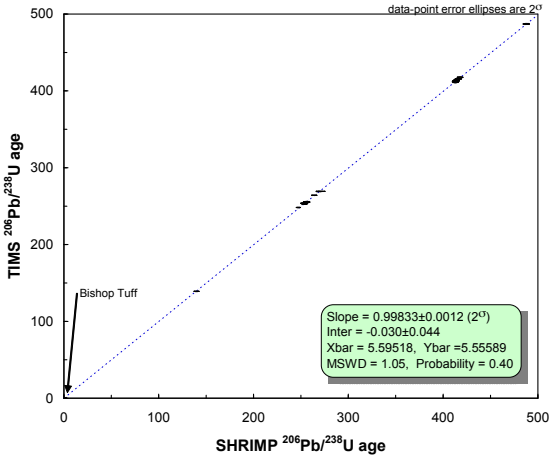

Figure 2. Twenty-nine of 32 grain slope fit for Phanerozoic SHRIMP vs. CA-ID-TIMS doubly dated samples at GA.

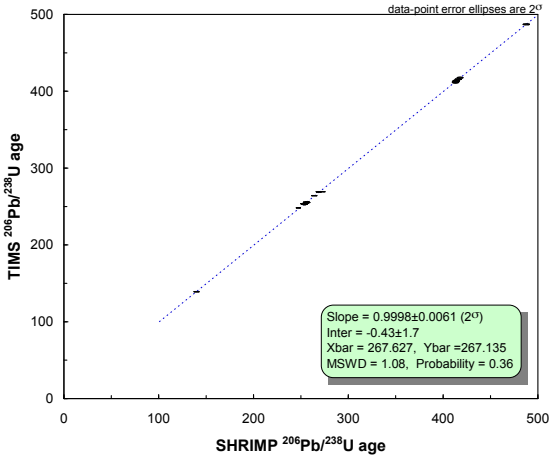

Figure 3. Twenty-eight of 32 grain slope fit for Phanerozoic SHRIMP vs. CA-ID-TIMS doubly dated samples from GA.

References

Ickert, RB, Mundil R, Magee, CWJr, Mulcahy, SR. (2015) The U-Th-Pb systematics of zircon from the Bishop Tuff: A case study in challenges to high-precision Pb/U geochronology at the millennial scale. Geochimica et Cosmochimica Acta 168, 88-110.

Positive primary column, primary secondary ion operation of SHRIMP

Magee, CW,Jr.[1], Hyder, JH[2] and Butres, R[2]

1: Geoscience Australia. Canberra ACT Australia
2: Australian Scientific Instruments. Fyshwick ACT Australia

The original SHRIMP was designed to handle all four polarity permutations of primary and secondary beam charge. However, it was determined early on that in the absence of an electron gun, the use of negative oxygen primary ions for positive secondary ion yield was the most useful for geochronology and other cation analyses for which the instrument was typically used. The commercial SHRIMP II instrument was designed on the assumption that only oppositely charged primary and secondary ions would be analysed. However, the similar ion optical design allows the SHRIMP II to be retrofitted to enable same polarity secondary and primary ions with a few key changes. Recently, Schmitt and Zack (2012) showed that the use of a positive O_2^+ primary beam in a 1270 ion probe allows for vast improvements in counting stats on low Pb conductive minerals, such as rutile.

Unlike the 1270, the SHRIMP II is not equipped for off-the-shelf +,+ operation from the factory. So a few changes were made.

Polarity reversal in the CAMECA ion microscopes is relatively straightforward, because both the primary and secondary column are ground referenced, and only the ion source and the sample are held at potential. As the SHRIMP has a floating primary column, using positive ions for both primary and secondary ion requires stacking the voltage, so that the source is at almost the combined potential relative to ground. As the Duo (and Duo power supply) to ground potential is 19.3 kV, components not designed for this voltage need to be reassessed and upgraded, if necessary.

The key issue on the commercial SHRIMP II instruments is the gas feed line that goes from a gas supply at ground, through a ~1 atmosphere insulator to a needle valve to drop the pressure, through a pressure gauge to measure the pressure, and then into the duoplasmatron. The gauge is powered by an isolation transformer that is only rated to 15kV. What we have done is to ground the bleed valve and gauge, and move the vacuum break to the low pressure side of the gas feed line. Low pressure discharge is prevented by the use of a bead-filled insulator supplied by ASI, an approach used on 1980's era PHI quadrupole SIMS.

Positive ion extraction from the duoplasmatron utilizes an intermediate aperture with zero offset (as electrons are repelled, not attracted, by the accelerating voltage) and use of only one of the three ring magnets. Operation in this mode is generally straightforward, although the emission of like-charged secondary ions results in the Primary Beam Monitor (PBM) being less than, not greater than the true primary beam current. Additionally, the opposite direction of primary beam deflection due to the sample potential causes a spot position shift that has to be compensated for by a change in the working distance.

Preliminary results show that Baddeleyite and zircon act as insulators and do not emit in the absence of a charge-compensating electron gun. However, in rutile, count rates of up to 50,000 cps $^{206}Pb^{+}$ can be achieved in Mesoproterozoic rutiles, allowing better counting statistics than are possible with the dimmer O_2^{-} primary beam. The development work required to ascertain accuracy and precision is ongoing.

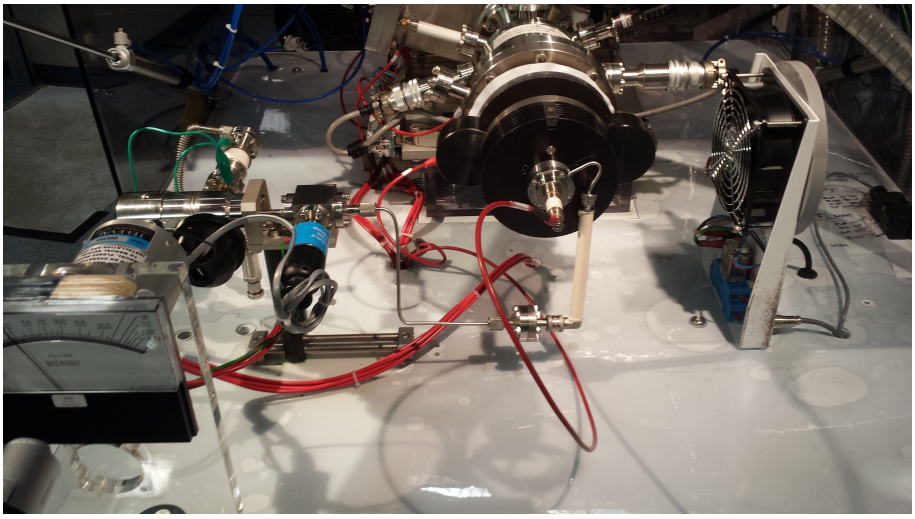

Figure 1. Alteration of gas feed line for voltage stacking on a SHRIMP II instrument. The green alligator clip bypasses the old gas line insulator, grounding the gas gauge and needle valve. The low pressure gas line insulator is below and to the right of the duoplasmatron, and successfully holds off 20kV. Rewiring in the HV cabinet is not shown.

References

Schmitt, AK, Zack, T. (2012) High-sensitivity U-Pb rutile dating by secondary ion mass spectrometry (SIMS) with an O_2^{+} primary beam. Chemical Geology 332, 65-73

SHRIMP Stable Isotope (-SI): first results for triple-oxygen using synthetic and natural olivine, with application to meteorites and other planetary materials

McKibbin, SJ[1], Ávila, JN[2], Holden, P[2], Ireland, TR[2], Friedrichs, B[3], Pack, A[3] and Claeys, Ph[1]

1: Vrije Universiteit Brussel, Brussels, Belgium.
2: Australian National University, Canberra, Australia.
3: Georg-August-Universität, Göttingen, Germany.

Introduction

Triple oxygen isotope data are powerful tools for investigating the provenance of early Solar System materials ($^{18}O/^{16}O$ and $^{17}O/^{16}O$ expressed as $\delta^{18}O$ and the mass-independent component, or deviation from a mass-dependent fractionation reference line, $\Delta^{17}O$ [e.g. 1]). They are often used to investigate relationships between meteorites (usually chondrites) and micro-meteoritic materials [e.g. 2]. Early investigations used in-situ approaches by Secondary Ion Mass Spectrometry (SIMS) [3,4,5] while a similar number of micrometeorites have since been investigated by higher precision Laser-assisted Fluorination Mass Spectrometry (LFMS) [6,7,8]. While LFMS is established as a tool in

planetary work where high precision is needed due to small isotopic variations, SIMS trades precision for the ability to probe a larger number of samples, and is particularly suited to addressing chondritic (nebular, rather than planetary) materials and has the advantage that small samples, such as micrometeorites, are preserved for further studies. Therefore, we are revisiting the potential of SIMS to screen large numbers of micrometeorites and other chondritic materials with a focus on the common mineral olivine (formula $[Mg,Fe]_2SiO_4$ with molar composition given by Mg# = 100 * Mg/(Mg+Fe)).

Methods

Previously, olivine has been synthesized for Sensitive High-mass Resolution Ion Micro-Probe (SHRIMP) work on Mn-Cr isotopes [9]. We have repurposed these olivine reference materials for triple-oxygen isotopes, to be analysed by SHRIMP Stable Isotope (-SI), a prototype SIMS instrument. Olivine separates and large grains (~2 mg) were fluorinated and analyzed by Thermo MAT 253 [1], and small individual grains analysed (via ~30 µm diameter sampling pits) by SHRIMP-SI [modified from the sulfur method of 10]. So far we have found no bias on $\delta^{18}O$ for SHRIMP as a function of Mg# in olivine in the range 90-50 that covers most meteoritic materials [11]. To assess variation in the abundance of ^{17}O that is unrelated to mass-dependent fractionation, we calculate $\Delta^{17}O$ as $\delta^{17}O - \delta^{18}O * 0.5305$ (updated from previous reference lines which were lower, e.g. 0.52 [12]) relative to VSMOW [1] and correcting San Carlos terrestrial mantle olivine to $\delta^{18}O = 5.19$ ‰.

Results and Discussion

Synthetic olivines are displaced to higher $\delta^{18}O$ and lower $\Delta^{17}O$ (Figure 1), are roughly intermediate to lithospheric and atmospheric compositions [1], consistent with their synthesis from industrial reagents that probably involved oxidation of metals. Correspondence between SHRIMP-SI and LFMS measurements is (except for very Fe-rich olivine) excellent for $\delta^{18}O$, while for $\Delta^{17}O$ we find a slight offset between the two techniques, although both find lower $\Delta^{17}O$ for synthetic olivine. By comparison with previous sulfur work by SHRIMP-SI that has achieved 0.1 ‰ (1-sigma) on the statistically similar variable $\Delta^{33}S$ [10], it can be seen that some improvement in precision should be possible. Current limitations probably include counting time, charge negation via electron gun or column, and detector efficiency. The latter might account for the offset in $\Delta^{17}O$.

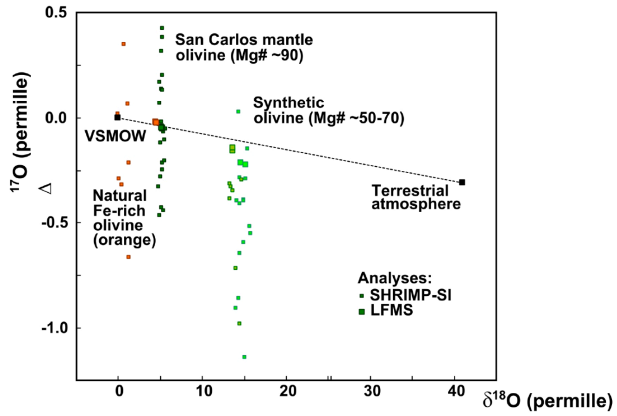

Figure 1: Triple oxygen isotope data for natural and synthetic olivine. LFMS in large points; SIMS data by SHRIMP-SI in small points. Isotope ratios were calculated relative to VSMOW using a reference line with slope 0.5305 rather than previous calibrations using 0.52. At the achieved precisions, the terrestrial mantle and atmosphere are resolved, and an atmospheric signature is visible in the synthetic olivines.

References

[1] Pack and Herwartz (2014) EPSL 390, 138-145.

[2] Soens et al. (2016) *SHRIMP Workshop, Granada (this meeting)*.

[3] Engrand et al. (2005) GCA 69, 5365-5385.

[4] Taylor et al. (2005) GCA 69, 2647–2662.

[5] Yada et al. (2005) GCA 69, 5789–5804.

[6] Suavet et al. (2010) EPSL 293, 313-320.

[7] Cordier et al. (2011) GCA 75, 5203-5218.

[8] Cordier et al. (2012) GCA 77, 515-529.

[9] McKibbin et al. (2013) GCA 110, 216-228.

[10] Ireland et al. (2014) Int. J. Mass. Spec. 359, 26-37.

[11] McKibbin et al. (2016) *Meteoritical Society Meeting*.

[12] Clayton (2008). *Reviews in Mineralogy*. 68, 5–14.

Rutile U/Pb geochronology and geochemistry by SHRIMP: some observations

McNaughton, NJ[1], Talavera, C[1], Porter, JK[12], Evans, NJ[12] and McInnes, BIA[1]

1: John de Laeter Centre for Isotope Research, Curtin University, Australia
2: Department of Applied Geology, Curtin University, Australia

Introduction

Rutile generally contains less U than other minerals traditionally used for SHRIMP U/Pb geochronology and yields poorer age precision as a result. However, rutile also carries trace elements, some of which reflect their environment of formation, including during ore genesis (e.g. Clark & Williams-Jones, 2004). Rutile, along with zircon, garnet and ilmenite, is a robust mineral during sediment transport and typically accumulates in more mature sedimentary rocks. Combining these attributes, detrital rutiles in siliciclastic sediments and sedimentary rocks provide a complementary source of information to zircon about sediment provenance. Given the increasing emphasis of zircon "chemical and isotopic fingerprints" in provenance studies, we are considering the same application in rutile.

Rutile standards

There are few suitable rutile standards available for SHRIMP studies. The earliest SHRIMP work by Clark et al. (2000) used a multigrain rutile standard (Windmill Hill - WH) separated from a granulite facies quartzite. Zircons from the same sample gave much older ages than the rutile, reflecting provenance ages, and indicated that the rutiles were either reset detrital or were metamorphic in origin. Nonetheless, with few exceptions, the SHRIMP U/Pb and Pb-Pb ages of analyses from multiple grains of WH are consistent. Luvizotto et al. (2009) and Zack et al. (2011) assessed a number of potential rutile standards and via collaboration we have confirmed that R10 appears to be the most homogeneous in age and U-content, and has sufficient U-content for our geochronology purposes.

SHRIMP methodology

The procedures for SHRIMP analysis of rutile have been previously published (Clark et al., 2000; Taylor et al., 2012). One key observation is that rutile excludes Th from its structure, allowing common Pb corrections by the 208-correction method with far greater precision than the more commonly used 204-correction method. However, rutile analysis by SHRIMP suffers from crystal orientation effects, which not only perturbs U/Pb calibrations (Taylor et al., 2012) but also makes measurements of U-contents uncertain as the count-rate on the reference peak ($Ti_3O_3^+$ at mass 192) varies by >4, depending on orientation alone.

The SHRIMP community generally uses an O_2^- primary beam for routine U/Pb geochronology, which is thought to give more consistent data for standards and unknowns, compared to O^-. All previous SHRIMP studies of rutile utilise a primary beam of O_2^-. Our preliminary studies of rutile analysis by SHRIMP using both a O_2^- and O^- primary beam, on the same grains during the same analytical session, show much less variation in the 192 reference peak count-rate per nanoamp for the O^- primary beam compared to O_2^- (Fig. 1). Further, the uncertainty in the U/Pb calibration for the O^- beam data is comparable to O_2^- beam data, suggesting the orientation effect observed in data collected with a O^- primary beam is minimal or absent. We further note that the 208-corrected $^{207}Pb/^{206}Pb$ age for the O_2^- and O^- data collected on WH during the same session are indistinguishable in accuracy and precision, suggesting there is no apparent advantage using the O_2^- primary beam, as uniformly done with zircons.

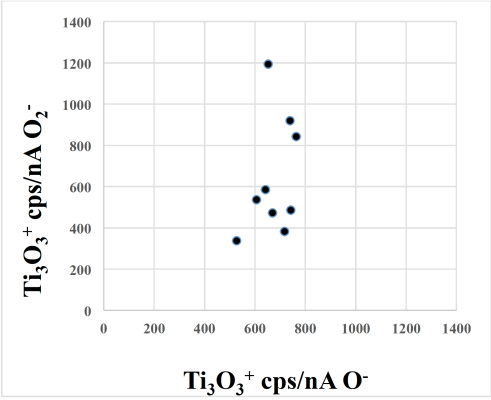

Figure 1. $Ti_3O_3^+$ (at mass 192) counts per second, per nanoamp of primary beam, for data collected with an O_2^- and O^- primary beam from the same grains of the Windmill Hill rutile standard. The grains are in random orientation.

However, as O_2^- primary beam-derived data is entrenched in routine SHRIMP U/Pb geochronology and trace element analyses in rutile are referenced to the mass 192 peak which varies by >4, we seek to address the problem of correcting for the rutile orientation effect from O_2^--derived data. To do this, it is necessary to have a rutile standard which is homogeneous in a trace element of interest. The multigrain WH standard is unlikely to be completely homogeneous in trace elements, but initial LA-ICPMS data shows only 7.5% variation (2σ; n=28 out of 28) from the reference value for U (Clark et al., 2000). There is similarly a coherent correlation between the apparent U-content and $Ti_3O_3^+$ from SHRIMP data (Fig. 2) confirming that the U-content of WH grains is reasonably constant and the apparent variation (in SHRIMP data) may be due to orientation effects alone.

Trace elements in rutile

Tungsten and Sn are trace elements in rutile that appear to be reliable fingerprints of mineralisation (Clark & Williams-Jones, 2004; Meinhold 2010). Hence an exploration strategy for gold is: (i) stream sediment sampling, (ii) rutile separation, and (iii) analysis for W without Sn, whereas Sn±W enrichment may reflect base metal mineralisation. As rutiles that formed during mineralisation also preserve the age of mineralisation, it is desirable to measure both age and W-Sn-contents during the same analysis. Tungsten can be measured in a rutile SHRIMP run table at both mass 200 (WO^+) and 216 (WO_2^+), where it is normally sufficiently abundant to peak centre. However, as with U, the orientation effect from using the O_2^- primary beam must be corrected for. The count-rate for the most abundant Sn species at mass 252 (Sn_2O^+) is too low for peak-centring measurements in all but Sn-rich rutiles.

Conclusions

Protocols for rutile geochronology and geochemical analyses by SHRIMP may have to be reconsidered in the light of observations presented herein.

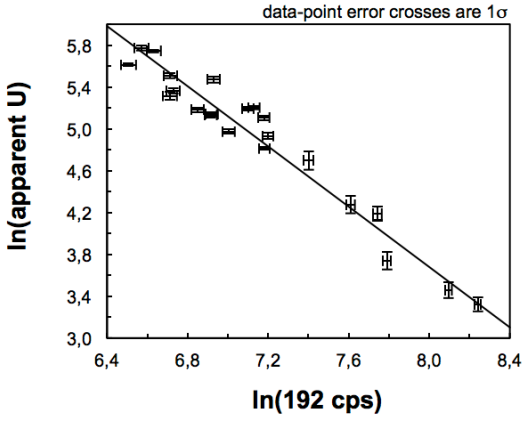

Figure 2: Ln-ln plot of multigrain WH standard data using a O2- primary beam in a single SHRIMP session. Plot of the apparent U-content (i.e. ln U (ppm) with calculated U-contents using SQUID with

analyses referenced to the 192 peak: Ti3O3+) vs 192 (counts/second). The grains are in random orientations.

References

Clark, DJ, Hensen, BJ, Kinny, PD. (2000) Geological constraints for a two-stage history of the Albany-Fraser Orogen, Western Australia. Precambrian Research 102, 155-183.

Clark, JR, Williams-Jones, AE. (2004) Rutile as a potential indicator mineral for metamorphosed metallic ore deposits. Rapport Final de DIVEX, Sous-project SC2, Montreal, Canada. 17 pp.

Luvizotto, GL, Zack, T, Meyer, HP, Ludwig, T, Triebold, S, Kronz, A, Munker,C, Stockli, DF, Prowatke, S, Klemme, S, Javob, DE, von Eynatten, H. (2009) Rutile crystals as potential trace element and isotope mineral standards for microanalysis. Chemical Geology 261, 346-369.

Meinhold, G. (2010) Rutile and its applications in Earth Sciences. Earth-Science Reviews 102, 1-28.

Taylor, R, Clark, C, Reddy, SM. (2012) The effect of grain orientation on secondary ion mass spectrometry (SIMS) analysis of rutile. Chemical Geology 300-301, 81-87.

Zack, T, Stockli, DF, Luvizotto, GL, Barth, MG, Belousova, E, Wolfe, MR, Hinton, RW. (2011) In situ U-Pb rutile dating by LA-ICP-MS: ^{208}Pb correction and prospects for geological applications. Contributions to Mineralogy and Petrology 162, 515-530.

The δ^{18}O zircon isotope composition & U-Pb geochronology on SHRIMP IIe/MC - An example from the foreland of the Variscan orogenic belt (S Poland)

Mikulski, SZ[1], Krzemińska, E[1] and Czupyt, Z[1]

1. Polish Geological Institute- National Research Institute, Warszawa, Poland

U-Pb age analyses combined with oxygen isotopic ratios on dated zircons grains becomes high effective analytical routine being increasingly used in regional geological investigations. The microanalytical study of zircon oxygen isotopic composition expresses as δ^{18}O, allows discriminating among possible sources of magma origin in terms of possible contributions of mantle and crustal components and detecting the roles of assimilation and magma mixing and potential hydrothermal influence (Bindeman, 2008). In this study we used a narrow range of δ^{18}O = 5.3±0.3‰, characteristic for mantle crystallized zircons (Valley, 2003), as a reference of relative mantle vs. crustal melt interactions. Every incorporation of higher δ^{18}O material (e.g. supracrustal rocks) that is crustal contamination can strongly affect oxygen isotopes in igneous rocks resulted in modification of diagnostic values towards higher δ^{18}O in magmatic zircon. Typical Phanerozoic *I*-type granitoids, which were formed by melting of igneous rocks derived from an arc processes tend to, have δ^{18}O values below 9‰. In contrast *S*-type granitoids derived by melting of clay- rich sedimentary rocks have higher values of δ^{18}O up to 15 ‰. The U-Pb dating's of igneous rocks associated with orogenic processes, and studies of their petrogenesis on the basis of δ^{18}O isotopic composition measured on the exactly the same spot may provide valuable information on the magma genesis, as well as the overall evolution of a crustal blocks.

We present a new set of integrated U-Pb and O isotope data of zircon samples derived from the Małopolska Block (MB) of Variscan Foreland, from the area known as one of the Baltica's proximal terrane. Although U-Pb zircon age results achieved on SHRIMP II were recently published (Żelażniewicz et al., 2008), but U-Pb & O isotope investigation in the considering area of the MB remains unique. Along the SW margin of the (MB) in the vicinity of the Krakow–Lubliniec Fault Zone (KLFZ), silicic calc-alkaline igneous plutons intruded from c.a. 310 Ma to 290 Ma (^{206}Pb/^{238}U, mean age 300.3 ±3.2 Ma for n=18), with no record of inherited components. The presence of euhedral to subhedral cores in some zircon grains compared with particular patterns of the U-Pb results has been interpreted as two stages of zircon growth at 304 ±2 Ma and then at 294 ±3 Ma. In general the MB magmatism was coeval with post-collisional granite intrusions in the Central European Variscides (*op cit.*). In the considering area of the KLFZ, especially on the MB occurs porphyry Mo-Cu-W mineralization.

The zircon SEM cathodoluminescence (CL) imaging were made on HITACHI SU 35 with innovative optics (Fig.1). The U-Pb and O isotope measurements were carried out in PGI-NRI on SHRIMP IIe/MC during two analytical cycles, starting from geochronology in March, 2015 and after regular routine of changing polarity, completed in June 2015. U-Pb and O isotopic compositions were subsequently measured in the same grains and areas after polishing and cleaning procedure. Selected areas in the grains were analysed for U, Th and Pb isotopes using a procedure similar to that described by Williams and Claesson (1987) but for O isotopes according to routine decribed by Ickert et al. 2008. The compositions were measured relative to zircon standard Temora (U/Pb = 416 Ma and $\delta^{18}O$ = 8.2‰ VSMOW) accompanied with SL reference material. U-Pb for each spot was collected in sets of five scans through the mass range. The spots for analysis were selected to avoid textural fractures and inclusions but to check some unusual features of zircon cores.

Two hundred and twenty analyses were performed on one hundred eighty zircon grains from five samples from MB, forenland area and about one hundred from other three localities within Sudetian Variscides. In practice, from 18 to approximately 60 results (U-Pb&O) have been obtained. In this report the $^{206}Pb/^{238}U$ ages are preferred because they have smaller uncertainties (also on Fig.1).

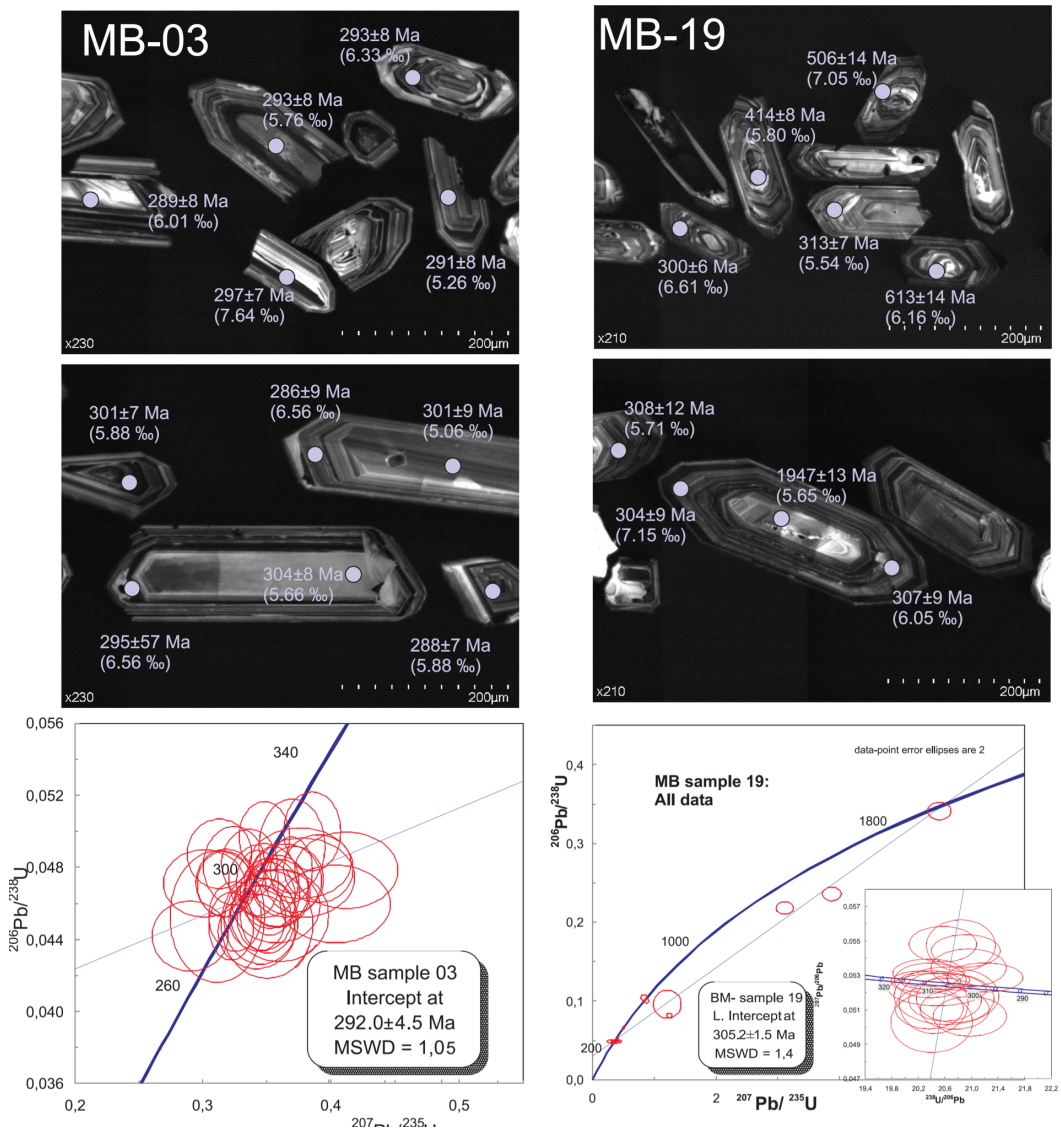

Figure1. Representative CL images of zircon samples 03 (porphyritic dacite) and 19 (micrograno-diorite) from Variscan Foreland MB showing igneous oscillatory zoning and a few inherided cores. Selected spot locations and $\delta^{18}O$ and Pb –Pb age results are marked. Below, the appropriate concordia diagrams showing lower intercept age defined as crystallization time.

The weighted average $^{206}Pb/^{238}U$ ages of five samples from MB varies from 283 ±3.8 Ma to 305 ±4 Ma that is actually similar to previously obtained chronology on the only one sample (Żelaźniewicz et

al., 2008) for the MB. However, our detailed age investigation reveals also several inheritances. Sometimes (see sample 19 on Fig.1) older cores were recorded in 8 from 33 analysed grains. In general inherited zircons in the MB igneous rocks define an age range of *ca*. 411-1947 Ma displaying predominant Neoproterozoic population (6 grains) with minor Mesoproterozoic group. The oxygen results on zircons from MB samples gave a narrow range of mean average values $\delta^{18}O$ between 6.33 ±0.14‰ and 6.72 ±0.20‰ (*vs.* SMOW). Two extreme examples shown on fig. 1, (sample 03, porphyritic dacite and sample 19, micrograno-diorite) reveal of 40% and 36% of the mantle grains.

Conclusions

The overall results of oxygen isotopes on SHRIMP IIe/MC, show evident homogeneity in $\delta^{18}O$ values in the studied zircons from the Małopolska Block (MB) that was the foreland of the Variscan orogenic belt in the southern Poland. Surprisingly, there is a significant amount of mantle related zircons (~5.3 ±0.6 ‰ 2σ) within each of the tested MB samples emplaced within the age range from 305 to 283 Ma (U-Pb). For comparison in zircons from the Variscan granites and related rocks (also from the Western Europe) the values of $\delta^{18}O$ higher than 7 ‰ have been observed (e.g. Mikulski et al., 2014, Sola et al. 2009). Studied zircons are characterized also by the presence of inherited zircons displaying predominant Neoproterozoic (590-680 Mas) population with minor Mesoproterozoic group (ca. 1.200-1.300 Ma). The last one group of inherited zircons is quite common in the pyroclastic and epicalstic rocks in SE Poland on the East European Platform.

The newly obtained crystallization ages and the isotopic composition of zircons may be used to reconstruct the evolution of magmatic systems of MB, thus they provide insights into the formation of the continental crust of MB proximal terrane.

References

Bindeman I. (2008) Oxygen isotopes in mantle and crustal magmas as revealed by single crystal analysis. Reviews in Mineralogy & Geochemistry, 69, 445-478.

Ickert, RB, Hiess, J, Williams, I S, Holden, P, Ireland, TR, Lanc, P, Schram, N, Foster, J, Clement, SW. (2008) Determining high precision, in situ, oxygen isotope ratios with a SHRIMP II: Analyses of MPI-DING silicate-glass reference materials and zircon from contrasting granite. Chemical Geology, 257, 114-128.

Mikulski, SZ, Krzemińska, E, Czupyt, Z, Williams, IS. (2014) The metallogenic evolution of the Kłodzko-Złoty Stok Intrusion (Sudetes, SW Poland) in the light of a SHRIMP reconnaissance study of $\delta^{18}O$ zircon isotope composition. Workshop on accessory minerals, University of Warsaw, September 2014*,* 26-27, Warsaw.

Sola, AR, Williams, IS, Neiva, AMR, Ribeiro ML. (2009) U–Th–Pb SHRIMP ages and oxygen isotope composition of zircon from two contrasting late Variscan granitoids, Nisa-Albuquerque batholith, SW Iberian Massif: Petrologic and regional implications. Lithos 111, 156 -167.

Valley, JW. (2003) Oxygen isotopes in zircon. In: Hanchar JM, Hoskin PWO (eds) Zircon, Reviews in Mineralogy and Geochemistry, 53. Mineralogical Society of America/Geochemical Society, Washington, DC, 343–385

Żelaźniewicz, A, Pańczyk, M, Nawrocki, J, Fanning, M. (2008) A Carboniferous/Permian, calc-alkaline, Itype granodiorite from the Małopolska Block, Southern Poland: implications from geochemical and U-Pb zircon age data. Geological Quarterly, *52*(4), 301-308.

Tectonic evolution of the southern boundary of Western Dharwar Craton, India: evidence from petrological and geochronological data

Miyanari, A[1], Das, K[1], Hidaka, H[2] and Bose, S[3]

1: Department of Earth and Planetary Systems Science, Hiroshima University, Japan
2: Department of Earth and Planetary Science, Nagoya University, Japan
3: Department of Geology, Presidency University, India

The south-western boundary of Archean (>3.0 Ga) Dharwar craton, India exposes granulite to amphibolite facies rocks that record multiple cycles of metamorphism (and deformation) and evolved

thorugh cycles of orogenesis. Crustal-scale dynamic processes are evident from the juxtaposition of deep-crustal high-grade granulites and mid-crustal amphibolites occurring in a regional-scale tectonic zone e.g. Mercara Shear Zone in the Kodagu district of Karnataka. Alkaline plutons are reported to be emplaced at Neoproterozoic age with inherited Archean ages from zircon U-Pb dating using LA-ICP-MS (Santosh et al., 2014). The orogenic connection between such belt of India, Madagascar and Sri-Lanka may provide information that these were formed a part of the Neoproterozoic continent Azania (Collins and Pisarevsky, 2005). However, tectonothermal events and their ages as revealed from the high-grade metamorphic rocks from this cratonic-margin orogenic belt are yet to be studied. This study aims to link the nature and style of tectonothermal evolution and their ages from the metapelitic granulites and associated gneissic rocks from Madikeri area situated at the centre of the Mercara Shear Zone.

Microstructural study in aluminous granulite indicates that coarse-grained assemblages formed during peak to pre-peak metamorphic stage include porphyroblastic garnet, sillimanite and quartz. Subsequently, post-peak stage yielded reaction corona of orthopyroxene, cordierite and spinel surrounding these porphyroblastic garnet, possibly indicating a stage of decompression and exhumation of deep crust. At the last stage of retrogressive cooling and hydration biotite grew on preexisting ferromagnesian minerals. P-T conditions of these stages are estimated by geothermobarometers, e.g. 8-10 kbar, 800-930 ^{o}C (peak condition); 4.5-6 kbar, 600-830^{o}C (early retrograde condition), 500-750 ^{o}C (final retrogression). Also, P-T pseudsections imply the evolution through an overall clockwise P-T path. As for SHRIMP dating, aluminous granulite, mafic granulite and garnet-kyanite-biotite gneiss were executed as sample. Also, aluminous granulite, garnet-kyanite-biotite gneiss and enderbite gneiss were used for EPMA dating. The results of zircon U-Pb age dating by SHRIMP and monazite U-Th total Pb age dating by EPMA indicate at least four events; ~3.2 Ga, 2.7-3.2 Ga, 2.5-2.7 Ga, 0.73-0.83 Ga. Particularly, the rim part of zircon grains from aluminous granulite yields $^{207}Pb/^{206}Pb$ age of ~0.8 Ga, with many data plotted on a clear discordia in Tera-Wasserburg plot.

These results imply (1) ~2.9 Ga; basin was formed with supply from craton, (2) 2.7-2.9 Ga; the shallow crust suffered prograde metamorphism, (3) 2.5-2.7 Ga, age of charnockite magmatism during Dharwar Orogeny with metamorphic peak (Ghosh et al., 2004), (4) 0.73-0.87 Ga; exhumation of deep crust during retrograde metamorphism along the crustal scale shear zone (stretching lineation and S-C fabric formation as last deformation event).

References

Collins, AS, Pisarevsky, SA. (2005) Amalgamating eastern Gondwana: The evolution of the Circum-Indian Orogens. Earth-Science Reviews 71, 229–270.

Ghosh, JG, Wit, MJ, Zartman RE. (2004) Age and tectonic evolution of Neoproterozoic ductile shear zones in the Southern Granulite Terrain of India, with implications for Gondwana studies. Tectonics 23, 3006.

Santosh M, Yang Q, Y, Mohan M R, Tsunogae T, Shaji E, Satyanarayanan M, 2014, Cryogenian alkaline magmatism in the Southern Granulite Terrane, India: Petrology, geochemistry, zircon U–Pb ages and Lu–Hf isotopes. Lithos 208–209, 430–445.

Impact of the IBERSIMS SHRIMP (Macarena) on the Geological Knowledge of the Western Reguibat Shield, Northern West African Craton

Montero, P[1], Bea, F[1], Haissen, F[2], Molina, JF[1] and Mouttaqi, A[3]

1: Department of Mineralogy and Petrology, University of Granada, Spain
2: LGAGE, Département de Géologie, Faculté des Sciences Ben Msik, Université Hassan II, Casablanca, Morocco
3: Office National des Hydrocarbures et des Mines, Rabat, Morocco

This report describes the most important findings and impact caused by the IBERSIMS SHRIMP (nicknamed Macarena) on the geological knowledge of the westernmost Reguibat Shield and associated pericratonic terranes of the Oulad Dlim massif, one the most interesting areas of the West African Craton (WAC). This area is located in the old Spanish Sahara currently ruled by the Kingdom of Morocco. Geological studies here were started by Spanish geologists at the end of the 19th century but were discontinued during the Polisario war. They were slowly resumed by Moroccan geologists

during 1999-2004 although limited the elaboration of geological maps and mineral exploration projects. The war situation since 1970 caused the lack of detailed geochemical studies and reliable geochronology, which until 2011 were nonexistent. The only previous geochronology was a K-Ar survey which, despite of this technique unreliability for dating high-grade metamorphic rocks, has been the base for structural division of the Oulad Dlim Massif in different units.

Despite the difficulties derived from military restrictions —an unmapped anti-tank and anti-personal mine fields made the area very dangerous for field geology— a joint team of geologist from the Universities of Granada, Casablanca and El Jadida began working in this area in 2010, just before the SHRIMP was installed in Granada. Since then six field expeditions and an enormous amount of SHRIMP U-Th-Pb and oxygen isotopes work have been done in the zone. Here we summarize the most important results and briefly show how these data are changing the geological interpretation of the zone:

1) Archean TTGs and greenstones (Montero et al., 2014): The Aghaylas TTG suite plus some greenstone belts form the regional rocks of the Archean sector of Reguibat. The Aghaylas Suite TTG gneisses have SHRIMP U–Pb zircon crystallisation ages between 3.04 ± 0.01 Ga and 2.92 ± 0.10 Ma, and whole-rock Nd model ages between TCR = 3.03 Ga and 2.92 Ga. Zircon U-Pb ages coincide with whole-rock Nd model ages this indicating that the main episode of new crust formation in the area occurred at 3.1–3.0 Ga; this is significantly different from other sector of the WAC. The Tichla greenstone belt was formed between 3.03 ± 0.01 Ga and 3.01 ± 0.01 Ga, though a metasediment Nd model age of 3.39 Ga indicates the contribution of an older crust.

2) Kalsilite syenites (synnyrites) (Bea et al., 2013, 2014): The Archean to Proterozoic transition in the West Reguibat is marked by the intrusion of several small massifs of kalsilite and nepheline syenites with extremely high K_2O (up to 19 wt.%) and K_2O/Na_2O (> 10). These rocks were believed to be Pan-African nepheline syenites, the presence of kalsilite was not known. We identified this mineral and determined the presence of two syenite types, one kalsilite-bearing and the other nepheline-bearing. The two syenites yielded the same 2.46 Ga zircon U-Pb crystallization ages. These mark the Archean-to-Proterozoic transition in the area. Remarkably, these are the oldest kalsilite-bearing rocks known so far and the only ones that are older than Palaeozoic. They give evidence of the singularity of the subcontinental mantle underneath the Reguibat Shield and the early cratonization of the area.

3) First evidence of the Cambrian Rifting (Bea et al., 2016): Derraman, a body situated in the Oulad Dlim Massif west of the Archean terranes was previously considered as a Proterozoic nepheline syenite. It is in fact a hypersolvus aegirine-riebeckite granite with zircon U-Pb ages of 524 Ma that likely represent the first manifestation of the Cambrian rifting known in the area.

4) Oulad Dlim carbonatites (Montero et al., 2016): The Oulad Dlim massif contains some carbonatite complexes of previously unknown age. The largest and best studied are Gleibat Lafhouda, composed of magnesio-carbonatites, and Twihinate, composed of calcio-carbonatites. Gleibat Lafhouda is hosted by Archean gneisses and schists. It has a SHRIMP U–Th–Pb zircon crystallization age of 1.85 ± 0.03 Ga. Twihinate is much younger. It is hosted by Late Silurian to Early Devonian deformed granites and has a zircon crystallization age of 104 ± 4 Ma, which is within error of the age of the carbonatites of the famous Richat Structure in the southwest Reguibat Shield. Remarkably, the Twihinate carbonatites contain abundant inherited zircons with ages that peak at ca. 420 Ma, 620 Ma, 2050 Ma, 2466 Ma, and 2830 Ma. This indicates that their substratum has West African rather than, as previously suggested, Avalonian affinities.

5) Silurian-Devonian Laknouk granitoids (Montero et al., 2016): The Oulad Dlim Massif was not known to contain Palaeozoic granite bodies. The westernmost crystalline outcrops were reported as consisting of Archean granitic gneisses. However, we found that this complex is in fact Silurian-Devonian formed of fine-grained I-type 421 Ma granites intruded by coarse-gained I-type transitional to A-type 410 Ma granites with biotite, epidote, titanite and Ca-rich garnet as varietal minerals. These are the first rocks of this age described in the pericratonic terranes of the WAC. Given that their mineralogy, geochemistry and Sr-Nd isotopes are compatible with being supra-subduction granites, the finding opens an unexpected way for understanding the geology of this area.

6) Ongoing work: Most materials of the Oulad Dlim massif, excepting the Laknouk massif, seem to be Pan-African. We are working actively on them. Shortly after this meeting we have found that

the central part of the Pan-African belt contains a huge block of Archean granites previously unknown. Preliminar SHRIMP work on two samples shows lead-loss discordias with upper intersection U-Pb ages close to 2.9 Ga, close to those of the TTGs of the Reguibat Rise. This finding casts doubts on the current tectonic interpretation of the Oulad Dlim Massif.

References

Bea, F.; Montero, P.; Haissen, F.; and El Archi, A. 2013. 2.46 Ga kalsilite and nepheline syenites from the Awsard pluton, Reguibat Rise of the West African Craton, Morocco. Generation of extremely K-rich magmas at the Archean–Proterozoic transition. Precambrian Research, 224, 242-254.

Bea, F.; Montero, P.; Haissen, F.; Rjimati, E.; Molina, J. F.; and Scarrow, J. H. 2014. Kalsilite-bearing plutonic rocks: The deep-seated Archean Awsard massif of the Reguibat Rise, South Morocco, West African Craton. Earth-Science Reviews, 138, 1-24.

Bea, F.; Montero, P.; Haissen, F.; Molina, J. F.; Michard, A.; Lazaro, C. et al. 2016. First Evidence for Cambrian Rift-related Magmatism in the West African Craton margin: The Derraman Peralkaline Felsic Complex. Gondwana Research, 36, 423-438.

Montero, P.; Haissen, F.; El Archi, A.; Rjimati, E.; and Bea, F. 2014. Timing of Archean crust formation and cratonization in the Awsard-Tichla zone of the NW Reguibat Rise, West African Craton. A SHRIMP, Nd-Sr isotopes, and geochemical reconnaissance study. Precambrian Research, 242, 112-137.

Montero, P.; Haissen, F.; Mouttaqui, A.; Molina, J. F.; Errami, A.; Sadki, O. et al. 2016. Contrasting SHRIMP U-Pb zircon ages of two carbonatite complexes from the peri-cratonic terranes pf the Reguibat Shield: Implications for the lateral extension of the West African Craton. Gondwana Research, in press, http://dx.doi.org/10.1016/j.gr.2015.12.005.

Extension-related Neoarchean granites from the Campo Belo metamorphic complex, southern São Francisco craton, Brazil: Geochronological and geochemical constraints

Moreno, JA[1], Baldim, MR[1], Semprich, J[1], Oliveira, EP[1], Verma, SK[2], Teixeira, W[3]

1: Department of Geology and Natural Resources, University of Campinas, Brazil
2: División de Geociencias Aplicadas, Instituto Potosino de Investigación Científica y Tecnológica (IPICYT), Mexico
3: Instituto de Geociências, Universidade de São Paulo, Brazil

The Campo Belo metamorphic complex (CBMC), located in the southern São Francisco craton, is a huge complex mainly composed of late-Archean migmatitic gneisses and granitoids. The complex was mainly affected by amphibolite facies metamorphism although granulitic rocks have been described in some areas. The oldest and most widespread unit in the complex is the Fernão Dias orthogneiss with an age of 2.84 Ga, which is intruded by three granitic plutons named the Bom Sucesso, Rio do Amparo and Lavras granites. The present work focuses on the study of these three granitic plutons.

LA-SF-ICP-MS U-Pb dating reveals a long period (ca. 100 My) of Neoarchean granitic magmatism in the CBMC. It could have started with the intrusion of a highly porphyritic biotite granite at ~2747 Ma, followed by the emplacement of a foliated hornblende biotite granite at ~2727 Ma and the subsequent intrusion of the Rio do Amparo, Bom Sucesso and Lavras granites at ~2716 Ma, ~2695 Ma and ~2646 Ma, respectively. This Neoarchean granitic activity seems to end with the intrusion of peraluminous leucocratic dikes at ~2631 Ma. The isotopic composition of the Campo Belo granites characterized by mostly negative εNd_i values (Rio do Amparo: –2.0 and +3.1; Bom Sucesso: –3.6, –3.1 and +0.9; Lavras granites: –5.6, –2.5 and –0.2) and old Nd model ages (2.8–3.1 Ga) suggests significant reworking of Mesoarchean crust although with involvement of juvenile material, which seems to be more important in the Rio do Amparo granite. The elevated number of inherited zircons displayed by the Rio do Amparo granite (>50% of the analyses) and the Bom Sucesso granite (ca. 30% of the analyses) also supports an important crustal reworking.

All the studied samples are high-silica granites ranging from 69.3 to 75.0 wt.% SiO_2, showing mostly alkali-calcic and calc-alkalic compositions (MALI (Na_2O+K_2O–CaO by weight) = 5.46–8.69; Fig. 5C). The Bom Sucesso and Lavras granites as well as the foliated hornblende biotite granite are characterized by relatively high (Na_2O+K_2O)/CaO ratio, Fe-number, and Zr, Nb, Ce and Ga contents, along with apatite- and zircon-saturation temperatures >800 ºC, sharing chemical features of A-type

granites. They are classified as A_2-type granites that could have formed by high-T partial melting of a TTG older crust. The Bom Sucesso biotite-bearing granite evolved through crystal fractionation of feldspar, ferromagnesian minerals and Th-REE-accessory minerals. Whereas the A-type hornblende biotite granites (i.e., the Lavras and foliated granites) show a more complex petrogenesis that could involve accumulation, mixing, mingling and assimilation processes as well as melting of a similar source at different times. On the other hand, the Rio do Amparo granite, although sharing features of A-type, is a peraluminous I-type granite formed by partial melting of a 2.77 Ga tonalite or medium to high-K basalt, after which, it experienced an evolution via crystal fractionation of feldspar, biotite, Fe-Ti oxides and Th-REE-accessory minerals and assimilation of older country rocks.

The 2727–2646 Ma high-K magmatism in the Campo Belo complex is likely related to a major extensional period as suggested by the geochemical compositions of the studied granites along with the high zircon inheritance detected in the Bom Sucesso and Rio do Amparo granites. An extensional setting for the CBMC between 2750 and 2660 Ma has also been proposed by Teixeira et al. (1998) due to the existence of undeformed rocks of the Ribeirão dos Motas mafic-ultramafic. Our data agrees well with previously published information about such peculiar granite-genesis in the Archean-Paleoproterozoic transition around the world (e.g., Champion and Sheraton, 1997; Mitrofanov et al., 2000; Zhou et a., 2015).

References

Champion, D.C., Sheraton, J.W., 1997. Geochemistry and Nd isotope systematics of Archaean of the Eastern Goldfields, Yilgarn Craton, Australia: implications for crustal growth processes. Precambrian Research 83, 109–132.

Mitrofanov, F.P., Zozulya, D.R., Bayanova, T.B., Levkovich, N.V., 2000. The World's Oldest Anorogenic Alkali Granitic Magmatism in the Keivy Structure on the Baltic Shield. Geochemistry 374, 238–241.

Teixeira, W., Cordani, U.G., Nutman, A.P., Sato, K., 1998. Polyphase Archean evolution in the Campo Belo Metamorphic Complex, Southern São Francisco Craton, Brasil: SHRIMP U-Pb zircon evidence. Journal of South American Earth Sciences 11, 279–289.

Zhou, G.Y., Wu, Y.B., Gao, S., Yang, J.Z., Zheng, J.P., Qin, Z.W., Wang, H., Yang, S.H., 2015. The 2.65 Ga A-type granite in the northeastern Yangtze craton: Petrogenesis and geological implications. Precambrian Research 258, 247–259.

Sources of the youngest (15-20 ka) loess in Poland as determined from detrital zircon data

Nawrocki, J[1] and Pańczyk, M[2]

1: Geophysical Laboratory, Polish Geological Institute – NRI, Warszawa, Poland
2: Micro-area Analysis Laboratory, Polish Geological Institute – NRI, Warszawa, Poland

Loess deposits in the western Ukraine and southern Poland form the westernmost part of a widely distributed loess mantle named the 'East European Loess Province'. In the Lublin, Volhynia and Podole Uplands, loess sediments were deposited mostly during later periods of the Pleistocene. The loess sources and directions of aeolian transport have been defined on the basis of mineralogical studies in the context of palaeogeography. Chlebowski & Lindner (1975) and Chlebowski et al. (2003) postulate that winds from west and north-west transported the youngest loess. They also assume that aeolian material was derived from mixed (i.e. local and distant) sources. Studies of the anisotropy of magnetic susceptibility (AMS) were carried out in order to define the directions and strength of palaeowind during sedimentation of the youngest loesses in Poland and western Ukraine. The majority of the sections studied indicate a palaeowind direction from W-SW to E-NE, with a mean azimuth of 258^o (Nawrocki et al., 2006).

Six sections of the youngest loess in Poland were chosen for isotope studies of detrital zircon grains (Fig.1A). More than four hundred crystals were selected for single-grain U-Pb dating. These grains were processed on the SHRIMP IIe device in the laboratory of Polish Geological Institute - NRI.

More than 80% of area of Poland was covered by postglacial deposits at time of loess deposition. A substantial part of clastic material forming several till horizons and glaciofluvial sands and gravels was derived from Scandinavia. Because of this the Precambrian zircon grains with the age spectrum characteristic for the Baltic Shield were expected. However, the obtained results are completely different. Most of the zircon grains have provided the Variscan, Caledonian and Cadomian ages (Fig. 1B). It means that main sources of the loess were located in the mountain regions of Poland. The Holy Cross Mts., Carpathians and the Sudetes were not covered totally by the ice sheet during the Quaternary. The fine-grained material with the Variscan, Caledonian and Cadomian zircons could also be distributed along the rivers flowing out from the mountain areas.

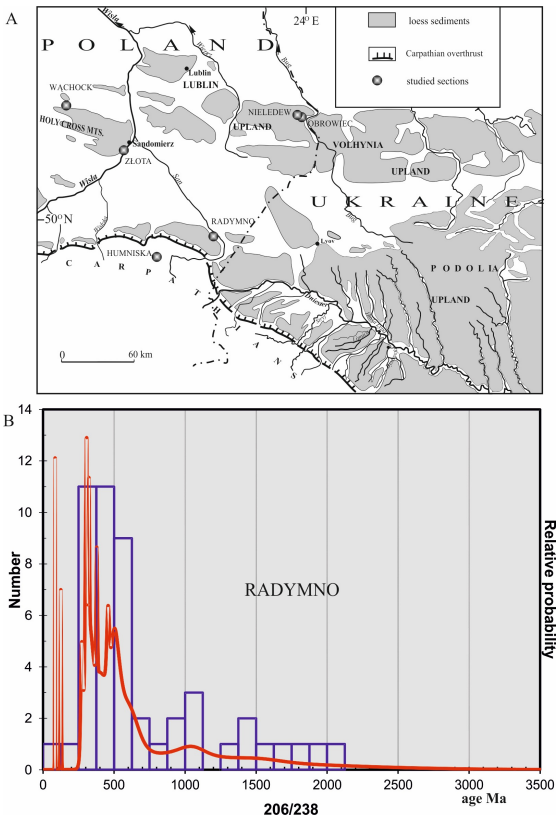

Fig. 1. (A) Location of studied sections on the background of map with loess distribution in SE Poland and Western Ukraine. (B) Binned frequency and probability density distribution plots of detrital zircon grains from the youngest loess of Radymno section.

References

Chlebowski, R, Lindner, L. (1975) Wpływ podłoża na skład minerałów ciężkich głównych wysp lessowych NW części Wyżyny Małopolskiej. Acta Geologica Polonica 25, 163-178.

Chlebowski, R, Lindner, L, Barczuk, A, Bogucki, A, Gozhik, P, Łanczont, M, Wojtanowicz, J. (2003) Accumulation conditions of the younger upper loess of Sandomierz Basin, Mid-Carpathian Foreland and Podolian Upland on the basis of the geological and mineralogical studies. Annales Universitatis Marie Curie-Skłodowska 58 (B), 7-64.

Nawrocki, J, Polechońska, O, Boguckij, A, Łanczont, M. (2006) Palaeowind directions recorded in the youngest less in Poland and western Ukraine as derived from anisotropy of magnetic susceptibility measurements. Boreas, 35, 266-271.

The Geological Survey of Canada's "SHRIMP tools": helping the laboratory meet its Open Data obligations

Rayner, N, Viljoen, D, Pestaj, T and Davis, B

J.C. Roddick Ion Microprobe Laboratory, Geological Survey of Canada, Ottawa, Ontario, Canada

SHRIMP labs generate large quantities of results for scientists both internal and external to their home organization. The storage, tracking and retrieval of data, along with associated metadata is an ongoing challenge. Added to this, SHRIMP facilities in publically funded laboratories may have mandated requirements to manage data in a way that makes it accessible and open to a wide variety of stakeholders (including the public).

In most cases, the scientific unit of interest in a SHRIMP analysis is the ***sample*** (commonly a specific lithology/unit from a unique location) however a single sample may have many sources of SHRIMP data. These may include multiple minerals from the same unit, the same mineral on multiple SHRIMP mounts, or the same SHRIMP mount analysed during multiple sessions or with multiple calibrations. The retrieval and compilation of all the results for a single sample for different minerals, mounts, sessions, or calibrations can be time consuming.

Many SHRIMP laboratories are using Ludwig's VBA-based Excel Add-In SQUID2 for their U-Pb geochronology data reduction (Ludwig, 2003). This incredibly powerful, customizable and complex piece of programming has the added benefit that it integrates seamlessly with Ludwig's Isoplot Add-In to generate the necessary calculations and plots utilized to interpret isotopic results. SQUID parses individual sample results on separate worksheets and preserves SHRIMP data reduction metadata such as analyses of standards, calibration error, specifics on the task and interpolation methods used on a separate sheet in the same workbook. However, each "SQUIDed" workbook contains only the data from a single analytical session and this poses challenges when data from a single sample straddles multiple sessions/workbooks.

While other data-reduction protocols are under-development by the wider geochronology community, we anticipate ongoing reliance on Excel workbooks. In light of the need to store, track, organize, retrieve and disseminate results in a timely way, the Geological Survey of Canada (GSC) has developed a number of software tools that help to integrate:

1) SQUID reduced U-Pb data from Excel spreadsheets

2) Data reduction metadata

3) Sample imagery (e.g. CL/BSE)

4) Post-analysis reflected light imagery and

5) SHRIMP instrument analytical conditions

Analytical results from SQUID, instrument conditions, and file/folder locations are stored in an Oracle database permitting rapid retrieval and compilation of all U-Pb geochronology results and associated metadata for a given sample.

An Excel VBA Add-In and external stand-alone applications are used to transfer data to the Oracle database. Once the database is populated with the results and instrumental parameters, data for an individual sample can be extracted as an Excel 2010 file using a "ZinfoExporter" tool, a Windows application. The resulting Excel workbook, referred to as a "Zinfo" file (GSC samples are given a laboratory number called a Z-number) includes U-Pb results from all analytical session/mounts/ calibrations, regardless of mineral. Each SHRIMP analysis is linked to the original SQUID workbook, the Adobe PDF file containing the SEM images and to the reflected light screen snap taken immediately after analysis. Analysis-specific analytical parameters including the primary beam intensity and sample stage coordinates, and session-specific parameters including the multiplier and discriminator settings, Kohler aperture, and calibration error are also reported in the Zinfo file. This permits easy quality assurance/quality control checks of the data. Data interpretation (concordia plots/ weighted mean calculations) can be carried out using Isoplot in the Zinfo file. A consistent set of

columns is output by the ZinfoExporter, thus simplifying the preparation of publication data tables that include more than one sample.

Part of the GSC's analytical protocol includes the analysis of secondary standards to independently verify the accuracy of the Pb/U calibration and identify any requirements for intra-element mass fractionation corrections. Data validation tools were developed to track average $^{206}Pb/^{238}U$ and $^{207}Pb/^{206}Pb$ ages of the secondary standards, as well as user-defined analytical parameters (e.g. average UO/U) for both the primary and secondary standards within the SQUID workbook. These too are uploaded to the Oracle database where they can be queried to track long term trends in instrumental performance.

The goal in developing these tools was to meet the laboratory objectives of quality control/quality assurance plus facilitated dissemination of results. The implementation of these tools has permitted the GSC's SHRIMP laboratory to partially automate the validation, storage, retrieval and compilation of laboratory results on the basis of sample, avoiding the need to cut/paste from multiple worksheets and the associated risk of error.

The GSC SHRIMP Tools provide a framework for more efficient and consistent SHRIMP data management. This facilitates the population of public-facing databases which underpin web accessibility via sites like the Canadian Geochronology Knowledgebase (CGKB, http://atlas.gc.ca/geochron/en/). The CGKB is one of many ways the GSC is fulfilling its Open Data mandate of providing accessible, high-quality geoscience data to Canada and the world.

References

Ludwig, K. R. (2003), User's manual for Isoplot/Ex rev. 3.00: a geochronological toolkit for Microsoft Excel. in Special Publication 4, pp. 70, Berkeley, Berkeley Geochronology Centre.

Isotope U-Pb ratio of "imperfect" baddeleyite crystals from carbonatites of the Proterozoic alkaline-ultramafic Tiksheozero massif (N Karelia, Russia)

Rodionov, NV, Belyatsky, BV, Antonov, AV, Lepekhina, EN, Balashova, YuS, Berezhnaya, NG and Sergeev, SA

Centre of Isotopic Research, AP Karpinsky Geological Institute (VSEGEI), St-Petersburg, Russia

Baddeleyite (ZrO_2) in recent years is widely used in the practice of the U-Pb dating, first of all, basic, ultrabasic and alkaline intrusive rocks [Amelin et al., 1999; Rasmussen et al., 2008]. The prospect of this mineral as a geochronometer determined by its predominantly magmatic origin, the crystal structure features (monoclinic, very high crystallization temperature, a small degree of mechanical durability) and chemical composition (relatively high U content in the absence of common Pb, as well as high Hf concentration which allows the use of Lu-Hf isotope systematics for additional dating) [Heaman, LeCheminant, 1993]. The main advantage compared to the zircon is a resistant baddeleyite U-Pb isotope system [Heaman, 2009], which allows to obtain concordant estimations of the crystallization age of the baddeleyite-hosted geological bodies as the Archean-Proterozoic and Phanerozoic as well [Bayanova, 2006]. However, a detailed study of baddeleyite U-Pb isotope systematics by SIMS has found the so-called "crystal orientation effect" [Wingate, Compston, 2000], which leads to significant (2–10 %) variations in the measured individual $^{206}Pb/^{238}U$ ratios [Li et al., 2010; Schmitt et al., 2010; Rodionov et al., 2012].

Baddeleyite in carbonatites of Tiksheozero massif (TM) is widely distributed as a mineral phase, as well as inclusions in zircon and has a homogeneous internal structure and a clear zoning, especially evident in the cathodoluminescence, and the inclusions of other mineral phases are usually absent. Age and geochemistry of baddeleyite from TM carbonatites was studied by us earlier for samples from 154 drill-hole [Rodionov et al., 2009, 2015; Frantz et al., 2013].

In this work, we studied the U-Pb baddeleyite systematics from magnetite phoscorite of 146 drill-hole at a depth of 96–107 meters (Fig.1). Local isotope analysis was carried out on an ion probe high resolution SHRIMP-II. As a standard used «Phalaborwa» baddeleyite with the known isotopic $^{206}Pb/$

^{238}U ratio equals to 0.37652, corresponding to age 2.06 Ma [Heaman, 2009]. Isotopic Pb/U ratio was measured according to the procedure, described in the papers [Wingate, Compston, 2000, Rodionov et al., 2012] and basically repeating the Pb-U zircon measuring procedure on SHRIMP-II. Individual analysis consisted of five cycles (150 sec per cycle), each cycle representing one pass through the mass stations: $^{196}(Zr_2O)$, ^{204}Pb, 204.5 background, ^{206}Pb, ^{207}Pb, ^{208}Pb, ^{238}U, $^{248}(ThO)$, $^{254}(UO)$. The "208-method" was used for common Pb correction, because it is more reliable for low-Th/U minerals such as baddeleyite, whereby the proportion of common Pb was estimated from the difference between measured $^{208}Pb/^{206}Pb$ and the radiogenic ratio expected for the age and measured $^{232}Th/^{238}U$ of the mineral.

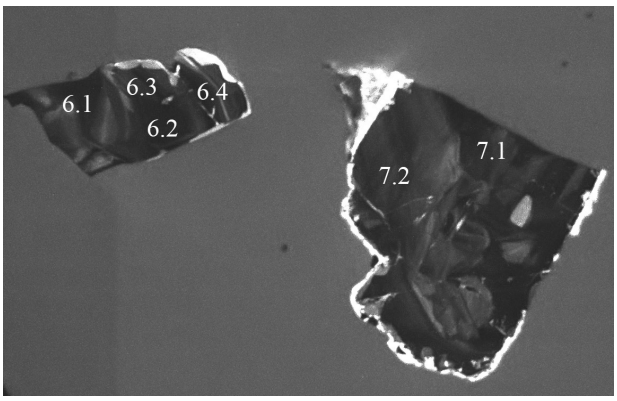

Fig.1. CL image of typical baddeleyite crystals from 146 sample

56 U-Th-Pb isotopic analyses in 18 baddeleyite crystals were conducted. U, Th and radiogenic Pb contents are characterized by moderately high values: from 6 to 204, an average of 59 ppm of U, from 0.3 to 35 ppm (averaged 7) Th, radiogenic Pb – 18 ppm (averaged), whereas in the previously studied baddeleyite from 154 drill-hole – Th: 1–6, U up to 23, Pb_{rad} 7.0 ppm (averaged). U-Pb and Pb-Pb baddeleyite age coincides within the error – the age according to the discordia intercepts was: -47 ± 85 & 1991 ± 11 Ma (MSWD = 1.9, 2s), according to 54 baddeleyite analyses calculated average $^{207}Pb/^{206}Pb$ age (at correction of the isotopic composition upon the ^{208}Pb) corresponds to: 1993 ± 8 (MSWD = 0.77, probability = 0.9 (Fig.3).

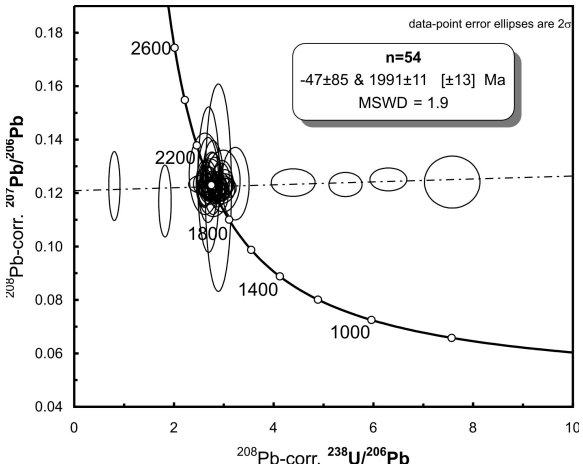

Fig.2. Diagram with discordia constructed on 54 analytical points of baddeleyite from 146 sample

These estimates coincide well with the known age of this massif [Rodionov et al., 2009, 2015], but three crystals from 18 showed unexpectedly high deviations of U/Pb ratios for the first time. The main part of data-points gives the scatter in $^{238}U/^{206}Pb$-ratio after correction on ^{208}Pb from 2.55 to 3.1 (Fig.2) which corresponds to the age from 2136 to 1809 Ma, the remaining 7 analyses of the three grains scattered from 0.81 to 7.65 (5200-800 Ma). Furthermore, the constructed on these data and concordant baddeleyite cluster pseudo-discordia can formally indicate Pb loss processes within baddeleyite, that is not observed till now during the study of baddeleyite crystals by local analysis methods, in contrast to the generally recognized "orientation effect" [Rubatto, Scambelluri, 2003]. At the same time, similar effects in the dating of individual grains of baddeleyite using ID-TIMS and LA-ICP-MS analytical

methods is well known due to the complexity of the chemical dilution for ID-TIMS and excessive fractionation for the LA-ICP-MS.

A detailed morphology study of the dated crystals shows "imperfections" only those grains, which were found the greatest deviations in U-Pb ratio. Baddeleyite separation performed using standard procedure including concentration table and handpicking under a binocular microscope. Micro-analytical study found among grains separated as simple transparent «normal» grains as well more complex crystals intergrown with pyrochlore and zircon which showed intriguing results. Three grains with the highest spread of the ratio are darker in transparent light, enriched by intergrowths with other minerals, and one of them is characterized by clear zircon overgrowth (4 over discordant points). The other relatively concordant results were obtained from more transparent crystals without any visible imperfections.

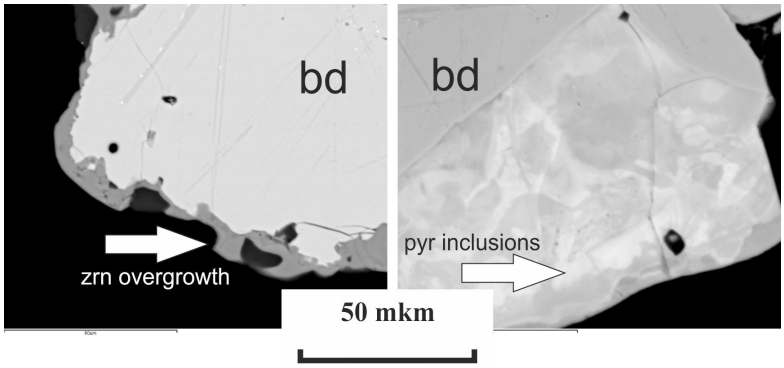

Fig.3. Detail structure (BSE) of baddeleyite crystal which has the greatest variation in U/Pb ratios

Perhaps, these separation and complex mineralogy factors have resulted in some excessive spread of uranium-lead ratio exceeds the highest ever previously observed during SIMS analysis: tens of percent instead of 2-10%. It can be doubtfully explained by the well-known "orientation effect" only. In our opinion, in this case another "matrix effect" engines operate, among which is necessary to highlight the disturbance of baddeleyite crystal lattice during initial stage of transformation, or due to an interaction with other minerals.

The study was done as a part of CIR works under the project of "Thematic and methodological works within 2016 aimed in development of laboratory and analytical methods under the State Geological Survey".

References

Amelin, Yu, Li, Ch, Naldrett, AJ. (1999) Geochronology of the Voisey's Bay intrusion, Labrador, Canada, by precise U-Pb dating of coexisting baddeleyite, zircon, and apatite. Lithos 47, 33–51.

Bayanova, TB. (2006) Baddeleyite: a promising geochronometer for alkaline and basic magmatism. Petrology 4, 187–200.

Frantz, NA, Rodionov, NV, Lokhov, KI. (2013) Carbonatites age of the Tiksheozero massive (North Karelia, Russia). Goldschmidt Conference Abstracts, 1106, DOI: 10.1180/minmag.2013.077.5.6.

Heaman, LM, LeCheminant, AN. (1993) Paragenesis and U–Pb systematics of baddeleyite (ZrO2). Chemical Geology 110, 95–126.

Heaman, LM. (2009) The application of U–Pb geochronology to mafic, ultramafic and alkaline rocks: an evaluation of three mineral standards. Chemical Geology 261, 43–52.

Li, QL, Li, XH, Liu, Y, Tang, GQ, Yang, JH, Zhu, WG. (2010) Precise U–Pb and Pb–Pb dating of Phanerozoic baddeleyite by SIMS with oxygen flooding technique. Journal of Analytical Atomic Spectrometry 25, 1107–1113.

Rasmussen, B, Fletcher, IR, Muhling, JR. (2008) Pb/Pb geochronology, petrography and chemistry of Zr-rich accessory minerals (zirconolite, tranquillityite and baddeleyite) in mare basalt 10047. Geochimica et Cosmochimica Acta 72, 5799–5818.

Rubatto, D, Scambelluri, M. (2003) U-Pb dating of magmatic zircon and metamorphic baddeleyite in the Ligurian eclogites (Voltri Massif, Western Alps). Contributions to Mineralogy and Petrology 146, 341–355.

Rodionov, NV, Belyatskii, BV, Antonov, AV, Presnyakov, SL, Sergeev, SA. (2009) Baddeleyite U-Pb SHRIMP II age determination as a tool for carbonatite massifs dating. Doklady Earth Sciences 428 (7), 1166–1170.

Rodionov, NV, Belyatsky, BV, Antonov, AV, Kapitonov, IN, Sergeev, SA. (2012) Comparative in-situ U–Th–Pb geochronology and trace element composition of baddeleyite and low-U zircon from carbonatites of the Palaeozoic Kovdor alkaline–ultramafic complex, Kola Peninsula, Russia. Gondwana Research 21, 728–744.

Rodionov, NV, Belyatsky, BV, Antonov, AV, Simakin, SG, Sergeev, SA. (2015) Geochemical features and age of baddeleyite from carbonatites of the Proterozoic Tiksheozero alkaline–ultramafic pluton, North Karelia. Doklady Earth Sciences 464(4), 474–479.

Schmitt, AK, Chamberlain, KR, Swapp, SM, Harrison, TM. (2010) In situ U–Pb dating of micro-baddeleyite by secondary ion mass spectrometry. Chemical Geology 269, 386–395.

Wingate, MTD, Compston, W. (2000) Crystal orientation effects during ion microprobe U–Pb analysis of baddeleyite. Chemical Geology 168, 75–97.

Age complexity in the composite Uivak Gneiss of the Saglek Block, Labrador

Sałacińska, A[1], Kusiak, MA[1], Whitehouse, MJ[2], Dunkley, DJ[1,3], Wilde, SA[3] and Kielman, R[2]

1: Institute of Geological Sciences, Polish Academy of Sciences, Warsaw, Poland
2: Swedish Museum of Natural History, Stockholm, Sweden
3: Department of Applied Geology, Curtin University, Perth, Australia

The Saglek Block of Nain Province in Northern Labrador forms the westernmost part of the North Atlantic Craton (Fig.1). It is one of the few regions on Earth where early Archaean crust is preserved (Collerson, 1983; Schiøtte et al., 1989; Collerson et al., 1991). The block comprises gneisses regionally metamorphosed to either granulite-facies from 2740 to 2707 Ma or amphibolite-facies at *c.* 2702 Ma (Krogh & Kamo, 2006). It is divided by the major, north- trending Handy Fault, which is interpreted as juxtaposing two different crustal levels of differing metamorphic grade, with amphibolite-grade gneisses to the east and granulites to the west (Fig.1; Bridgwater et al., 1975; Bridgwater et al., 1990).

The Saglek Block is dominated by two suites of metaigneous gneisses: the Uivak I suite (>3.6 Ga), comprising fine-to-medium grained tonalite-trondhjemite-granodiorite (TTG) gneisses, and the less extensive Uivak II augen gneiss (ca. 3.4 Ga), consisting of Fe-rich porphyritic granodiorite and diorite (Collerson & Bridgwater, 1979; Collerson, 1983). The Uivak suites are tectonically juxtaposed and interlayered with supracrustal assemblages, along with several generations of pegmatite. Two assemblages of heterogeneous supracrustal gneisses are recognized: the Nulliak assemblage, which occurs as macro-scale tectonic lenses in Uivak gneisses, and the more extensive Upernavik assemblage, which is distinguished as a younger assemblage through the absence of metabasaltic Saglek dykes that intrude the Nulliak and Uivak gneisses. Some studies, on the basis of zircon dating, have proposed the presence of enclaves or tectonic intercalations of pre-Uivak I felsic crust, such as the monzonitic ca. 3.95 Ga Nanok Gneiss (Regelous & Collerson, 1996) and the tonalitic >3.95Ga Iqaluk Gneiss (Komiya et al., 2015).

The study area is located on the east coast of the Labrador Peninsula between Saglek and Hebron Fiords. Four samples of felsic orthogneiss were chosen from the lower-grade eastern side of the Handy Fault, at sites mapped as Uivak I Gneiss: Johannes Point Cove (L1419, Fig. 2A), Tigigakyuk Inlet (L1434; L1440, Figs. 2B&C) and Big Island (L1443, Fig.2D). Samples L1419 and L1434 were chosen from layers of finer-grained, homogeneous grey gneiss with minimal leucosome. Samples L1440 and L1443 were slightly coarser-grained. Sample composition (granodiorite-tonalite) and mineralogy (mostly plagioclase and quartz, with minor K-feldspar and biotite, and accessory zircon and apatite) are consistent with published descriptions of Uivak I Gneiss (e.g. Collerson, 1983). Sample L1434 contains Mg-rich augite and hornblende, which are absent in the other samples. Most samples have a granoblastic texture, although L1440 preserves some partially recrystallized phenocrysts. Plagioclase

(oligoclase) is partially altered to sericite. Quartz with undulose extinction occurs in granoblastic domains and as inclusions in feldspar. Microcline is present in all samples.

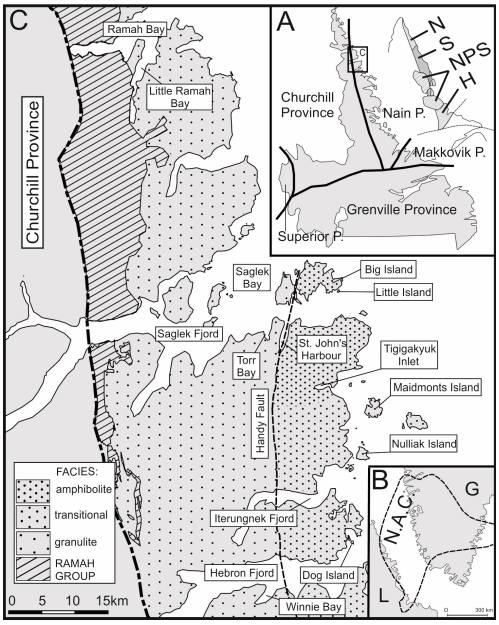

Fig.1. Geological map of the Saglek block between Ramah Bay and Hebron Fiord. N-Nachvak Block, S-Saglek Block, NPS-Nain Plutonic Suite, H-Hopedole Block, L-Labrador, G-Greenland, N.A.C-North Atlantic Craton (modified from Schiotte et al., 1989 and Bridgwater & Schiotte, 1991).

Fig.2. Samples of felsic orthogneisses analysed in this study: (A) Johannes Point Cove, sample L1419; (B&C) Tigigakyuk Inlet, samples L1434 and L1440, respectively; and (D) Big Island, sample L1443.

U-Pb isotopic dating of zircon separated from the four samples was performed on a CAMECA IMS1280 secondary ion mass spectrometer (SIMS) at the Natural History Museum (Stockholm, Sweden). Concordant age data obtained from zircon cores with characteristic igneous growth structures (Fig.3) from samples L1419, L1440 and L1443 fall within the interval 3.67-3.76 Ga, consistent with estimates for the protoliths of Uivak I gneisses by Schiotte et al. (1989) and Bridgwater and Schiotte (1991). Older xenocrystic ages comparable to those found by Krogh & Kamo (2006, 3.81 Ga and 3.99 Ga) and (Collerson, 1983, 3.91Ga) were not obtained. However, a few 3.58 Ga to 3.43 Ga concordant ages from zircon with magmatic structures were identified in the samples. These may indicate that the protoliths are younger than previous estimates, with older ages being xenocrystic. The younger age data could also be due to partial Pb loss during the 2.7Ga metamorphic event. Metamorphic ages from zircon rims (ca. 2745 Ma; L1440) are consistent with previous estimates (Schiotte et al. 1989; Collerson, 1983; Krogh & Kamo, 2006). Most data from sample L1434 scatter along concordia around 3.57 Ga, with zircon grains lacking the strong oscillatory zoning found in other samples, consistent with growth in a slightly more mafic magma, as indicated by sample chemistry and mineralogy.

The results may be interpreted as indicating that the Uivak I Gneiss are not a simple magmatic suite, but rather a composite containing TTG protoliths of different generations, likely the result of crustal recycling. However, in common with the early Archean of West Greenland (Whitehouse and Kamber, 2005) and the Neoarchean Lewisian complex (Whitehouse and Kemp, 2010), identifying true protolith ages from data that spread along concordia is problematic and it requires more data to address this problem.

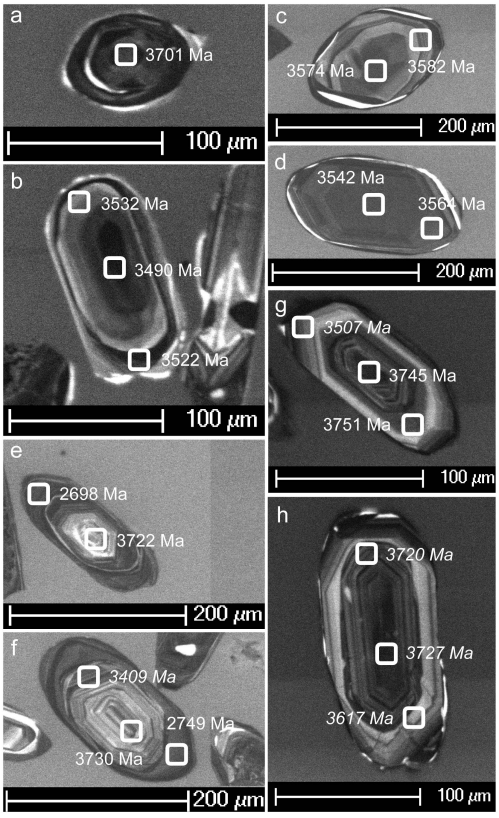

Fig.3. Cathodoluminescence images of selected zircon grains analysed by SIMS, together with $^{207}Pb/^{206}Pb$ ages; (A,B) sample L1419; (C,D) sample L1434; (E,F) sample L1440; (G,H) sample L1443 (Italics text – ages are discordant and/or comtaminated by common Pb).

Acknowledgements

This research was conducted thanks to a grant to MK from the Polish National Science Centre; NCN (nr 2014/15/B/ST10/04245) and funds to MJW from the Knut and Alice Wallenberg Foundation and the Swedish Research Council. Fieldwork was carried out with the permission and support of Parks Canada and the Nunatsiavut Government.

References

Bridgwater, D, Collerson, KD, Hurst, RW, Jesseau, CW. (1975) Field characters of the early Precambrian rocks from Saglek, coast of Labrador. Geol. Sum. Can., Pap. 75-1, Part A, 287-296.

Bridgwater, D, Mengel, F, Schiotte, L, Winter, J. (1990) Research on the Archean rocks of northern Labrador, progress report 1989: Current Research. Newfoundland Department of Mines and Energy, Report 90-1: 227-236.

Bridgwater, D, Schiotte, L. (1991) The Archaean gneiss complex of Northern Labrador - A review of current results, ideas and problems, 153-166.

Collerson, KD. (1983) Ion microprobe zircon geochronology of the Uivak gneisses: implications for the evolution of early terrestrial crust in the North Atlantic Craton, Houston, Texas. Lunar and Planetary Institute Technical Report 83-03: 28-33.

Collerson, KD, Bridgwater, D. (1979) Metamorphic development of early Archean tonalitic and trondhjemitic gneisses, Saglek area, Labrador. [in:] Baker, F. (ed), Trondhjemites, dacites and related rocks. Amsterdam, Elsevier, 205-273.

Collerson, KD, Cambell, LM, Weaver, BL, Palacz, ZA. (1991) Evidence for extreme mantle fractionation in early Archaean ultramafic rocks from northern Labrador. Nature, 349: 209–214.

Krogh, TE, Kamo, SL. (2006) Precise U-Pb zircon ID-TIMS ages provide an alternative interpretation to early ion microprobe ages and new insights into Archean crustal processes, northern Labrador. *Geological Society of America Special Papers*, 2006, 405:91-103.

Komiya, T, Yamamoto, S, Aokia, S, Sawaki, Y, Ishikawa, A, Tashiro, T, Koshida, K, Shimojo, M, Aoki, K, Collerson, KD. (2015) Geology of the Eoarchean, > 3.95 Ga, Nulliak supracrustal rocks in the Saglek Block, northern Labrador, Canada: The oldest geological evidence for plate tectonics. Tectonophysics, 622:40-66.

Regelous, M, Collerson. KD. (1996) Sm-147-Nd-143, Sm-146-Nd-142 systematics of Early Archaean rocks and implications for crust-mantle evolution. Geochimica Et Cosmochimica Acta, 60:3513-3520.

Schiotte, L, Compston, W, Bridgwater, D. (1989) Ion-probe U-Th-Pb zircon dating of polymetamorphic orthogneisses from northern Labrador, Canada. Canadian Journal of Earth Sciences, 26:1533-1556.

Whitehouse, M.J., Kemp, T. (2010) On the difficulty of assigning crustal residence, magmatic protolith and metamorphic ages to Lewisian granulites: constraints from combined U-Pb and Lu-Hf isotopes. Geological Society, London Special Publications, 335: 81-101.

First REE analyses in zircon by SHRIMP at Geosciences Institute of São Paulo University: REEdiffusion from apatite inclusion inside Temora zircon

Sato, K, Tassinari, CCG, Basei, MAS,Onoe AT and Siga Junior, O

Geosciences Institute, University of São Paulo, Brazil

Analytical Technique

The Rare Earth Elements (REE) isotopic compositions in zircons were measured on SHRIMP II at Institute of Geosciences of University of São Paulo - Brazil. SHRIMP IIe uses LabView 8.5 as a communication platform between the computer and the spectrometer by SHRIMP software (version 2.90), which was developed by Australian Scientific Instruments (ASI).

SHRIMP IIe Setup - primary ion beam

Köhler aperture = 120 μm, beam diameter = 20-30 μm, O^{-2} beam density ~ 4 ηA, and raster time = 2 minutes. Secondary ion beam: source slit = 80 μm, mass resolution to light rare earth element (LREE) (La - Eu) is > 5000 (1%), Figure 1 and mass resolution to heavy rare earth element (HREE) ranged 3500 - 5000 with energy filter applied in the electrostatic analyzer (ESA). The integration times for acquiring data in the NIST610 used for all REE isotopes are 5s and for ^{91}Zr = 15s. The peak auto center were done for all peaks, and the integration times for zircon REE isotopes are: ^{91}Zr = 1s, ^{139}La = 40s, ^{140}Ce=20s, ^{141}Pr =20s, ^{143}Nd=20s, ^{146}Nd=20s, ^{147}Sm=20s, ^{149}Sm=20s, ^{151}Eu=20s, ^{155}Gd=20s, ^{157}Gd=20s, ^{159}Tb=20s, ^{161}Dy = 5s, ^{163}Dy=5s, ^{165}Ho=5s, ^{166}Er=5s, ^{167}Er=5s, ^{169}Tm=5s, ^{171}Yb=5s, ^{172}Yb=5s, ^{175}Lu=5s and ^{178}Hf=5s. The peak auto center are done only to ^{91}Zr, ^{165}Ho, ^{169}Tm, ^{175}Lu and ^{178}Hf.

Data reduction

Excel data sheet was used for offline data reduction. To correct the continuous drifting of ^{91}Zr and REE isotopes during peak jump mode analyses, it was calculated the drift rate (slope) of ^{91}Zr during all time interval (Figure 2B). All REEisotopes were normalized relative to reference isotopes of ^{91}Zr interpolated, therefore relative REE/^{91}Zr ratios were determined (Figure 2B) for calculation of REE concentration. All measurements were calibrated against NIST 610 international standard. Zr_2O value of 66.99% obtained in zircon standard 91500 (Wiedenbeck and others, 2004) was used for determination of REE isotopes sensitivity factor between NIST and zircon. The REE isotopes sensitivity factor obtained (around 1.165, Figure 3), is applied for REE isotopes correction in zircon sample. Chondrite value used to normalization of REE in zircon was McDonough and Sun (1995).

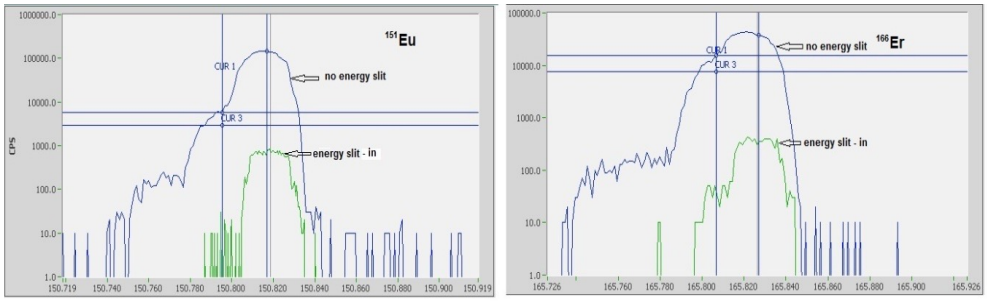

Figure 1 - Black: no energy slit; green: ESA energy slit applied. ^{153}Eu (left) and 166Er (right) intensities decrease120 times after applied energy slit but interference problems were solved.

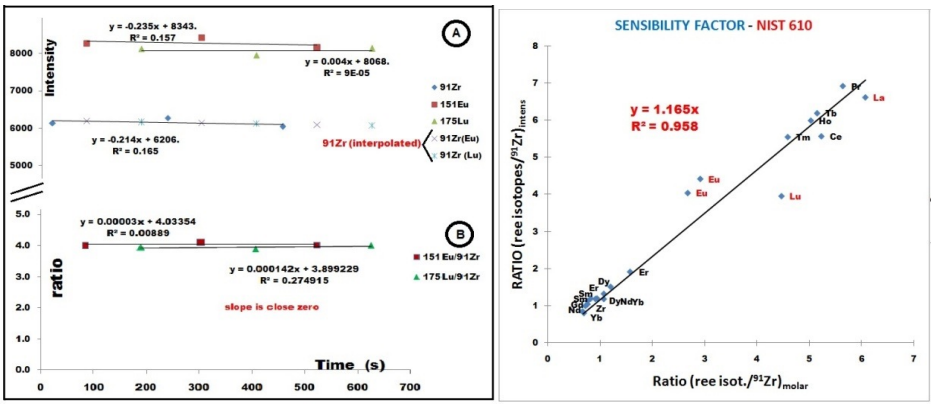

Figure 2(left) - Figure 2A shows ^{91}Zr, ^{151}Eu and ^{175}Lu intensities (total counts - NIST 610). The ^{91}Zr intensity (lozenge symbol) decreases during analysis with negative slope of -0.214. The "x" symbol represents ^{91}Zr interpolated intensities. Figure 2B show REE isotope ratios relative to ^{91}Zr interpolated. The ratio slopes (drift) are very close to zero value. Figure 3 (right) - Sensitivity factor - The sensitivity factor is around 1.16. Lu present low sensitivity (~0.9) while Eu show high sensitivity factor (~1.5).

Result and discussions

The REE data obtained from zircon by SRHIMP were normalized using chondrite value (McDonough and Sun, 1995). Figure 4 show REE data obtained from 91500 zircon standard. The mean value of 12 analyzes were plotted in the Figure 5 to comparison with the mean value obtained by Wiedenbeck et al., (2004). Simple mean value obtained in this work is very close of Wiedenbecket al. (2004) data, but slightly lower.

Figure 6 shows REE data plot obtained for OG1 zircon standard. The figure present normal behavior of an igneous zircon with a positive Ce and a slight negative Eu anomalies, followed by a continue LREE to HREE enrichment. In the same way the REE data obtained for Temora zircon crystals indicates a normal pattern, except when the measures were done close to apatite inclusion (Figure 7). It is possible to observe an inflection occurring among Sm and La (see Figure 7), probably due to small REE diffusion that occur close to apatite inclusion that is rich in LREE. This probable LREE diffusion, coming from apatite, occurs in small scale (lower than 50 microns from inclusion border).On the other hand, HREE trend lines are normal.

HREE in Temora, OG1 and FC1zircon standards normally present a positive correlation. Lu vs U data obtained from OG1 and Temora were plotted in the figures 8 and 9 respectively. The figures show that Lu and U present a relative good tendency with a positive correlation and with R^2 value > 0.48. U concentration from OG1 shown in the figure 6 ranged from 103ppm to 210ppm. HREE trending lines (figure 6) grow from U =103 ppm to U = 210 ppm. In the same way, HREE trending lines at Temora zircon crystals (figure 7) grow in U content function.

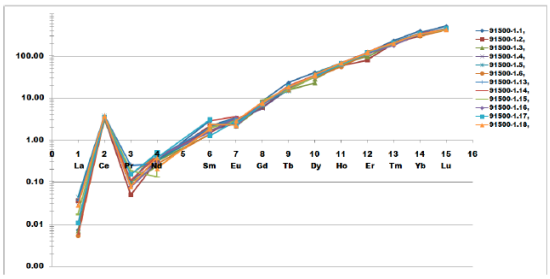

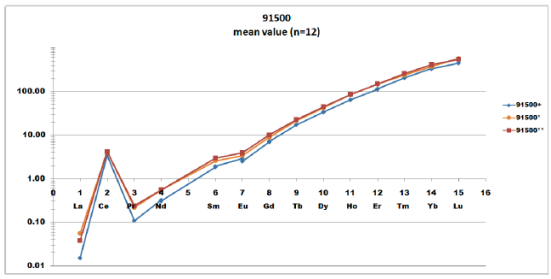

Figure 4 (left): REE/chondrite data at 91500 zircon standard - 12 analyses; Figure 5 (right): comparison between this work (+ blue line, mean value - N=12) and Wiedenbeck et al., 2004 SIMS data (= orange line), Wiedenbeck et al., 2004 SIMS/La-ICP-MS mean value (** = brown line)*

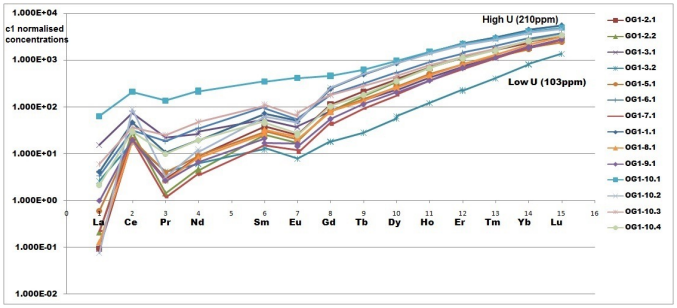

Figure 6 - OG1 zircon standard - HREE increases as U concentration function

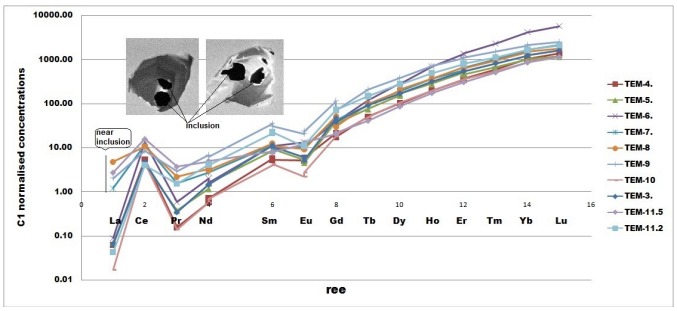

Figure 7 (right) - Temora zircon with apatite inclusion. Near apatite inclusion (< 50µm) LREE content increases but keeping for HREE a normal trend.

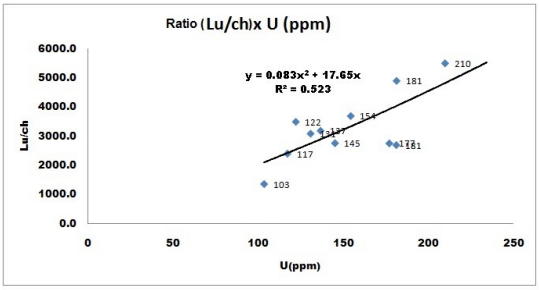

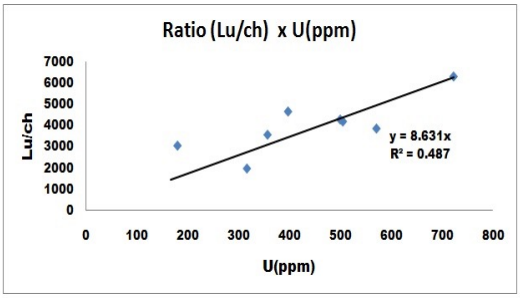

Fig. 8 - OG1- HREE (Lu/ch, ch = chrodrite) and U show positive correlation. Fig. 9 Temora 2 - HREE (Lu/ch) and U present positive correlation. Numbers indicated at Fig.8 represent uranium content (ppm)

Acknowledgements

The authors are grateful for Ian Williams for his REE analyses suggestions and SHRIMP setup.

References

McDonough, WF, Sun S. (1995) The composition of the Earth. Chemical Geology 120, 223–253.

Wiedenbeck , M, Hanchar, JM, Peck WH, Sylvester, P, Valley, J, Whitehouse, M, Kronz, A, Morishita, Y, Nasdala, L, Fiebig, J, Franchi, I, Girard, JP, Greenwood, RC, Hinton, R, Kita, N, Mason, PRD, Norman, M, Ogasawara, M, Piccoli, PM, Rhede, D, Satoh, H, Schulz-Dobrick, B, Skår, Ø, Spicuzza, MJ, Terada, K, Tindle, A, Togashi, S, Vennemann, T, Xie, Q, Zheng,YF. (2004) Further Characterization of the 91500 Zircon Crystal. Geostandard and research geoanalytical. 28, n1, 9-39.

Volcanoes: eruptive style, pre-eruptive evolution and risk (VESPER)

Scarrow, JH[1], Chamberlain, K[2], Preece, K[3], Bea, F[1], Montero, P[1], Cambeses, A[1], Barclay, J[3] and Brown, R[4]

1. Department of Mineralogy and Petrology, Faculty of Sciences, University of Granada, 18071 Granada, Spain
2. R&D Center for Ocean Drilling Science (ODS), JAMSTEC, Yokosuka, 237-0061, Japan
3. School of Environmental Sciences, University of East Anglia, Norwich Research Park, Norwich, NR4 7TJ, UK
4. Department of Earth Sciences, Durham University, Science Labs, Durham, DH1 3LE, UK

This new project will use the compositions and crystal cargoes of erupted magmas to study the preeruptive behaviour of a magmatic system. The aim is to understand its relationship to, and control on, periodicity and eruptive style of volcanic eruptions. To do this we will undertake detailed characterisation of whole-rock composition and mineral chemistry of volcanic rocks from an active intra-plate volcanic centre, Ascension Island. This will also permit consideration of new knowledge about zircon behaviour within a well-constrained system.

We shall characterise inherited, assimilated and magmatic zircons, where present, in the Ascension system. Experimental and numerical modelling predict pre-existing zircons which survive being dissolved in magmas suffer thermal shock. This affects their structure and U-Th-Pb isotopic system and, so, ages (Bea and Montero, 2013). This is reflected in heterogeneities such as irregular patches and zoning. Detailed petrographic study will permit comparison of natural examples of thermal shock with experimental and modelling results.

Recent detailed field mapping and geochemical characterisation of volcanic deposits on Ascension Island shows that there have been >75 explosive eruptions and >40 effusive sub-aerial eruptions in the last million years. Only a few of these show clear evidence for magma mixing prior to eruption. We will use zircon and geochemical data to understand the nature of such interactions.

The main objective of the project is to obtain information about magma storage conditions and plumbing systems in relation to effusive and explosive volcanic activity (cf., Preece et al., 2013; Chamberlain et al., 2016). Such information may be used to consider future behaviour and so possible short-term, within event, and longer term, between events, potential risks.

References

Bea F., Montero P. 2013. Chemical Geology, doi: 10.1016/j.chemgeo.2013.04.014

Chamberlain et al. 2016. Journal of Volcanology and Geothermal Research, doi: 10.1007/s00445-016-1046-z

Preece K., Barclay J., Gertisser R., Herd R. 2013. Journal of Volcanology and Geothermal Research, doi: 10.1016/j.jvolgeores.2013.02.006

A synthesis of triple-oxygen isotope analyses on Antarctic micrometeorites

Soens, B[1], Goderis, S[1], McKibbin, S[1], Pittarello, L[1], Van Ginneken, M[1,2], Debaille, V[2] and Claeys, P[1]

1: AMGC, Vrije Universiteit Brussel, Belgium.
2: Laboratoire G-Time, Université Libre de Bruxelles, Belgium.

Introduction

Micrometeorites (MMs) are extraterrestrial dust particles ranging in size between 10 μm and 2 mm [1], which form the main part of the extraterrestrial flux to Earth (~40000 tons/year) [2]. Traditionally, MMs have been recovered from a variety of depositional environments including deep-seas, deserts, lakes and by melting large volumes of Antarctic ice or snow [3-5]. Over the last decade, large and fresh accumulations of MMs have been discovered in sediment traps on top of glacially eroded granitic summits in the Transantarctic Mountains [6]. Similar deposits have also been found during the 2012-2013 Belgian-Japanese MICROMETA expedition in the Sør Rondane Mountains (East Antarctica), and are currently under investigation. Due to differential production and transportation mechanisms, these microscopic particles of the near-Earth interplanetary dust complex sample parent bodies different from those of meteorites [7-9]. Oxygen isotope ratios are one of the most powerful diagnostic tools to determine the origin of extraterrestrial material, because the combined mass-dependent and mass-independent effects on the three isotopes (^{16}O,^{17}O, and ^{18}O) are well known [10]. Mass-dependent and mass-independent effects during the atmospheric entry of micrometeoroids predominantly reflect fractionation (i.e. from a single source) or mixing of two or more sources (e.g., between nebular reservoirs or with terrestrial oxygen), respectively. Here we present an overview of the available oxygen isotopic data from literature and briefly discuss how the application of SHRIMP-SI (Sensitive High-Resolution Ion Microprobe – Stable Isotope) may facilitate the identification of MM parent bodies.

Methods

Previous work on the oxygen isotope compositions of MMs have been done by Ion Microprobe (IP) or Laser Fluorination Isotope Ratio Mass Spectrometry (LF-IRMS). While IP was capable of processing large datasets in short time spans, such studies typically lacked the precision required for detailed interpretation of the different MM groups (±1‰ for $\delta^{18}O$ and ±0.7‰ for $\Delta^{17}O$ [3,11-13]). Conversely, LF-IRMS achieved higher precisions (±0.3‰ for $\delta^{18}O$ and ±0.2‰ for $\Delta^{17}O$ [14-17]), but is slow and destructive. The prototype SHRIMP-SI is designed for low-mass isotope systems such as oxygen and sulfur. For the latter, precisions of ~0.1‰ on the mass-independent variable $\Delta^{33}S$ have been achieved [18]; we are extending these measurements to oxygen and expect similar precisions.

Results

In short (Fig.1), Suavet *et al*. [11] identified isotopic MM groups 1 and 2 as associated with the different classes of carbonaceous chondrites (i.e. CV, CO, CM, CR). The former group corresponds to CO/CV chondrites, whereas the latter has a larger affinity towards CM/CR chondrites. Group 3 appears related to ordinary chondrites (classes H, L, LL), while the enigmatic group 4 may only be associated to the rare Rumuruti (R) chondrites. However, such MMs are strongly overrepresented compared to the macroscopic R chondrite analogues and would require an extreme degree of mass-dependent fractionation (i.e. evaporation), which is not observed for isotopic group 3. Alternatively, this ^{18}O-rich group 4 may have sampled an unknown meteorite parent body (or bodies). The implementation of SHRIMP-SI for triple-oxygen isotopic analysis on MMs combines the advantages of both IP and LF-IRMS into one procedure. This non-destructive, highly precise approach allows the acquisition of qualitative triple-oxygen isotope data, but preserves sample for other geochemical techniques (e.g., Laser Ablation Inductively Coupled Plasma Mass Spectrometry) to specify the parent bodies of MMs (in particular isotopic group 4).

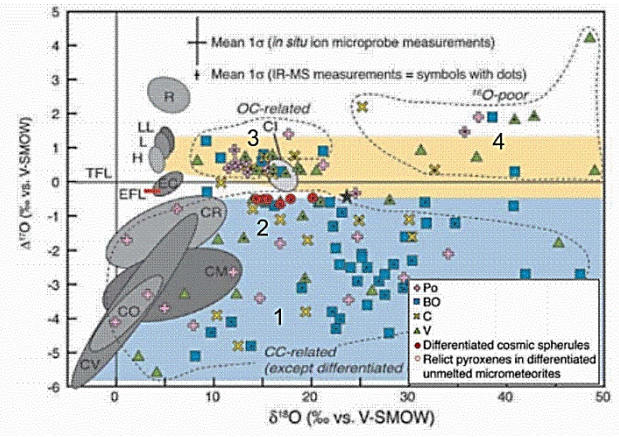

Figure 1: Oxygen isotope systematics of MMs (points) and potential chondritic sources (elliptical fields). The coloured fields illustrate the effect of mass dependent fractionation during melting (loss of lighter isotopes in proportion to their masses) and mixing with terrestrial atmospheric oxygen (star) from starting chondritic compositions (see inset figure). TFL: Terrestrial Fractionation Line, EFL: Enstatite Fractionation Line, EC: Enstatite chondrites. Po: Porphyritic, BO: Barred Olivine, C: Cryptocrystalline, V: Glassy MMs. Image adapted from [19].

References

[1] Rubin A.E. and Grossman J.N. 2010. Meteorit. Planet. Sci. 45:114-122.

[2] Love S.G. and Brownlee. D.E. 1993. Science 262:550-553.

[3] Engrand C. et al. 2005. Geochim. Cosmochim. Acta 69:5365-5385.

[4] Brownlee D.E. 1985. Annu. Rev. Earth Pl. Sc. 13:147-173.

[5] Duprat J. et al. 2007. Adv. Space Res. 39:605-611.

[6] Rochette P. et al. 2008. Proc. Nat. Acad. Sci. 105:47:18206-18211.

[7] Engrand C. and Maurette M. 1998. Meteorit. Planet. Sci. 33:565–580.

[8] Gounelle M. et al. 2009. Proc. Nat. Acad. Sci. 106:6904–6909.

[9] Cordier C. and Folco L. 2014. Geochim. Cosmochem. Acta 146:18–26.

[10] Clayton R.N. et al. 1973. Science 182:485-488.

[11] Clayton R.N. et al. 1986. Earth Planet. Sci. Lett. 79:235–240.

[12] Taylor S.R. et al. 2005. Geochim. Cosmochim. Acta 69:2647–2662.

[13] Yada T. et al. 2005. Geochim. Cosmochim. Acta 69:5789–5804.

[14] Suavet C. et al. 2010. Earth Planet. Sci. Lett. 29:313-320.

[15] Suavet C. et al. 2011. Geochim. Cosmochim. Acta 75:6200-6210.

[16] Cordier C. et al. 2011. Geochim. Cosmochim. Acta. 75:5203-5218.

[17] Cordier C. et al. 2012. Geochim. Cosmochim. Acta 77:515-529.

[18] Ireland T.R. et al. 2014 Int. J. Mass Spec. 359:26-37.

[19] Folco L. and Cordier C. 2015. EMU Notes in Mineralogy, 15, 253-297.

Single spot profiles along human enamel/dentine junction - a sensitive and high spatial resolution $\delta^{18}O$ record of the past environmental variation provided by SHRIMP IIe/ MC study

Soltysiak, A[1], Krzeminska, E[2], Czupyt, Z[2]

1: Department of Bioarchaeology, Institute of Archaeology, University of Warsaw, Poland
2: Polish Geological Institute-National Research Institute, Warszawa, Poland

Organisms through their life absorb elemental and isotopic composition from surrounding environment. Also dental tissues, with high apatite share, keep an oxygen isotopic signals from period of enamel successive mineralization. Temperature depended oxygen isotope fractionation between biogenic apatite and ingested water is influenced by specific physiology of an organism but also by climatic and geographical factors. It makes possible to use $\delta^{18}O$ values of tooth enamel as indicators of paleotemperature and ancient environmental proxy, applicable for bioarcheological research. However, one of the essential issues is the difficult choice between the preservation of dental remains and the use of destructive techniques. This problem may be solved at least partially by developing a proper protocol for *in situ* analysis on ion microprobes, and that was the aim of our experiments. The technique that offers a high spatial resolution of microsampling with sensitive detection of isotopic ratios can effectively support the interpretation of $\delta^{18}O$ variability in the past. Available ion microprobes as CamecaSIMS 1280HR and SHRIMP IIe/MC are very promising tools for low-destructive measurement of $\delta^{18}O$ oxygen isotopic ratios in thin incremental layers of tooth enamel with a spatial resolution of a few micrometers.

The method of $\delta^{18}O$ measurements along mammalian enamel/dentine junction (EDJ) proposed by Aubert et al., 2012 and Blumenthal et al., 2014, has been expanded in PGI-NRI and tested on human teeth (Krzemińska et al, in press). Following previous studies (Blumenthal et al., 2014), the aprismatic innermost of enamel has been used for isotopic analyses as more mineralized and less affected by diagenesis than other areas of enamel.

In this study we briefly discuss the crucial points of a new analytical procedure optimized for $\delta^{18}O$ *in situ* measurements within the innermost enamel layer on SHRIMP IIe/MC. To test the new protocol, we have used a series of human teeth representing (1) Tell Majnuna, a 4th millennium BCE cemetery in Northern Mesopotamia located in relatively hot and arid area of the Middle East with high seasonal differences in precipitation and temperature (Sołtysiak, 2010), and (2) modern Warsaw that is located in the zone of mild continental climate of present day central Poland with mild winters, no dry season, relatively warm summers and much lower seasonality in precipitation. Both deciduous and permanent teeth were used to test the protocol.

The mount preparation procedure was preceded by initial impregnation by epoxy resin that stabilizes all components facilitating precise cutting in the labial-lingual plane to expose a longest and best preserved innermost part of enamel. As a next step selected half of sectioned tooth is positioned upon double-sided tape together with a large number of transparent and inclusion free chips of Durango apatite grains and then embedded again into epoxy resin (Struers Epofix or Araldite). Hardened megamounts are polished, cleaned, photographed and coated with a conductive gold layer according to regular SHRIMP routine. Imaging is limited only to areas documented using transmitted light (TL) photographs of megamount surface. Instrumental configuration and analytical procedures were similar to those detailed by Aubert et al., 2012.

For $\delta^{18}O$ profiles single spots are placed within innermost enamel layer according to maturation chronology along the axis of growth, from the incisal (older) to apical (newer) enamel (in direction shown by arrow on Fig. 1). The distance between neighboring spots varies from 0.10 mm to 0.12 mm, matching to the thickness of each incremental layers. It corresponds to temporal resolution of less than one month of the process of enamel formation, that overall continues for 4–5 years in case of permanent teeth. Measurements are taken using Sample Auto Analysis SAA Setup mode with options “no video” & “no focus”, to shorten usual distances between points. It is important to cover more than 95% of length of exposed enamel layer, omitting only cracked or damaged parts. The innermost layer is easy visually identified on TL images as a thin layer adjacent to the enamel-dentine junction with visible aprismatic incremental zones. In the course of experiments aimed at recognition whether authentic biogenic signal is detected, two complementary ways of validation were applied: (1) a typical control using the reference material (Durango-apatite) after every three spots within studied samples

and (2) comparison of two independent lines of measurements (labial and lingual side) and their patterns control. It is possible to identify spots on both sides that correspond roughly to the same formation time, and $\delta^{18}O$ values there should differ no more than the standard measurement error. The graphical form of stable oxygen isotope composition with standard errors is presented on the diagrams for each side and tooth separately. In result, c. 60-100 single $\delta^{18}O$ values can be obtained from each side of human tooth. If the measurements have followed the chronology of enamel mineralization, the changes in oxygen isotopic ratios may reflect short-term temporal changes in environmental conditions.

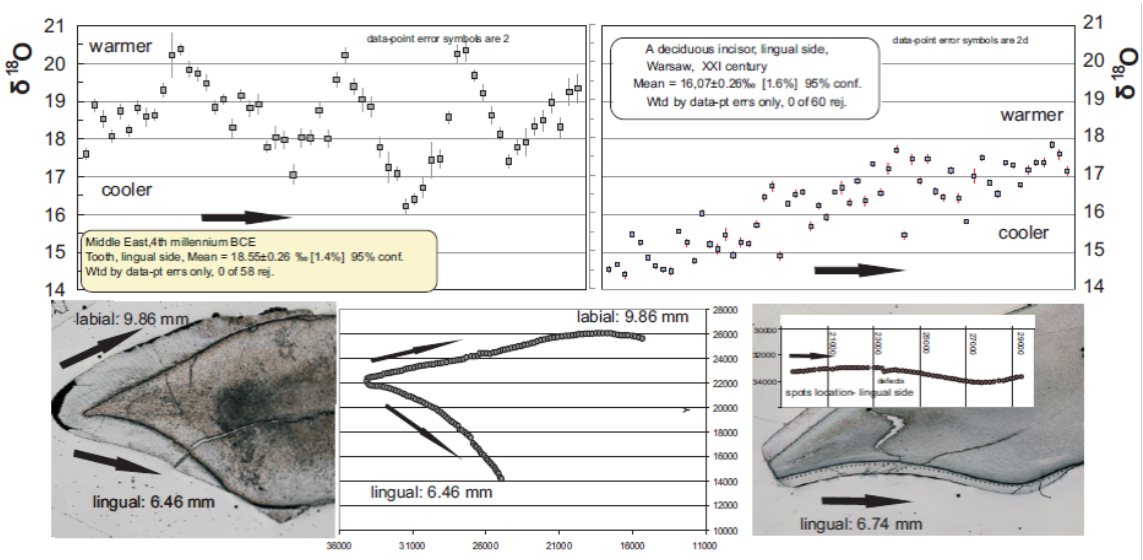

Fig.1. Comparison of δ18O profiles along human EDJ (lingual parts)_ an examples from two different climate areas: Tell Majnuna, NE Syria (upper left) and central Poland (upper right) showing different environmental records: semi-arid steppe climate with hot and dry seasons (strong seasonality) and mild continental with no dry seasons and lower temperatures (mild seasonality), respectively. The track of single spots locations (buttom) within innermost incremental layers of enamel visible on transmitted light photographs done after SHRIMP sessions merged with Y -Z diagrams (sample stage coordinates) that document the positions of each spot.

The range of $\delta^{18}O$ values with average about 18.55‰ indicates (Fig.1) a warmer environment and differences in the level of rainfall than average 16.07‰. The first pattern with strong sinusoidal fluctuations corresponds to the conditions with high seasonal differences in temperature (positive correlation) and rainfall (negative correlation) within few years, reflecting natural seasonality of the semi-arid steppe climate, characteristic for Northern Mesopotamia. The modern enamel of a deciduous incisor shows much less variable pattern that may be due to stable conditions during pre-natal early phase of enamel formation and gradual increase in $\delta^{18}O$ values may be the consequence of breast-feeding during post-natal final mineralization phase.

Conclusion

The results of this study confirm that SHRIMP IIe/MC may be used for successful analysis of $\delta^{18}O$ temporal sub- annual variation due to ecological or dietary changes. It opens a new research possibilities for bioarchaeology and forensic science.

Acknowledgements

The research on teeth from Tell Majnuna was financed by the National Science Centre (NCN) in Poland, grant No. 2013/10/M/HS3/00554.

The preparation of analytical protocol for stable isotope sequential analyses was supported by Polish Geological Institute – NRI internal grant no: 61.32071502.00.0 in 2015.

References

Aubert, M, Williams, IS, Boljkovac, K, Moffat, I, Moncel, M.-H, Dufour, E and Grün R. (2012) In situ oxygen isotope micro-analysis of faunal material and human teeth using a SHRIM P II : a new tool for palaeo-ecology and archaeology. J. Archeological Sci., **39**: 3184–3194.

Blumenthal, SA, Cerling, TE, Chritz ,KL, Bromage, TG, Kozdon, R, Valley, JW. (2014) Stable isotope time-serie in mammalian teeth: in situ $\delta^{18}O$ from innermost enamel layer. Geochim. et Cosmochim. Acta, **124**: 223–236

Krzeminska, E, Sołtysiak, A, Czupyt, Z. (in press) Reconstructing seasonality using $\delta^{18}O$ in incremental layers of human enamel: a test of the analytical protocol developed for SHRIMP IIe/MC ion microprobe. Geological Quarterly, *in press*

Sołtysiak, A. (2010) Death and decay at the dawn of the city. Interpretation of human bone deposits at Tell Majnuna. Areas MTW, EM and EMS, Warszawa: Instytut Archeologii UW

Conventional mechanical crushing versus Selfrag Lab. pulverization

Takehara, M[1] and Horie, K[1,2]

1: Geoscience Research Group, National Institute of Polar Research, Tachikawa-shi, Tokyo, Japan
2: Department of Polar Sciences, The Graduate University for Advanced Studies (SOKENDAI), Japan

Mineral separation is an essential process in sample preparation before SHRIMP U-Pb analysis. In particular, enhancement of recovery rate of minerals is important for U-Pb dating if quantitative comparisons are to be attempted between polychromic zircon populations.

Focused on pulverization process in the mineral separation process for U-Pb zircon geochronology, we compared the recovery rates of zircon between conventional fragmentation with a stampmill and high-voltage selective fragmentation with Selfrag Lab machine. Nearly equal weights of rock (TEMORA2; Black et al., 2004) are crushed by each crushing method. After pulverization, the conventional method (rinsing with water, heavy liquid separation, and magnetic separation with ferrite and Nd magnet) is applied. Weights of the products of each step were measured. Based on the sample weight, recovery rate of heavy and non-magnetic mineral including zircons were calculated and compared between two pulverizing processes.

Weights of TEMORA2 rock fragments and recovery rates are shown in Table 1. Recovery rate of heavy and non-magnetic mineral including zircons by Selfrag are slightly higher than stamp mill pulverization (stamp mill: 0.02680 g, 0.007%, Selfrag: 0.03607 g, 0.009%). However, the difference is so small that it is difficult to judge whether this is caused by difference of pulverization method or heterogeneity of component in TEMORA2 rock fragments. On the other hand, in the case of light minerals, recovery rate using Selfrag is much higher than one using stamp mill. Selfrag can keep the shape of crystals better than stamp mill, so relatively coarse-grained light minerals, such as feldspar and quartz can be survived during pulverizing process.

Table 1. Weights and recovery rates of TEMORA2 zircon obtained using stamp mill and Selfrag Lab.

	rock sample	pulverization	elutriation (rinsing with water)	heavy liquid separation	non-magnetic fraction
Selfrag	378.5 g	307.9 g (81.3%)	-	9.32 g (2.5%)	0.0361 g (0.00953%)
Stamp mill	383.0 g	290.0 g (75.7%)	98.9 g (25.8%)	6.62 g (1.7%)	0.0268 g (0.00700%)

Values in brackets are recovery rate (ratio of weight of product from each separation process divided by weight of rock sample before all separation processes.)

References

Black, LP, Kamo, SL, Allen, CM, Davis, DW, Aleinikoff, JN, Valley, JW, Mundil, R, Campbell, IH, Korsch, RJ, Williams, IS, Foudoulis, C. (2004) Improved 206Pb/238U microprobe geochronology by

the monitoring of a trace-element-related matrix effect; SHRIMP, ID–TIMS, ELA–ICP–MS and oxygen isotope documentation for a series of zircon standards. Chemical Geology 205, 115–140

Zircon U-Pb geochronology and geochemistry of the Utsubo granitic pluton, Hida Belt, central Japan

Takehara, M[1], Horie, K[1,2] and Williams, IS[3]

1: Geoscience Research Group, National Institute of Polar Research, Tachikawa-shi, Tokyo, Japan
2: Department of Polar Sciences, The Graduate University for Advanced Studies (SOKENDAI), Japan
3: Research School of Earth Sciences, Australian National University, Acton, Australia

Geochronological information and the chemical evolution of magmas are essential considerations in the growth of continental crust. A plutonic complex with compositional zonation produced by a single intrusion of magma provides an especially good opportunity to understand the detailed timescale of magmatic evolution. In this study, we discuss the timescale of chemical evolution in the Utsubo granitic pluton using precise zircon U-Pb dating, zircon oxygen isotope analysis and the Ti-in-zircon thermometer.

The Utsubo granitic pluton is situated in the Hida belt, the northernmost geotectonic unit in the Inner Zone of the Southwest Japan Arc. The granitic rocks in the Hida belt are Early Triassic to Early Jurassic in age, and traditionally are classified as Funatsu type or Simonomoto type. Recently, the calc-alkaline plutons in the Hida belt have been divided into two types based on petrology, and Sr and Nd isotopic compositions: Type-1 has a limited range in initial Sr and Nd isotopic values and Type-2 has a wider range (Arakawa and Shinmura, 1995).

The Utsubo granitic pluton, emplaced into the Hida gneiss, is a Type-1 pluton and has normal lateral compositional zoning: tonalite, granodiorite, pink coarse-grained granite, and fine-grained granite from its margin to center (Kano, 1990). Zircon grains extracted from tonalite, granodiorite and coarse-grained granite yielded 192.2 ± 1.4, 190.0 ± 1.3 and 188.5 ± 1.4 Ma, respectively. The geochronological results indicate that the time interval from tonalite to coarse-grained granite is 3.7 ± 2.0 Ma.

The mean oxygen isotope composition ($\delta^{18}O_{VSMOW}$) in zircon decreases slightly (by ~0.54‰) for a ~12% increase in SiO_2, tonalite to granite (Fig. 1). The calculated whole rock $\delta^{18}O$ based on the correlation between $\Delta^{18}O_{(WR\text{-}zircon)}$ and silica content ($\Delta^{18}O_{(WR\text{-}zircon)} = 0.0612 \cdot (SiO_2) - 2.50$; Lackey et al., 2008) is 7.81 ‰ (tonalite), 8.13 ‰ (granodiorite), 8.05 ‰ (granite), using the SiO_2 contents measured by Arakawa and Shinmura (1995). Closed-system differentiation of mafic magmas typically produces an increase in whole-rock $\delta^{18}O$ of ~0.5‰ for each 10% increase in SiO_2 (Taylor & Sheppard, 1986). Lackey et al. (2008) reported that the whole-rock $\delta^{18}O$ of calc-alkaline systems (the Tuolumne suite) increases by ~ 1.0‰ for each 10% increase in SiO_2, while the $\delta^{18}O$ of the zircons is relatively constant.

The zircon crystallization temperatures of the Utsubo granitic rocks, calculated from the Ti content of zircon using the equations of Watson et al. (2006) and Fu et al. (2008), are shown in Fig. 2. The Utsubo granitic rocks contain zircon and titanite ($CaTiSiO_5$). The TiO_2 activity of the Utsubo granitic melt is unknown but it can be assumed to range from ~0.6 to 0.9 because zircon was saturated in this melt and rutile is not observed. The zircon crystallization temperatures were calculated assuming TiO_2 activity is 0.7. The mean zircon crystallization temperature of the Utsubo granitic rocks is constant. On the other hand, the zircon saturation temperatures calculated by the methods of Watson & Harrison (1983) increase with increasing SiO_2. Bulk rock compositions of SiO_2, Al_2O_3, Na_2O, CaO, K_2O, and Zr were obtained from Arakawa & Shinmura (1995). The zircon saturation temperature of the Utsubo granitic rocks increases from ~730 to ~790°C with the increase in SiO_2.

We will discuss the meaning and importance of the geochemical data obtained from zircons through the magmatic process in the zoned pluton.

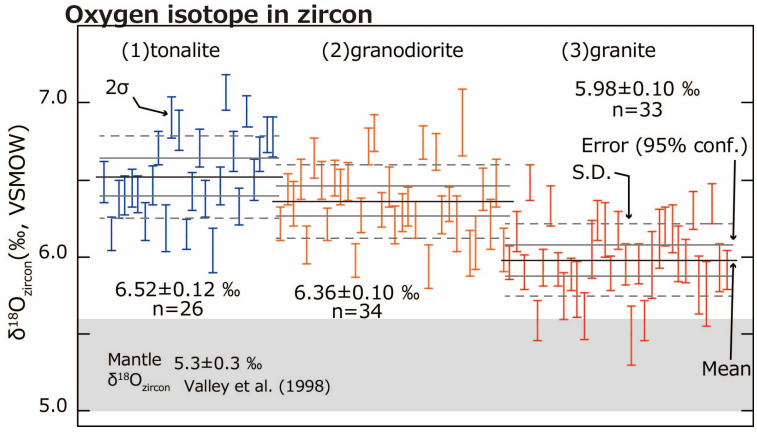

Fig. 1 Plot of $\delta^{18}O$ in zircon from the Utsubo granitic pluton. Error bars are 2σ. $\delta^{18}O$ in zircon from mantle-derived magmas are from Valley et al. (1998).

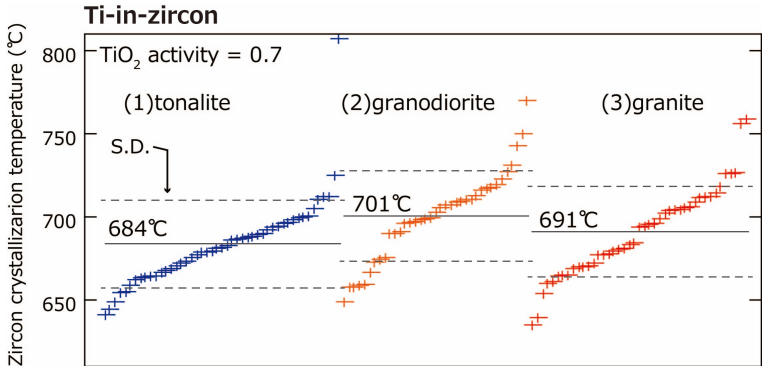

Fig. 2 Plot of zircon crystallization temperature from the Utsubo granitic pluton. Crystallization temperatures are calculated assuming TiO_2 activity is 0.7. Each cross represents the analysis of a single spot. Mean crystallization temperatures are 684°C (tonalite), 701°C (granodiorite), 691°C (granite), respectively.

References

Arakawa, Y, Shinmura, T. (1995) Nd-Sr isotopic and geochemical characteristics of two contrasting types of calc-alkaline plutons in the Hida belt, Japan. Chemical Geology, 124, 217-232.

Kano, T. (1990) Granitic rocks in the Hida complex, central Japan. Mining Geology, 40, 397-413.

Taylor, HP, Sheppard, SM. (1986) Igneous rocks; I, Processes of isotopic fractionation and isotope systematics. Reviews in Mineralogy and Geochemistry, 16, 227-271.

Watson, EB, Wark, DA, Thomas, JB. (2006) Crystallization thermometers for zircon and rutile. Contributions to Mineralogy and Petrology, 151, 413-433.

Fu, B, Page, FZ, Cavosie, AJ, Fournelle, J, Kita, NT, Lackey, JS, Valley, JW. (2008) Ti-in-zircon thermometry: applications and limitations. Contributions to Mineralogy and Petrology, 156, 197-215.

Watson, EB, Harrison, TM. (1983) Zircon saturation revisited: temperature and composition effects in a variety of crustal magma types. Earth and Planetary Science Letters, 64, 295-304.

Valley, JW, Kinny, PD, Schulze, DJ, Spicuzza, MJ. (1998) Zircon megacrysts from kimberlite: oxygen isotope variability among mantle melts. Contributions to Mineralogy and Petrology, 133, 1-11.

SHRIMP dating of high-Th zircons

Talavera, C, Kennedy, AK and McNaughton, NJ

John de Laeter Centre, Curtin University of Technology, Bentley, WA, Australia

Introduction

Zircon can host variable amounts of U and Th although the variation of the Th/U ratio is generally restricted to the range of 0.1 to 1.0, but it can reach values up to 100-1000 in some carbonatites and nepheline syenite pegmatites (Belousova et al., 2002). Carbonatitic zircons typically have low U (<1 up to 100s ppm) and high Th (up to 1000s ppm) (e.g. Belousova et al., 2002, Downes et al., 2016, Midende et al., 2014, Tichomirowa et al., 2014). The high concentration of Th makes these zircons more suitable for Th/Pb dating rather than the usual U/Pb dating.

Sample

Carbonatites from the Canary Islands are located in the western part of Fuerteventura and crop out as subvertical dykes or along shear zones in the Basal Complex, the oldest unit of this island (Fig. 1A). Zircons from this carbonatite are subhedral, often broken, and up to 500 µm long. The Cathodoluminescence (CL) imaging shows two groups of zircons: 1) zircons with typical magmatic oscillatory zoning; and 2) dark zircons with slight or no oscillatory zoning (Fig 1B). Some zircons also show different stages of a later alteration process (Fig. 1B).

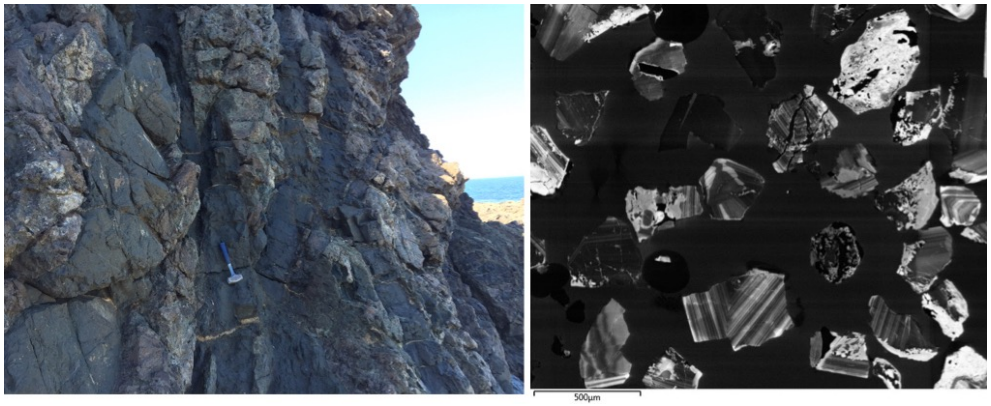

Fig. 1: A) Field photograph of dykes of Fuerteventura Carbonatite (FC). B) CL image of FC zircons. Field of view 500 microns.

Analytical methodology

Analytical procedure broadly followed those described by Compston et al. (1984) and Williams (1998). Data were collected during six scans through the mass range of $^{196}Zr_2O^+$, $^{204}Pb^+$, Background, $^{206}Pb^+$, $^{207}Pb^+$, $^{208}Pb^+$, $^{232}Th^+$, $^{238}U^+$, and $^{254}UO^+$ with count times of 2, 10,10, 50, 10, 20, 5, 5, 2 seconds, respectively.

The high Th content of the carbonatitic zircons (and subsequent tripping of the electron multiplier) from Fuerteventura zircons prevented us using the conventional run table and $^{232}Th^+$ was substituted for $^{248}ThO^+$ to obtain the $^{232}Th/^{238}U$ ratio and the Th concentration. This modification required the calculation of a new equation relating the measured and real $^{232}Th/^{238}U$, when reducing the SHRIMP data. This equation was calculated empirically by measuring $^{232}Th/^{238}U$ in different well-characterised zircon standards (Fig. 2). The resulting equation subsequently used to process our data was:

$$(^{232}Th/^{238}U)_{real} = 1.527 * (^{232}Th/^{238}U)_{measured} + 0.012$$

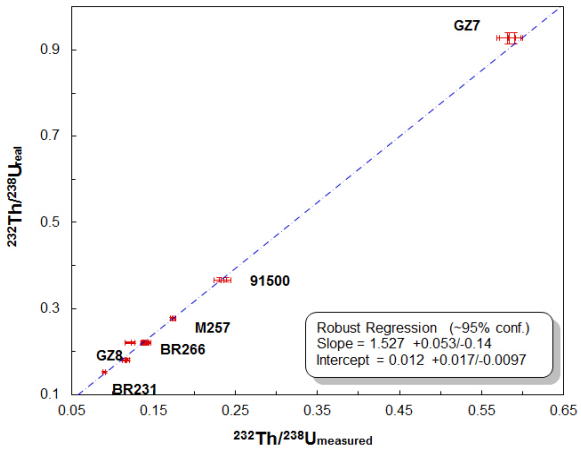

Fig. 2: $(^{232}Th/^{238}U)_{measured}$ versus $(^{232}Th/^{238}U)_{real}$ plot for six different zircon standards.

Results

Thirty one zircons from FC were analysed in a subsequent session. The zircons are characterised by low U and high Th contents, ranging from 0.2 to 899 ppm and from 97 to 16671 ppm, respectively. Despite the extremely high thorium concentration, no obvious matrix effect was observed: i.e no correlation between Th concentration and Th/Pb age or percentage of common lead was detected.

The two CL groups of zircons described above show slightly different U and Th contents. The oscillatory zoned group has relatively high U (up to 899 ppm) and high Th (522-7,220 ppm) whereas the darker zircons have lower U concentration (up to 335 ppm) and much higher Th concentration (up to 16,671 ppm). However, the $^{208}Pb/^{232}Th$ age ranges of both groups are similar.

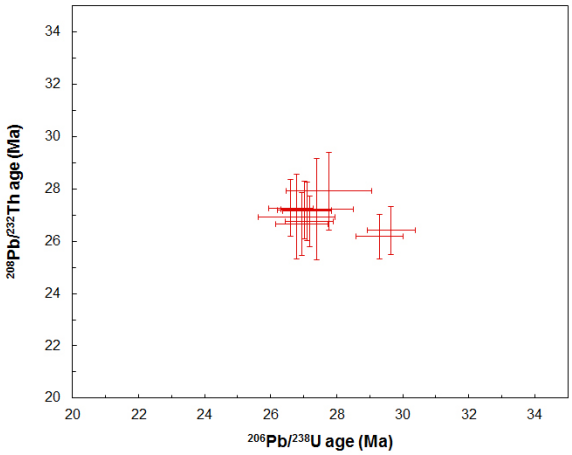

Fig. 3: $^{206}Pb/^{238}U$ age versus $^{208}Pb/^{232}Th$ age for zircons from the Fuerteventura Carbonatite. Error bars are 95% c.l.

The calculation of the $^{208}Pb/^{232}Th$ age of this carbonatite is based on 33 of 38 analyses on zircons from both groups which have less than 1% of common lead and high Th concentrations (1,404 up to 16,671 ppm). Thirty one analyses plot in a single population with a $^{208}Pb/^{232}Th$ age of ~ 27 Ma. There are also two possible older ages. The calculation of the $^{206}Pb/^{238}U$ age is, however, based on only ten analyses which have > 150 ppm of U and <1% of common Pb. Eight analyses plot in a single population with a $^{206}Pb/^{238}U$ age of ~ 27 Ma. There are also two possible older ages.

The $^{208}Pb/^{232}Th$ and $^{206}Pb/^{238}U$ ages seem to be similar but a mismatch between both ages has been recognised in two zircon grains (Fig. 3). The zircons with older $^{206}Pb/^{238}U$ ages have a $^{208}Pb/^{232}Th$ age similar to the crystallisation age within uncertainty. The reason of this inconsistency is currently unknown and further work is needed.

Conclusion

Based on the experiment described above, the $^{208}Pb/^{232}Th$ dating of low-U carbonatitic zircons seems to provide a precise and reliable age and it may represent the best approach for dating this type of rock. This study suggests that Th, unlike U (White and Ireland, 2012), does not have a significant matrix effect on either the $^{208}Pb/^{232}Th$ or $^{206}Pb/^{238}U$ age in high-Th zircons.

References

Belousova, EA, Griffin, WL, O'Reilly, SY, Fisher, NI. (2012) Igneous zircon: trace element composition as an indicator of source rock type. Contributions to Mineralogy and Petrology 143, 602-622.

Compston, W, Williams, IS, Meyer, CE. (1984) U-Pb geochronology of zircons from lunar breccia 73217 using a sensitive high-mass resolution ion microprobe. Proceedings of the fourteenth Lunar and Planetary Science Conference, Par 2. Journal of Geophysical Research 89, B525-B534.

Downes, PJ, Dunkley, DJ, Fletcher, IR, McNaughton, NJ, Rasmussen, B, Jaques, AL, Verrall, M, Sweetapple, MT. (2016) Zirconolite, zircon and monazite – (Ce) U-Th-Pb age constraints on the emplacement, deformation and alteration history of the Cummins Range Carbonatite Complex, Halls Creek Orogen, Kimberley region, Western Australia. Mineralogy and Petrology 110, 199-22.

Midende, G., Boulvais, P, Tack, L, Melcher, F, Gerdes, A, Dewaele, S, Demaiffe, D, Decrée, S. (2014) Petrography, geochemistry and U-Pb zircon age of the Matongo carbonatite Massif (Burundi): Implication for the Neoproterozoic geodynamic evolution of Central Africa. Journal of African Earth Sciences 100, 656-674.

Tichomirowa, M, Whitehouse, MJ, Gerdes, A, Götze, J, Schulz, B, Belyatsky, BV. (2013) Different zircon recrystallization types in carbonatites caused by magma mixing: Evidence from U-Pb dating, trace element and isotope composition (Hf and O) of zircons from two Precambrian carbonatites from Fennoscandia. Chemical Geology 353, 173-198.

White, LT, Ireland, TR. (2012) High-uranium matrix effect in zircon and its implications for SHRIMP U-Pb age determinations. Chemical Geology 306-307, 78-91.

Williams, IS. (1998) U-Th-Pb Geochronology by Ion Microprobe. In: M.A. McKibben, Shanks, W.C., Ridely, W.I. (eds), Applications of Microanalytical Techniques to Understanding Mineralizing Processes.

Boron Isotope Analysis on SHRIMP II

Williams, M[1], Holden, P[1], Rubatto, D[1,2] and Magee, C[3]

1: Research School of Earth Sciences, Australian National University, Canberra, Australia
2: Institute of Geological Sciences, University of Bern, Bern, Switzerland
3: Australian Scientific Instruments, Canberra, Australia

Boron is a useful elemental and isotopic tracer for a variety of geological processes, and particularly those related to fluid-rock interaction. As an incompatible element, boron is concentrated in surface reservoirs where variations in temperature, pH and fluid-rock ratios produce an array of geochemical reservoirs with different boron abundances and isotopic compositions. The heterogeneity of subduction zone inputs in terms of boron abundance and $\delta^{11}B$ can be exploited to constrain fluid production and migration within the slab, and also relative contributions of different reservoirs to arc magmatic suites. The ability to conduct in-situ boron isotope analysis of hydrated minerals presents an additional tool to constrain metamorphic and geochemical evolution in such systems. Here we present results of development for boron isotope analysis on SHRIMP II at the Research School of Earth Sciences, ANU.

Initial analytical testing for boron isotopes in positive mode ($^{10}B^+$, $^{11}B^+$) used a single electron multiplier, and was conducted on three instruments: SHRIMP RG (ANU), SHRIMP II (ANU) and SHRIMP IIe (Geoscience Australia). Analysis of positive secondary ions results in slightly reduced ionisation yield (relative to $^{10}B^{16}O^-$, $^{11}B^{16}O^-$), but all isobars are effectively resolved at mass resolution of 1600-1800 (not possible for negative mode, where $^{12}C^{14}N^-$ requires ≈ 12,000). A duoplasmatron was utilized to produce a 1-35nA $^{16}O^-/^{16}O_2^-$ primary beam, focused through a Köhler aperture to provide a

30-100µm spot. Helmholtz coils were used on the source chamber to minimise isotopic dispersion due to ambient magnetic field. Analysed targets include the NIST and MPI-DING glasses, various phyllosilicates (serpentine, chlorite, biotite-phlogopite, and white micas) and tourmaline. Instrumental mass fractionation on the order of 30-40‰ is observed for SHRIMP II for both single- and multi-collector analysis.

Single collector boron isotope analyses were conducted with 10 scans (300s collection time; 15-17 min/spot). Testing for sequential collection of $^{6}Li^{+}$, $^{7}Li^{+}$, $^{10}B^{+}$, $^{11}B^{+}$, $^{24}Mg^{++}$, and/or $^{16}O^{+}$ suggests that limiting the runtable mass range to 3-4amu is necessary for optimal analysis of boron isotopes. The $^{24}Mg^{++}$ ion is a feasible internal standard for estimation of boron abundance for Mg-bearing minerals (e.g. serpentine, chlorite, some micas), while the $^{16}O^{+}$ ion may prove sufficient for Mg-poor minerals. The collector transfer system and retardation lens (at 7000-7500V) were utilized to minimise the influence of low-energy ions, resulting in typical signal losses on the order of 10-20%. Repeated analysis of a selection of glass reference materials (2.3 to 350ppm B) over multiple sessions yielded internal uncertainties on $\delta^{11}B$ averages of 0.7-2.6‰ (2SE, n = 6-23), and reproducible averages between sessions. For glass reference materials, relative sensitivity is approximately 50-80 c/s/nA/ppm and is composition dependent. NIST610 and GOR-128G glass reference materials were used as primary reference materials (Kasemann et al., 2001; Jochum et al., 2006 respectively). A systematic bias of up to 3‰ was observed across a range of synthetic and natural glass compositions (NIST, Gorgona Komatiite, St. Helens Andesite; greater than bias observed on similar large-format instruments, e.g. Marschall & Monteleone, 2015).

Multicollector boron isotope analysis was also conducted on SHRIMP II with a dual Faraday Cup setup, using 6-10 scans (up to 200s collection time; 6-9 min/spot). The reference material B4 (Elba Island schorl; Tonarini et al., 2003) was used as a primary standard. Repeated analyses of B4 tourmaline during typical sessions (0.5-2 days) yield a $\delta^{11}B$ repeatability of 0.4-0.8‰ (2σ) after correcting for instrumental drift. Analysis of secondary reference tourmalines yields reproducibility of mean $\delta^{11}B$ between sessions on the order of 0.5-0.8‰ (2σ). At this level of precision, matrix effects are identifiable across the Mg-Fe (dravite-schorl) solid solution, and also with changes in Li and Al content. Analysis of reference tourmalines (Dyar et al., 2001) and natural tourmalines for which TIMS data are available suggest modest matrix bias associated with variation in Mg# (up to -3‰ relative to B4; negative bias towards either endmember). For common metamorphic dravites (Mg# 0.5-0.9), bias is likely within analytical uncertainty. Multicollector boron isotope analysis by SHRIMP has allowed the identification of isotopic heterogeneity in zoned tourmalines, and may assist in interpretation of fluid-rock interaction histories within metamorphic and metasomatic lithologies.

References

Dyar, MD, Wiedenbeck, M, Robertson, D, Cross, LR, Delaney, JS, Ferguson, K, Francis, CA, Grew, ES, et al. (2001) Reference Minerals for the Microanalysis of Light Elements. Geostandards Newsletter, 25(2-3), 441-463.

Jochum, KP, Stoll, B, Herwig, K, Willbold, M, Hofmann, AW, Amini, M, Aarburg, S, Abouchami, W, et al. (2006) MPI-DING reference glasses for in situ microanalysis: New reference values for element concentrations and isotope ratios. Geochemistry, Geophysics, Geosystems, 7(2), Q02008.

Kasemann, S, Meixner, A, Rocholl, A, Vennemann, T, Rosner, M, Schmitt, AK, Wiedenbeck, M. (2001) Boron and Oxygen Isotope Composition of Certified Reference Materials NIST SRM 610/612 and Reference Materials JB-2 and JR-2. Geostandards Newsletter, 25(2-3), 405-416.

Marschall, HR, Monteleone, BD. (2015) Boron Isotope Analysis of Silicate Glass with Very Low Boron Concentrations by Secondary Ion Mass Spectrometry. Geostandards and Geoanalytical Research, 39(1), 31-46.

Tonarini, S, Pennisi, M, Adorni-Braccesi, A, Dini, A, Ferrara, G, Gonfiantini, R, Wiedenbeck, M, Gröning, M. (2003) Intercomparison of Boron Isotope and Concentration Measurements. Part I: Selection, Preparation and Homogeneity Tests of the Intercomparison Materials. Geostandards Newsletter, 27(1), 21-39.

The deficiencies and excesses of the very young

Williams, IS[1], Rojas-Agramonte, Y[2,3,4] and Kröner, A[2,4]

1: Research School of Earth Sciences, The Australian National University, Canberra, ACT 2601, Australia
2: Beijing SHRIMP Centre, Chinese Academy of Geological Sciences, 26 Baiwanzhuang Road, 100037 Beijing, China
3: Departamento de Ciencias de la Tierra y de la Construcción, Universidad de las Fuerzas Armadas ESPE, Sangolquì, Ecuador
4: Department of Geosciences, University of Mainz, 55099 Mainz, Germany

Debate continues about the extent to which material from the continental crust is recycled into magmas produced in intra-oceanic settings. The report by Pilot and others (1998), for example, that Palaeozoic and Proterozoic zircon had been found in gabbro recovered by drilling beneath the mid Atlantic Ridge was received with scepticism, only to have similar findings reported by Belyatsky and others (2008) several years later in a more extensive study of similar rocks. Intra-oceanic subduction zones are another setting in which there is the potential for mantle-derived magmas to incorporate upper crustal material.

The Lesser Antilles arc, developed during westward subduction of Atlantic oceanic lithosphere beneath the leading edge of the Caribbean plate, is one of the best global examples in which to examine how the involvement of subducted sediment affects the composition of mantle-derived magmas. Many of the Cenozoic volcanic rocks in the arc contain inherited zircon, the most likely source of which is eroded continental crust. Zircon dating of these rocks has proved to be a challenge; some are less than 1 Ma old. Achieving adequate analytical precision in the U-Pb analyses of such zircon using SHRIMP has involved departures from normal analytical conditions, for example the use of larger spots, longer counting times on Pb, and a primary ion beam that is not mass filtered. Particular care was also needed to minimise the common Pb on the surface of the mount.

Precision is not the main limiting factor in dating such zircon, however. The principal limitation is accurate correction for disequilibrium in the ^{238}U decay series. This series takes about 3 Ma to reach secular equilibrium, the main determining factor being the slow decay of the intermediate daughter product ^{234}U, with a half life of ~ 246 ka. Even if the U incorporated in a mineral has an equilibrium $^{234}U/^{238}U$ ratio (5.42×10^{-5}), the moderately slow decay of ^{230}Th, with a half life of ~ 76 ka, prevents secular equilibrium being reached for about 1 Ma. This radioisotopic bottleneck means that the production of ^{206}Pb is delayed, and even after secular equilibrium is achieved, a deficiency in ^{206}Pb remains.

Recognition of this situation is nothing new. Schärer included it as one of his examples in his discussion of the effects of excess ^{230}Th in the dating of young minerals with high Th/U, most notably monazite (Schärer, 1984). He proposed an addition to the simple ^{238}U decay equation that takes the effect of initial ^{230}Th into account:

$$^{206}Pb/^{238}U = (e^{\lambda 238 t} - 1) + \lambda_{238} / \lambda_{230} (f - 1)$$

where $f = Th/U_{mineral} / Th/U_{melt}$. This equation works well in the great majority of cases, but becomes increasingly inaccurate at ages less than 1 Ma.

A further modification to the equation has recently been proposed by von Quadt and others (2014), based on the work of Sakata and others (2013). This equation takes into account both initial ^{230}Th and the ingrowth of ^{230}Th from ^{238}U decay:

$$^{206}Pb/^{238}U = (e^{\lambda 238 t} - 1) + \lambda_{238} / \lambda_{230} (f - 1) (1 - e^{-\lambda 230 t}) e^{\lambda 238 t}$$

Both these equations are approximations. An accurate calculation of the $^{206}Pb/^{238}U$ expected in very young minerals requires all 17 intermediate decay products in the ^{238}U decay chain to be taken into account. In practical terms, however, only ^{234}U, ^{230}Th, and ^{226}Ra have half lives long enough to have a significant influence on the result. In deciding how best to calculate the ages of the youngest of the Lesser Antilles zircons we have revisited the question of U-series disequilibrium using the first-principles equations developed by Bateman (1910). We have compared the results of this relatively rigorous calculation with those from the approximations proposed by Schärer (1984) and von Quadt and others (2014). Our finding is that for zircon of 'normal' composition (Th/U = 0.5) older than 700 ka, the results from the three methods of calculation agree within about 0.4%. At 300 ka the discrepancy increases to about 3%, and the Schärer (1984) equation gives negative isotope ratios below

about 96 ka. The von Quadt et al. (2014) correction, in contrast, remains accurate within 10% of the measured age down to 50 ka. The discrepancy between corrected and uncorrected ages also increases with decreasing age. At 10 Ma the discrepancy is ~ 0.1%, at 1 Ma it is ~ 10%, at 500 ka it is nearly ~ 20%, at 250 ka it is ~ 35%.

Similar discrepancies are found for monazite (e.g. Th/U = 30). Above 700 ka the corrections agree within about 0.2%, at 300 ka the disagreement between the Schärer (1984) correction and the other two is about 4.5%, and at 100 ka it rises to ~ 55%, getting even larger for younger samples. The von Quadt et al. (2014) correction, on the other hand, is accurate within 4% as young as 50 ka. Our conclusion is that, for samples older than 1 Ma the simple equation of Schärer (1984) is perfectly adequate. For samples in the range 1.0–0.1 Ma the equation of von Quadt et al. (2014) works very well, but below 100 ka the best result is obtained using the equations of Bateman (1910). This issue having been resolved, the problem remaining is to make an accurate estimate of Th/U_{melt} (not necessarily the same as Th/U_{rock}), which is needed in order to calculate 'f '.

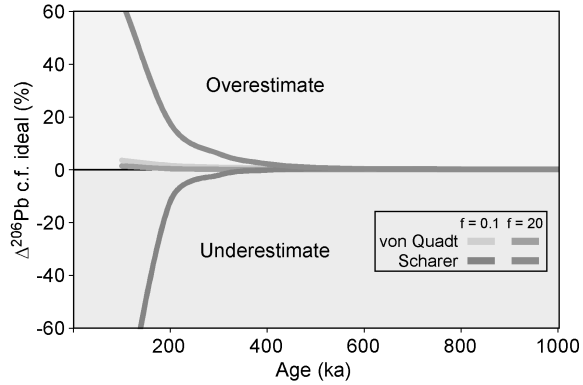

References

Bateman, H. (1910) The solution of a system of differential equations occurring in the theory of radio-active transformations. Proceedings of the Cambridge Philosophical Society, 15, 423–7.

Belyatsky, B, Lepekhina, E, Antonov, A, Shuliatin, O, Sergeev, S. (2008) Age and genesis of accessory zircon from MAR gabbroids. Geophysical Research Abstracts, 10, EUG2008-A-01314.

Pilot, J, Werner, C-D, Haubrich, F, Baumann, N. (1998) Palaeozoic and Proterozoic zirconz from the Mid-Atlantic Ridge. Nature, 393, 676–9.

Sakata, S, Hirakawa, S, Iwano, H, Danhara, T, Hirata, T. (2013) Correction of initial-disequilibrium on U-Th-Pb system for dating of young zircons. Abstracts, Goldschmidt 2013, A2116.

Schärer, U. (1984) The effect of initial ^{230}Th disequilibrium on young U-Pb ages: the Makalu case, Himalaya. Earth and Planetary Science Letters, 67, 191–204.

von Quadt, A, Gallhofer, D, Guillong, M, Peytcheva, I, Waelle, M, Sakata, S. (2014) U-Pb dating of CA/non-CA treated zircons obtained by LA-ICP-MS and CA-TIMS techniques: impact for their geological interpretation. Journal of Analytical Atomic Spectrometry, 29, 1618–29.

AMCG suite in NE Poland-subsequent datings of A-type granitoids on SHRIMP

Wiszniewska, J[1], Krzemińska, E[1], Krzemiński[1] and Williams, IS[2]

1: Polish Geological Institute- National Research Institute, Warszawa, Poland
2: Research School of Earth Sciences, Australian National University, Canberra, Australia.

The Mesoproterozoic magmatic activity has been recorded in a few localities in SW Fennoscandia including the area of Mazury Complex (MC) in Poland dominated by anorthosite–mangerite–charnockite–granite AMCG suite. AMCG plutonic rocks were emplaced along a linear zone of weakness, which facilitated melting of the lower crust. This part of Fennoscandia is buried by more than 1000 m of the Phanerozoic sediments at present but recognised by deep drillings. AMCG intruded

into the Palaeoproterozoic crust, forming a 200 km long, E–W trending anorogenic belt. This polyphase plutonic structure formed along of three anorthosite-norite massifs e.g. Ketrzyn, Suwalki and Sejny (Wiszniewska et al., 2002) is dominated by porphyritic A-type granitoids, and accompanied by subordinate charnockites and mangerites. AMCG suite provide an evidence that, two different crustal source-rocks can produce two different suites of rocks during the same melting episode (Duchesne et al., 2010). One of the melting product - the hornblende bearing granite suite, oxidized and H_2O-rich is associated with an anorthosite and ferrodiorite and charnockite suite, which formed under dry and more reduced conditions.

Several samples from MC area were recently dated by U-Pb method (Wiszniewska et al., 2007) and the most of them were analysed during last ten years by SHRIMP ion microprobe facilities at RSES, ANU Canberra and afterwards in PGI-NRI, Warsaw. New U–Pb ages however are related to the granitoid member of suite, that represent the most dominant phase across the region showing commonly known a rapakivi-like texture and A type chemical signature.

In this study, we report sensitive high-resolution ion microprobe (SHRIMP) U–Pb zircon ages from further localities within basement: (a) east- and westernmost parts of Suwalki Anorthosite Massif as well as from (b) subsequent boreholes located within Warmia area, as a western prolongation of MC, where the depth of the crystalline rocks occurrence violently increases. The zircon single grain samples have been selected from boreholes: Krasnopol 6 -depth of 1003m (KR), Filipow 1, depth of 1595m (FI), Debowiec Warminski 3- depth of 2771m (DW), Malbork 1- depth of 3668 m (MA), and Koscierzyna 1 - depth of 5199 m (KO).

U-Pb zircon analyses were realized according to “canonical” SHRIMP routine but using two different reference materials. The Temora3 mainly has been used as a primary standard, but in case of two samples standardization was leading on FC-1, giving error calibration of 0.47 % during 26 hours of automatic session. The uranium content was calibrate on SL13 reference zircon.

Despite distinct E-W spatial locations of two boreholes from MC area - samples KR and FI yield overlapping U–Pb crystallization ages of 1510±10 Ma and 1512± 17 Ma, respectively. The identical age of the similar type of rocks from two distant localities is consistent with other evidences suggested that long merged MC belt is composed of coherent intrusive bodies. The regional prolongation of MC intrusions group to the west in the Warmia area revealed somewhat younger ages towards to west from 1520±22 Ma (DW) to 1494 ±13 Ma (KO). As a tests on the beginning of analytical activity of PGI-SHRIMP Lab in 2015, the zircon measurements on mounts analyzed in 2005, have been repeated during one session. It documented that minimal sample damage during sputtering by SHRIMP primary beam really leaves the target intact for repeat analyses, future work and post analysis examination. The repetition has been done after short re-polishing and cleaning procedure of mini mount with DW and MA samples.The reconnaissance data in 2005 were limited to n=10 single spots on each sample and gave the simple weighted Pb-Pb mean age of 1520±22 Ma (sample DW, Fig.1- left) and 1497±21 Ma (sample MA). After these first estimation a number of single spots has been extended up to n=25 (DW) and to n=33 (MA). Most part of DW zircon analyses overlap on concordia curve defining an age of 1535.8±9.5 Ma (Fig. 1-right) or identical weighted Pb-Pb mean age of 1536±9.5 Ma.

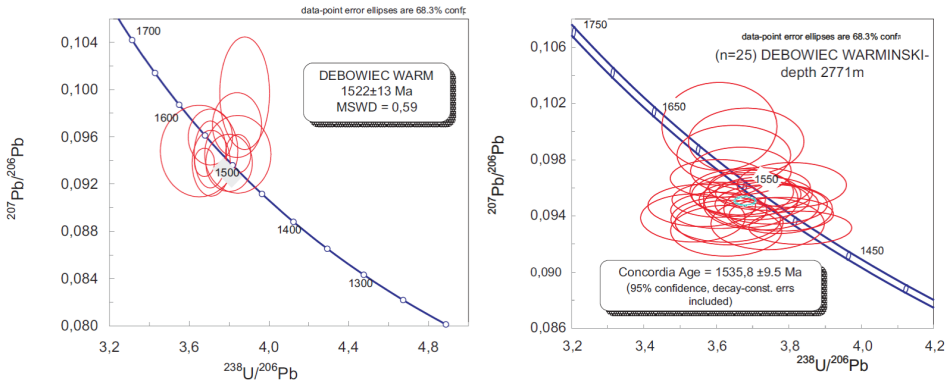

Fig.1. Tera–Wasserburg concordia diagrams of repeated U–Pb zircon measurements of the same sample DW (), with calculating the weighted Pb-Pb mean age (left) done in 2005, vs concordia age (right) done in 2015.

For sample MA, 28 from 33 analyses yielded concordia age at 1509.2±7.9 Ma, that slightly improved a precision of age estimation. A slight degree of zircon discordance and internal convolute shape of CL patterns are considered as an indicative of a complex isotopic evolution. Therefore, a new U-Pb titanite and apatite dating project has now been initiated to establish a more detailed records of the intrusive activity and define a spread of syn- to post-magmatic stages, using coexisting titanite or/ and apatite grains extracted from the same heavy mineral remains after zircon separation procedure.

Conclusions

The new U–Pb results indicate that there was no gap in within-plate igneous activity at this latitude of the Fennoscandian block and intrusions were emplaced probably during long overlapping events however the age database is still limited to the oxidized and H_2O-rich granite member of AMCG suite. The absolute ages of the charnockitic and anorthositic members of the suite seems to be critical to any AMCG genetic models.

Acknowledgments

Funding from projects 21.2101.0010 and 00.8520.1401.00.0 in PGI-NRI has supported most of this works.

References

Duchesne, J-C, Martin, H, Baginski, B, Wiszniewska, J, Vander-Auwera, J. (2010) The origin of the ferroan-potassic A-type granitoids: the case of the hornblende-biotite granite suite of the Mesoproterozoic Mazury Complex, Northeastern Poland The Canadian Mineralogist 48 (4)· 947-968.

Wiszniewska, J. (2002) Wiek i geneza rud Fe-Ti-V i skal towarzyszących w suwalskim masywie anortozytowym (NE Polska). Biuletyn PIG, 401, 1-96.

Wiszniewska, J, Kusiak, MA, Krzemińska, E, Dörr, W, Suzuki K., (2007) MesoproterozoicAMCG granitoids in the Mazury Complex, NE Poland- a geochronological update. W: Kozłowski, Wiszniewska J., ed. Granitoids in Poland. AM Monograph 1, 31–39.

Is an inter- and intra-conodont specimen $\delta^{18}O$ variability a key to their paleoecology? Example from the Upper Devonian of the Holy Cross Mountain (Poland)

Wójcik, K, Krzemińska, E and Czupyt, Z

Polish Geolgical Institute-National Research Institute, Warszawa, Poland

Introduction

Conodonts are extinct group of marine nektonic chordates known mostly after phosphatic denticles of their mouth apparatus, referred to as “elements”. These elements are 1 to 5 mm long and have lamellar concentric structure. This structure originated as a result of daily growth increments of successive lamellae of calcium phosphate, which were added from the outside, as in vertebrate enamel (Dzik, 2008). Usually there are from 40 to 70 laminas (each of 1 to 5 μm thick) in particular elements indicating the animals reached their maturity after approximately 2 months. The oxygen isotope composition of conodont bioapatite provide relatively robust record of palaeoseawater temperature through Paleozoic and Triassic (e.g. Joachimski et al., 2009; Trotter et al. 2015). In recent years the conodont elements have been intensely researched using conventional GIRMS and in-situ SIMS techniques (e.g. Wheeley et al., 2012). Our current SHRIMP ion microprobe analyses have been aimed at collecting the isotopic dataset of the Upper Devonian conodonts from the Holy Cross Mts. (central Poland). Multiple measurements of individual elements have been used to test both the inter- and intra-specimens variability for constraining a model of the Late Devonian conodont palaeoecology.

Samples and methods

A collection of 33 conodonts derived from eight samples from the Upper Devonian *linguiformis* – lower *expansa* interval from the Płucki and Zbrza sections (southern part of the Holy Cross Mts.; see Wójcik, 2012) has been analyzed. The collection includes 5 specimens of *Icriodus alternatus alternatus* (Frasnian, Płucki section), 3 specimens of *Polygnathus webbi* (Frasnian, Płucki section), 1

secimen of *Ancyrodella curvata* (Frasnian, Płucki section) and 24 palmatolepids (Frasnian and Famennian, Płucki and Zbrza sections).

Analyses of conodonts were undertaken on the SHRIMP IIe/MC in PGI-NRI following the protocols for ion microprobe analysis of conodonts set out by Trotter et al. (2008). The megamount has been prepared according to regular routine: namely single individuals were carefully positioned upon double-sided tape and potted by epoxy resin (Struers Epofix) together with proper amount of Durango3 grains. Before and after analytical session sample imaging has been prepared under optical microscope in reflected RL and transmitted TL light. Conductivity of target was obtained by gold, as an alternative to the routine of aluminum target application. The mount surface was coated by thin ~ 12 nm layer of high purity of Au. Two cycles of measurements of individual conodonts has been applied. After first session a deeper polishing allowed to expose a successive layers of bioapatitic dental tissue, which were embedded in a resin. The penetration of the focused Cs^+ primary beam does not destroy the sample, thus even a few re-polishing cycles are feasible. Single spots on quasi-profiles were run along and across each individual specimen. For bioapatitic conodont samples the apatite Durango3 has been used to calibrate oxygen isotopic composition (ref. $\delta\ ^{18}O = 9.80‰$). The reference material Durango3 was analyzed at the beginning of each session and after every three-four sample spots. Selected chips of transparent and inclusion-free Durango apatite usually yielded proper internal consistency of isotopic composition. The mean average value of $\delta^{18}O$ during first session was of 9.80 ± 0.08‰ (s.d. 0.37, n=41), and during the second session of 9.81 ± 0.07 ‰ (s.d.0.38, n=40), which is relatively close to the referenced value. The sample data were processed using POXI software.

Results

The oxygen isotope record on conodont elements from total 229 single spot measurements exhibit a wide range of $\delta^{18}O$ VSMOW values from 16.70± 0.12‰ to 20.72± 0.11‰. The number of measurements (n) located within one element was from 3 to 15 (Fig.1, table 1). Within each single conodont element, $\delta^{18}O$ can vary by up to ~3‰, but typical ranges are below 2‰ (table 1). The highest fluctuation was 2.73‰ recorded within one of largest conodont (FA23), which corresponds to the difference in temperature record to 6.5ºC. The mean composition of element was calculated as the unweighted mean of the accepted analyses. Regard to seven individuals, a double series analysis were applied, showing well repeatability intra-specimen average $\delta^{18}O$ values: discrepancy of the average mean $\delta^{18}O$ value not exceed 1.33 ‰. The mean $\delta^{18}O$ variability between different conodont elements within and between particular rock samples is generally lower about 2‰.

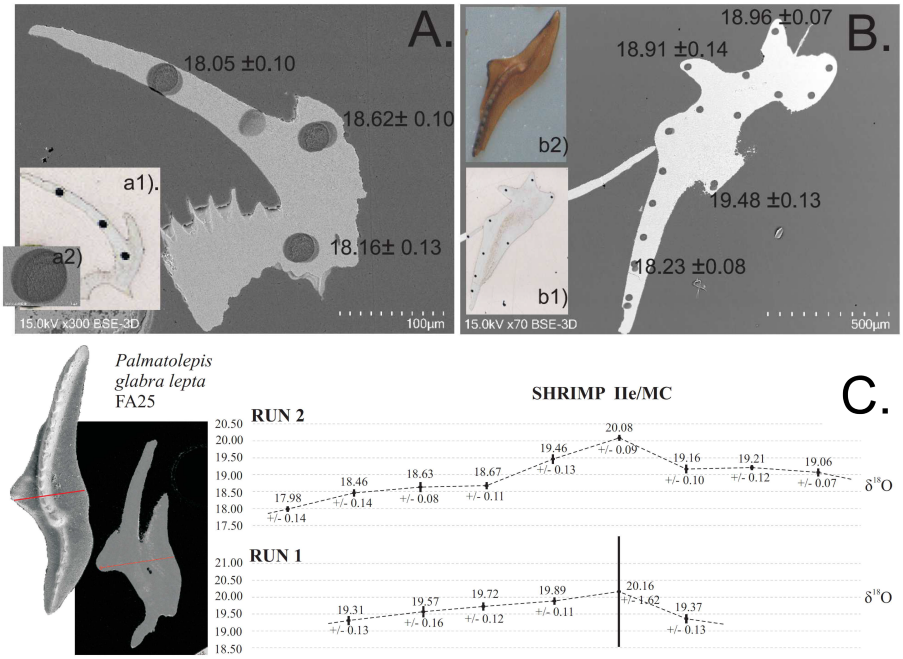

Figure 1. The record of single spot location with representative values of δ18O [‰]: A) BSE image of FA17 after II run (n= 3 spots, intra-element variations =0.57‰). B) BSE image of FA23 after II run (n= 15 spots, intra-element variations =1.44‰); a1) and b1) RL images after I run; a2) area of burned pit showing structure of bioapatite lamellae; b2) FA23 condont element from mount preparation stage. C) SEM image of FA25 and δ18O results across conodont element after I and II run.

Table 1. Summary of the isotopic heterogeneity of individual conodont elements detected during repeated measurement run I versus run II

Sample	Stratigraphy	Conodont ID	Species	run	n	(1) Intra-element max-min [‰]	(2) Mean $\delta^{18}O$ [‰]	±[‰]	s.d.	Discrepancy ±[‰]	Average temp. [° C]	Difference ±[°C]
1	Famennian, Lower *rhomboidea* Zone	FA5	*Palmatolepis glabra prima*	I	6	1.66	18.10	0.25	0.56	0.82	31.4	3.2
				II	5	1.11	18.82	0.21	0.48		28.2	
2		FA17	*Palmatolepis rhomboidea*	I	3	1.18	18.23	0.35	0.52	0.05	30.9	0.4
				II	3	0.57	18.28	0.17	0.30		30.5	
3	Famennian, Lower *marginifera* Zone	FA23	*Palmatolepis glabra lepta*	I	8	2.73	18.86	0.31	0.87	0.11	28.1	0.6
				II	15	1.44	18.97	0.11	0.43		27.5	
		FA24	*Palmatolepis glabra lepta*	I	7	1.90	18.94	0.26	0.72	0.01	27.7	0.0
				II	12	0.35	19.02	0.12	0.41		27.3	
		FA25	*Palmatolepis glabra lepta*	I	6	0.8	19.67	0.13	0.32	0.70	24.4	3.1
				II	9	2.1	18.97	0.21	0.62		27.5	
4		FA27	*Palmatolepis g. pectinata*	I	3	1.78	18.01	0.54	0.93	0.64	31.9	2.9
				II	4	1.79	18.65	0.42	0.84		29.0	
		FA28	*Palmatolepis g. pectinata*	I	3	0.59	19.79	0.17	0.30	1.33	28.3	1.5
				II	4	0.29	18.46	0.06	0.11		29.8	

Discussion and conclusions

The internal isotopic structure of given conodont element (intra-specimen $\delta^{18}O$ variability) is heterogeneous, although it seems to be stable within particular increments (fig. 1). Mean $\delta^{18}O$ values differ between particular conodont elements derived from the same sample (inter-specimen $\delta^{18}O$ variability) even if they belong to the same species. Nevertheless, the representatives of given species have a characteristic isotopic profile, unique for the sample, even if their mean $\delta^{18}O$ values are different (fig. 1). Several factors responsible for oxygen isotope variability in conodonts were discussed by Wheeley et al., (2012). Basing on the material from the Upper Devonian of the Holy Cross Mts. the following conclusions could be made:

1. We can easily exclude that the diagenetic overprint and preparation issues are responsible for the isotopic variability – otherwise all specimens of conodonts derived from the same samples should have the same isotopic composition, or at least intra-specimen isotopic trend.

2. The oxygen isotopes in present surface seawaters ($\delta^{18}O_{seawater}$) vary from 0 to +0.8 ‰ in a near-equatorial belt to +0.3 to +1.4 ‰ around tropics (LaGrande and Schmidt, 2006). Of course, some of the intra-element variations in $\delta^{18}O$ bioapatite composition <1.4‰ may reflect natural fluctuations of sea surface. Higher fluctuations could be produced only if conodont animals feed on changing depths. Is it possible all representatives of the same species feed exactly on the same depth in the same time? Did they swim as shoals? This is improbable, if to compare the $\delta^{18}O$ values differ between conodont elements of the same species from the same sample, although the isotopic trend within particular elements is similar. This is like all conodont animals of the species decided to dive exactly in the same time but each single animal dived on different depth.

3. Our data should be interpreted as a result of different food preferences of different species (different isotopic signature in different species within the same sample) and changes in food supply in time (different isotopic composition of the same species in different samples).

Acknowledgements

The contribution was financed from projects PGI –NRI 61.2401.1501.00.0

References

Dzik, J. (2008) Evolution of morphogenesis in 360-million-year-old conodont chordates calibrated in days. Evolution & Development, 10 (6): 769–777.

Joachimski, MM, Breisig, S, Buggisch, W, Talent, JA, Mawson, R, Gereke, M, Morrow, JR, Day, J, LeGrande, AN, Schmidt, GA. (2006) Global gridded data set of the oxygen isotopic composition in seawater. Geophysical Research Letters, 33, L12604.

Weddige, K. (2009) Devonian climate and reef evolution: Insights from oxygen isotopes in apatite. Earth and Planetary Science Letters, 284: 599–609.

Lécuyer, C, Amiot, R, Touzeau, A, Trotter, J. (2013) Calibration of the phosphate $\delta^{18}O$ thermometer with carbonate-water oxygen isotope fractionation equations. Chemical Geology, 347: 217–226.

Trotter, JA, Williams, IS, Barnes, CR, Lécuyer, C, Nicoll, RS. (2008) Did cooling oceans trigger Ordovician biodiversification? Evidence from conodont thermometry: Science, 32: 550–554.

Trotter, JA, Williams, IS, Nicora, A, Mazza, M, Rigo, M. (2015). Long-term cycles of Triassic climate change: a new $\delta^{18}O$ record from conodont apatite. Earth and Planetary Science Letters, 415: 165–174.

Wheeley, JR, Smith, MP, Boomer, I. (2012) Oxygen isotope variability in conodonts: implications for reconstructing Palaeozoic palaeoclimates and palaeoceanography. Journal of Geological Society, London, 169: 239–250.

Wójcik, K. (2012) Famennian Fusulinina (Foraminifera) from the Holy Cross Mountains (central Poland). Geological Journal, 47: 594–615.

Using oxygen ($\delta^{18}O$) time-series SHRIMP IIe/MC analyses of the mammalian enamel from Stajnia Cave (southern Poland) to trace a Vistulian (Weichselian, Late Pleistocene) short time climate variability

Zarski, M, Krzeminska E-and Czupyt, Z

Polish Geolgical Institute-National Research Institute, Warszawa. Poland

The positive correlation between oxygen stable isotope composition of mammalian dental enamel and oxygen composition of ingested water have been widely used to reconstruct some aspects of ancient environment and climate, thus there is potential climate proxy of the regions and time what the animals lived. Teeth grow incrementally over the span of months to few years. During this time bioapatitic enamel can capture a variations in oxygen ratio of the local water and preserving a continuous *time-series* of isotope $\delta^{18}O$ fluctuations.

Most frequently however the isotopic spatial variability the is implemented through “bulk sampling” of enamel. It provides a single analyze, that yields a single time-averaged value. Such data are referred for cave bear from Slovakian Medvedia Cave (Abedova, Sabol, 2008) in the Western Tatras Mts (latitude: 49º10′42″N, 19º 35′ 59″ E, altitude 1133 m). For time of Middle Plenivistulian (Middle Pleniglacial, MIS 3) at 39 -51 ka BP a three values of $\delta^{18}O$: 17.7‰, 18.0‰ and 18.9‰ have been obtained teeth analyses. To trace intra-tooth isotope fluctuations during the period of enamel formation a more sensitive methodology and higher spatial resolution is necessary. These requirements are fulfilled through SIMS technique using single spot *in situ* analyses along the enamel-dentine junction (EDJ) according to direction of growth (Blumenthal et al., 2014). We present a first data from the pilot project, where the remains of mammalian teeth were analyzed on SHRIMP IIe/MC using Cs+ primary source. The oxygen isotope analyses along innermost enamel layer teeth were realized in PGI NRI lab, according to the routine described by Blumenthal et al. 2014 and then used as a paleoenvironmental indicator.

The remains of dental tissues of Pleistocene fauna e.g. cave bear and reindeer, were sampled in Stajnia Cave in S Poland (latitude: 50º 3′57″ N, 19º 29′ 4″ E, altitude 362 m). The Stajnia Cave is one of the most important archaeological sites due to the finds of the first remains (teeth) of Neanderthals (*Homo neanderthalensis*) in Poland (Urbanowski et al., 2010) and several tens of thousands of flint artifacts of the Middle Palaeolithic Age. The faunal evidence is typical of the Vistulian (Weichselian).

The aim of study was to decipher and compare enamel records within one taxa from different sedimentary horizon (from C to H) of Stajnia Cave as well as within one stratigraphic horizon but different taxa: cave bear vs reindeer. For large sized mammals, body temperatures are kept constant and $\delta^{18}O$ [‰] enamel is not affected by metabolic processes. Thus the oxygen isotope composition of enamel bioapatite mostly reflects of composition of water consumed from local environmental source. The remains of teeth of reindeer were sampled from layers C, D, E and teeth of bear were taken from

D, E, H. The best preserved dental material however derived from layer E, that predated layer D with age of about 45-52,000 years BP (C14, T/U, OSL method), where a relics related to the Neanderthals have been discovered. A significant amount of spots (typically >50) were measured within each tooth. The $\delta^{18}O_{VSMOW}$ [‰]values from each sample were plotted against distance down the tooth enamel. A distance between spots was kept in range about 0.02 mm along the EDJ, that was enough to obtain temporal resolution of enamel incremental layer less than one month.

The analyses of cave bear enamel from the same layer E gave almost similar $\delta^{18}O$ patterns in range from 14.7±0.1‰ to 18.2±0.10‰. The $\delta^{18}O$ patterns reflect an individual metabolic behavior of bear and natural seasonal fluctuations of ingested water composition, correlating positively with local temperature e.g. warm/cold month and directly provide a record of climate variables at a particular site for short period of time e.g. few seasons – during enamel mineralization. Comparison of the isotopic values between taxa within the same level did show some significant differences (Fig.1), however the reindeer enamel yielded usually higher amplitude (>6‰) of $\delta^{18}O$ intra-tooth fluctuation. An overall oxygen ratio varies from 8.13±0.11‰ to 15.02±0.10‰ (layer E sample R4, n=98 spots) at the distance of EDJ about 12.87 mm. It reflects a drastic change of isotopic composition of ingested environmental water, where lower $\delta^{18}O$ value was correlated to relatively colder and wet climatic regime. In oppose to summer-winter smaller-scale variation, the most of reindeer examined teeth reveal one or two single higher excursion of $\delta^{18}O$, that is a real evidence of migrations.

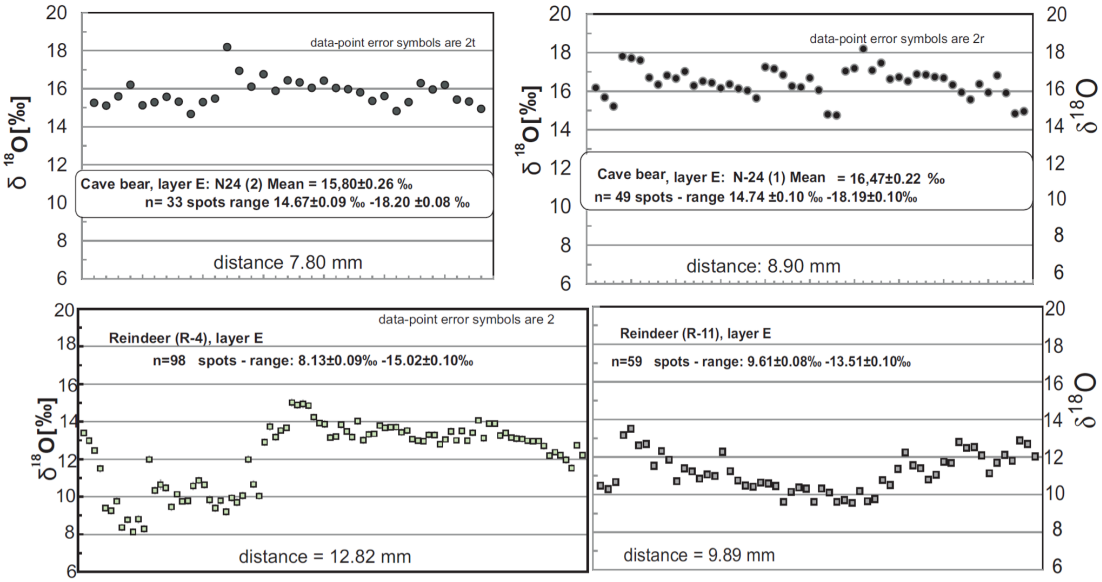

Fig. 1. Seasonal oxygen isotope intra-tooth variation detected by SHRIMP IIe/MC. Profiles of $\delta^{18}O$ along enamel/ dentine junction(EDJ). Examples of Cave bear and Reindeer tooth remains derived from a single fossiliferous horizon E, (age before 45−52,000 years BP) of Stajnia Cave.

Conclusions

Single spot $\delta^{18}O$ time-series analyses made by SHRIMP along EDJ perfectly track a natural inhomogeneity of enamel incremental layers. The long profiles (n>>50 spots) of intra-tooth $\delta^{18}O$ variation provided directly a record of seasonal changes of climatic variables from time of the Vistulian (Late Pleistocene). Intra-tooth $\delta^{18}O$ analysis on SHRIMP IIe/MC allowed to recognize of sub-annual (summer and winter) fluctuations with high time resolution. Teeth within a single fossiliferous horizon show the general similar isotopic range but sometimes distinct patterns thus a short time-series ($\delta^{18}O$ profiles) have also been used to indicate of long-distance movement pointing to migratory behavior of mammalians. The climate of Vistulian (Weichselian) was cold, characteristic of tundra areas with a typical vegetation and fauna, but based on oxygen isotope enamel record and its comparison between layers it can be concluded that from layer E upwards, the climate conditions became progressively drier and milder, that is consistent with the pollen record.

References

Abelova, M, Sobol M. (2008) Attempt on The reconstruction of palaeotemperature and palaeoenvironment in the territory of Slovakia during the Last Glacial based on oxygen and carbon isotopes from tooth enamel and bone collagen of cave bears. Acta Carsologica Slovacia 46. 10 -22.

Blumenthal, SA, Cerling TE, Chritz, KL, Bromage, TG, Kozdon, R, Valley JW. (2014) Stable isotope time-serie in mammalian teeth: in situ $\delta^{18}O$ from innermost enamel layer. Geochim. et Cosmochim. Acta, 124: 223–236.

Urbanowski, M, Socha, P, Dąbrowski, P, Nowaczewska, W, Sadakierska-Chudy, A, Dobosz, T, Stefaniak, K, Nadachowski, A. (2010) The first Neanderthal tooth found North of the Carpathian Mountains. Naturwissenschaften, 97, 411–415.